Global and Planetary Change 157 (2017) 114–138

Contents lists available at ScienceDirect

Global and Planetary Change

journal homepage: www.elsevier.com/locate/gloplacha

Invited review article

Hydrological and associated biogeochemical consequences of rapid global warming during the Paleocene-Eocene Thermal Maximum

Matthew J. Carmichael[a,b,*], Gordon N. Inglis[a], Marcus P.S. Badger[a,b,c], B. David A. Naafs[a], Leila Behrooz[a], Serginio Remmelzwaal[b,d], Fanny M. Monteiro[b], Megan Rohrssen[a,1], Alexander Farnsworth[b], Heather L. Buss[d], Alexander J. Dickson[e], Paul J. Valdes[b], Daniel J. Lunt[b], Richard D. Pancost[a]

[a] Organic Geochemistry Unit, School of Chemistry and Cabot Institute, University of Bristol, UK
[b] BRIDGE, School of Geographical Sciences and Cabot Institute, University of Bristol, UK
[c] School of Environment, Earth and Ecosystem Sciences, The Open University, UK
[d] School of Earth Sciences and Cabot Insitute, University of Bristol, UK
[e] Department of Earth Sciences, University of Oxford, UK

ARTICLE INFO

Keywords:
Paleohydrology
Data-model comparisons
Paleogene
Hyperthermals
Proxies
Climate models

ABSTRACT

The Paleocene-Eocene Thermal Maximum (PETM) hyperthermal, ~56 million years ago (Ma), is the most dramatic example of abrupt Cenozoic global warming. During the PETM surface temperatures increased between 5 and 9 °C and the onset likely took < 20 kyr. The PETM provides a case study of the impacts of rapid global warming on the Earth system, including both hydrological and associated biogeochemical feedbacks, and proxy data from the PETM can provide constraints on changes in warm climate hydrology simulated by general circulation models (GCMs). In this paper, we provide a critical review of biological and geochemical signatures interpreted as direct or indirect indicators of hydrological change at the PETM, explore the importance of adopting multi-proxy approaches, and present a preliminary model-data comparison. Hydrological records complement those of temperature and indicate that the climatic response at the PETM was complex, with significant regional and temporal variability. This is further illustrated by the biogeochemical consequences of inferred changes in hydrology and, in fact, changes in precipitation and the biogeochemical consequences are often conflated in geochemical signatures. There is also strong evidence in many regions for changes in the episodic and/or intra-annual distribution of precipitation that has not widely been considered when comparing proxy data to GCM output. Crucially, GCM simulations indicate that the response of the hydrological cycle to the PETM was heterogeneous – some regions are associated with increased precipitation – evaporation (P – E), whilst others are characterised by a decrease. Interestingly, the majority of proxy data come from the regions where GCMs predict an increase in PETM precipitation. We propose that comparison of hydrological proxies to GCM output can be an important test of model skill, but this will be enhanced by further data from regions of model-simulated aridity and simulation of extreme precipitation events.

1. Introduction

The Fifth Assessment Report (AR5) of the Intergovernmental Panel on Climate Change (IPCC, 2013) concluded that anthropogenic warming by 2100 is likely to exceed 2 °C above preindustrial temperatures for both stabilisation (RCP6.0) and high-emission (RCP8.5) greenhouse gas scenarios. Predicting the associated response of Earth's hydrological cycle is a fundamental endeavour, given the environmental and related socio-economic implications of such changes (e.g. Trenberth et al., 2003; Dai, 2006). Global warming is widely considered to cause an intensification of the hydrological cycle, with globally increased evaporative fluxes balanced by increased precipitation at around 2% K^{-1} (Allen and Ingram, 2002; Trenberth, 2011). Regionally, a 'wet-wetter dry-drier' style response is anticipated, with increased water vapour transport from moisture divergence zones into convergence zones (Held and Soden, 2006; Chou and Neelin, 2004). Beyond first-order predictions, regional variations in hydrological changes are more uncertain, with General Circulation Models (GCMs) exhibiting

* Corresponding author at: Organic Geochemistry Unit, School of Chemistry and Cabot Institute, University of Bristol, UK.
E-mail address: matt.carmichael@bristol.ac.uk (M.J. Carmichael).
[1] Now at: Department of Earth and Atmospheric Sciences, Central Michigan University, US.

http://dx.doi.org/10.1016/j.gloplacha.2017.07.014
Received 16 February 2017; Received in revised form 31 July 2017; Accepted 31 July 2017
Available online 12 August 2017

significant differences in their projected end-of-century climatology (Schaller et al., 2011; Knutti and Sedláček, 2013). Beyond predicting changes in mean annual or seasonal precipitation distributions, simulating variations in precipitation frequency, intensity and type are highly uncertain within numerical models (Dai, 2006; Sun et al., 2006), but potentially crucial to understanding localised hydrological responses.

The environmental impacts and feedbacks resulting from changes in the hydrological cycle are likely to be profound. Although current changes in runoff, erosion and coastal water quality are often dominated by direct human pressures such as land use change, water abstraction and increased fertiliser use (Fabricius, 2005; Walling, 2009), warming-induced hydrological changes will likely impart a significant impact on the hydrological cycle in coming decades (Jiménez Cisneros et al., 2014; Yang et al., 2003; Rabalais et al., 2009). Elevated global precipitation is predicted to result in increased soil erosion (Nearing et al., 2004; Zhang et al., 2012), although changes in seasonality of precipitation and the occurrence of high intensity events may increase erosion even in regions where total annual precipitation declines. On land, changes in precipitation and soil moisture will affect the vegetation distribution (Jiang et al., 2012; Yu et al., 2016), the extent of wetlands (Milzow et al., 2010; Acreman et al., 2009) and rates of organic matter decomposition (Jobbagy and Jackson, 2000; Conant et al., 2011), all with profound impacts on the carbon cycle. Moreover, changes in runoff will impact the delivery of freshwater, nutrients and terrigenous materials to continental shelves with associated impacts on biogeochemistry (Jiménez Cisneros et al., 2014), and intense storm activity could result in greater turbulent mixing (Meire et al., 2013).

Warmer-than-present intervals in Earth's history can serve as partial analogues for our future Earth (Lunt et al., 2013; Haywood et al., 2011), especially high atmospheric CO_2 end-of-century scenarios (White et al., 2001; Suarez et al., 2009). In particular, a coupled approach that integrates geologic proxy data with the results of modelling offers the possibility to evaluate whether GCMs are capable of adequately simulating the hydrological cycle of deep-time warm climates (Winguth et al., 2010; Speelman et al., 2010), with implications for understanding how best to utilise model projections for future prediction. Furthermore, the study of paleohydrology also has wide implications for understanding past changes in climate, biogeochemistry, and the carbon cycle.

In this paper, we explore changes in the hydrological cycle during the Paleocene-Eocene Thermal Maximum (PETM; Section 2), a greenhouse-gas induced hyperthermal warming event which occurred around 56 Ma (Westerhold et al., 2009). Despite extensive research on the environmental impacts of the PETM and several model-derived reconstructions of precipitation, a synthesis of proxy evidence is currently lacking. This is crucial, because much of the data reveal complex (Schmitz and Pujalte, 2003; Schmitz and Pujalte, 2007; Handley et al., 2012; Garel et al., 2013), or even contradictory interpretations (Bowen et al., 2004; Wing et al., 2005; Bowen and Bowen, 2008; Retallack et al., 2009). Furthermore, proxies are not direct indicators for changes in precipitation or evaporation, but rather more indirect evidence for how hydrological changes impacted sediments or biota. These proxies also respond to different temporal signals of hydrological change, but this process remains largely unconsidered (e.g. Foreman, 2014). In this paper, a compilation of proxy indicators that incorporate either direct or indirect signals of Eocene hydrological change is presented, focussing on the PETM but including some data for other transient hyperthermals and long-term changes associated with the Early Eocene Climatic Optimum (EECO). Crucially, by compiling results from different proxy approaches, a spatially distributed data set is generated, suitable for qualitative proxy-model comparison and for critical evaluation of the global hydrological cycle -and its consequences - during rapid global warming events.

2. Early Paleogene climate change

Early Paleogene (57–48 Ma) pCO_2 estimates are sparse and variable but generally indicate levels much higher than those of today (Royer et al., 2001; Fletcher et al., 2008; Doria et al., 2011; Yapp, 2004; Jagniecki et al., 2015; Anagnostou et al., 2016). As a consequence of putative pCO_2 increase, but also perhaps influenced by oceanographic change (e.g. Hollis et al., 2012), the early Eocene is characterised by gradual long-term warming. This culminated in the EECO (53–49 Ma), a long-term temperature maximum (Zachos et al., 2001; Littler et al., 2014). Sea surface temperature (SST) estimates inferred from inorganic and organic proxies for this interval indicate very high SSTs, including tropical temperatures warmer than today, > 30 °C (Pearson et al., 2001; Pearson et al., 2007; Inglis et al., 2015a), and markedly warmer SSTs at high latitudes, with estimates ranging between ~25 and 35 °C (Bijl et al., 2009; Creech et al., 2010; Hollis et al., 2012; Frieling et al., 2014; Inglis et al., 2015a). As such, a reduced equator-pole temperature gradient has been suggested for the early Eocene (Bijl et al., 2009; Inglis et al., 2015a; Tierney and Tingley, 2014), with significant implications for the global hydrological cycle (Speelman et al., 2010).

The early Paleogene is also characterised by a series of hyperthermal events, including the PETM which occurred around ~56 Ma and is associated with ~5 °C of warming in the deep ocean (Zachos et al., 2001; Tripati and Elderfield, 2005) and up to 8 °C of warming in the surface ocean (Sluijs et al., 2006; Zachos et al., 2006; Sluijs et al., 2007; Sluijs et al., 2011). The PETM is characterised by a ~3–6‰ negative carbon isotope excursion (CIE) which indicates the release of ^{13}C–depleted carbon into the ocean-atmosphere system (Dickens et al., 1995; Cramer, 2003; Lourens et al., 2005). The CIE occurs globally (McInerney and Wing, 2011) but differs in magnitude depending on both the archive and location (Schubert and Jahren, 2013; Section 3.4), leading to difficulties constraining the amount of carbon input. There is also little consensus over the source of carbon released during the PETM. Warming has been widely attributed to the dissociation of seafloor marine hydrates and the subsequent oxidation of methane to carbon dioxide (Dickens et al., 1995; Dunkley Jones et al., 2010), but this appears to be unable to explain the magnitude of the observed temperature rise (Zeebe et al., 2009). As such, additional carbon sources have been invoked, many of which represent biogeochemical feedbacks modulated by the hydroclimatic regime, including the decomposition of soil organic carbon in high-latitude permafrost (DeConto et al., 2012), enhanced terrestrial methane cycling in peat-forming environments (Pancost et al., 2007; Beerling et al., 2011) and/or increased carbon turnover in soils (Cotton et al., 2015). The drawdown of CO_2 that drove the PETM recovery is also thought to have been governed by biogeochemical feedbacks, including enhanced carbon storage in the terrestrial biosphere (Bowen and Zachos, 2010), increased efficiency in the biological pump (Bains et al., 2000) and/or enhanced marine carbonate preservation (Kelly et al., 2005).

3. Hydrological change during the PETM

Dramatic hydrological change during the PETM has been inferred from a range of sedimentological, geochemical and biological proxies. A compilation, and in some cases re-examination, of these proxies is essential for future data-model comparisons. Quantitative botanical proxies for precipitation are discussed first, followed by qualitative proxies for other hydrological changes.

3.1. Botanical proxies for change in precipitation

Fossilised plant remains provide two distinct methods for estimating ancient precipitation rates. Leaf Area Analysis (LAA) is a physiognomic approach whereby larger leaves predominate in climates with greater mean annual precipitation rates (Wilf et al., 1998). However, the LAA approach can underestimate precipitation (see Peppe et al., 2011 and

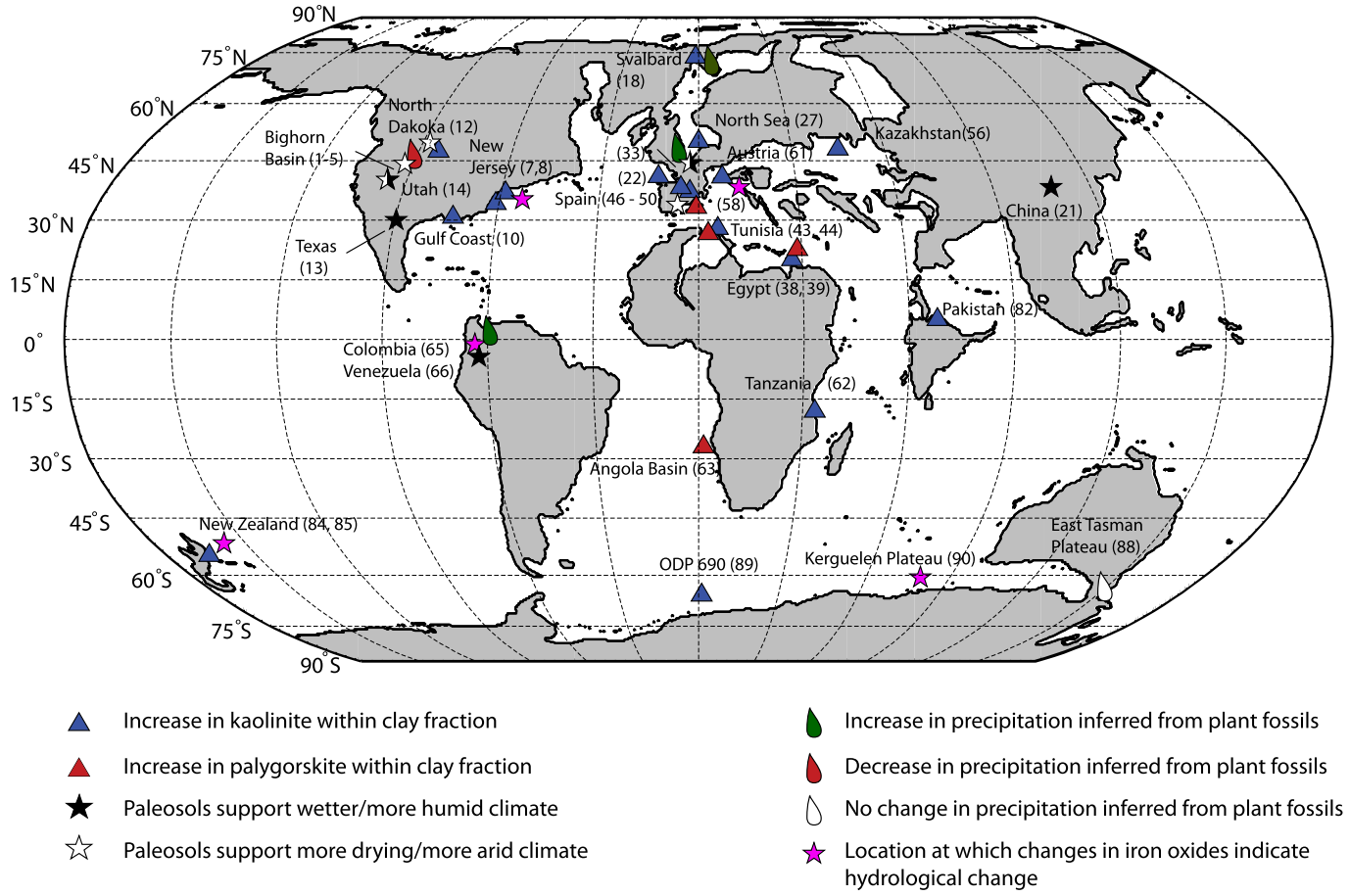

Fig. 1. Paleogeographic reconstruction for 56 Ma showing locations where PETM hydrological change has been inferred from changes in the distribution of clay mineralogy (triangles), paleosol characteristics and iron oxides (stars) and plant fossils (leaf symbols). Numbers provided after each location correspond to PETM sites and references provided in Supplementary Table 1.

references therein); as such, other physiognomic techniques have often been employed, including the Climate Leaf Analysis Multivariate Program (CLAMP; Wolfe, 1993; Wolfe, 1995) and digital leaf physiognomy (Royer et al., 2005). The second type of method compares the climatic tolerances of modern and fossil species and includes the Nearest Living Relative (NLR; Greenwood et al., 2003) and Co-existence Approach (CA; Mosbrugger and Utescher, 1997). Crucially, and unlike CLAMP, this approach can be applied to sporomorph assemblages (i.e. fossilised spores, seeds and pollen), as well as leaves. The location of plant-based reconstructions of precipitation for the PETM are shown in Fig. 1. The paleogeographic reconstruction comes from Getech Plc, and is a high-resolution version of that which appears in Lunt et al. (2016).

Leaf physiognomy has previously been applied within the Bighorn Basin, Wyoming. Wing et al. (2005) used LAA to produce estimates of precipitation shortly after the onset of the PETM and during the recovery phase. Using two distinct calibrations, the lower PETM flora yield MAP estimates of 800 mm/yr (+1140/−560 mm/yr) and 410 mm/yr, whilst the upper PETM flora yield MAP estimates of 1440 (+2060/−1000 mm/yr) and 1320 mm/yr. Comparison of these data to late Paleocene assemblages indicate that drying occurred near the onset of the PETM, followed by a return to background values during the recovery phase. Changes in the floral assemblage support LAA-derived interpretations, indicating a mesic and temperate community within the late Paleocene and seasonally dry tropical forests during the PETM (Wing and Currano, 2013), although the small number of species identified has precluded quantitative NLR precipitation estimates (Kraus et al., 2013).

Low-resolution NLR estimates have also been obtained from the East Tasman Plateau in the South West Pacific (Contreras et al., 2013). Here, samples from within the PETM yield similar estimates to the late Paleocene and early Eocene (1700–1800 mm/yr), although low concentrations of sporomorphs suggest they could reflect a change in depositional setting rather than a true paleoclimatic signal (Contreras et al., 2013). In other regions, there is no significant change in the abundance of dry indicator plant species during the PETM but floral data are consistent with a wetter climate (Jaramillo et al., 2010). In Columbia and Venezuela, the PETM is accompanied by an increase in plant diversity and an increase in the abundance of families related to wet tropical rainforests, suggesting stable or increasing precipitation during the PETM (Jaramillo et al., 2010). In the North Atlantic, an increase in the abundance of peat-forming flora during the body of the PETM has been argued to reflect enhanced regional precipitation and the development of waterlogged environments (Kender et al., 2012). Within PETM-aged sediments from Lomonosov Ridge in the high Arctic, abundances of fern spores indicative of wet climates also increase (Harding et al., 2011).

Other paleobotanic approaches further contribute to our understanding of PETM hydrology. For example, the presence or absence of inertinite (i.e. fossilised charcoal) can provide insights into the floral community and fire frequency (although we note that Denis et al., 2017 document increased polycyclic aromatic hydrocarbon (PAH) abundance at the PETM coeval with wetter Arctic conditions and argued that fire frequency is a function of ecology and vegetation distribution, not simply aridity). Within the Cobham Lignite (UK), prior to the PETM and during its immediate onset, fern spores and inertinite are abundant, suggesting a fire-prone and relatively dry peat-forming environment

(Collinson et al., 2009; Steart et al., 2007). However, during the PETM charcoal abundances decrease and wetland plant abundances increase, indicating a decrease in the fire regime and the development of more waterlogged conditions (Collinson et al., 2009). In contrast, in Kakahu, New Zealand, an increase in inertinite occurs during the PETM (Pole, 2010).

Collectively, insights from palaeobotanical precipitation proxies indicate a varied hydrological response during the PETM, with evidence for (seasonal) drying within the continental interior of the United States (e.g. Bighorn Basin) and stable (e.g. Contreras et al., 2013) or increasing precipitation (e.g. Collinson et al., 2009; Jaramillo et al., 2010; Kender et al., 2012) in higher-latitude and more coastal settings. However, changes in vegetation distribution are also highly regionally variable. Analysis of the Cobham lignite (Collinson et al., 2009) has indicated increased conifer abundance at the PETM, whilst North Sea assemblages suggest a decreasing abundance of conifers (Kender et al., 2012; Wing and Currano, 2013). Furthermore, a variety of locations indicate a lack of change in vegetation composition - including the US Gulf Coast (Harrington et al., 2004), North Dakota (Harrington et al., 2005) and Northern Europe (Steurbaut et al., 2003). Crucially, hydrological changes have been inferred from other proxies within these regions, underlining the importance of a multiproxy approach.

3.2. Paleosol morphology, mineralogy and geochemistry

PETM-aged paleosols provide both qualitative indicators of soil moisture conditions and quantitative estimates of precipitation rate. The soils of the Bighorn Basin provide one of the best continental records of terrestrial climate change at the PETM, with vertically-stacked paleosols yielding high-resolution insights into paleohydrology (Fricke, 2003; Secord et al., 2012). Kraus and Riggins (2007) presented a detailed analysis of two paleosol sequences which record transient fluctuations in regional hydrology during the PETM. Immediately after the carbon isotope excursion (CIE) onset at Polecat Bench, arid conditions are indicated by a lack of iron-oxide nodules and the presence of carbonate nodules; however, colour and mineralogical changes through the rest of the CIE reveal pronounced and perhaps cyclical hydrological variation. A similar pattern of transient drying events is inferred for the nearby Sand Creek (Kraus and Riggins, 2007) and this variability could correspond to ~21 kyr precessional cycles (Abdul Aziz et al., 2008). In a separate study of paleosols, also within the Bighorn Basin, Kraus et al. (2013) document a similar pattern with progressive drying at the onset of the PETM and wetting in the PETM recovery phase, suggesting these variations are caused by regional climatic changes, rather than localised controls. Intriguingly, Kraus et al. (2013) suggest that shifts to a drier climate occurred ahead of the PETM onset, and a moist climate continued beyond the event's termination, indicating a prolonged response.

Transient drying events are also supported by paleosol trace fossils, weathering indices, and paleosol geochemistry. Within paleosols at Polecat Bench, prismatic peds – interpreted as the casts of freshwater crayfish burrows - occur both before and after the event but are rare or absent in PETM-aged paleosols (Smith et al., 2008), reflecting a lowered water table and/or improved drainage on the floodplain. Weathering indices, including CIA (Chemical Index of Alteration) and CALMAG (CaO, MgO), in Bighorn Basin paleosols generally indicate a decline in precipitation (Adams et al., 2011). Manganese-rich nodules have also been observed within rhizocretions (mineralised root systems) within Bighorn Basin deposits. These are suggested to have formed under repeated redox alternations, likely related to seasonal flooding. Their occurrence is reduced during the main body of the PETM, again implying transient drying (Woody et al., 2014).

Whilst there is evidence from a range of proxies for transient drying within the Bighorn Basin, other studies from PETM-aged paleosols yield conflicting results for the US continental interior. Transfer functions based on the depth to carbonate nodular horizon have been applied to paleosols from the Axehandle Basin, Utah, to infer a PETM precipitation rate increase to 663 ± 147 mm/yr from a background of 393 ± 166 mm/yr (Retallack, 2005). However, clumped isotope analysis on dolomitic paleosol nodules from the same locality have also been used to infer increased aridity (VanDeVelde et al., 2013). Within western Texas, paleosols from the PETM have higher CIAs than those formed before the event, suggesting a possible role for increased humidity in weathering, although the increased production of carbonic acid in a high-CO_2 atmosphere could also have had an effect (White and Schiebout, 2008).

In other regions, such as the eastern Pyrenees, abundant calcite and soil nodules within the Claret Conglomerate (CC) indicate an arid or possibly sub-humid climate during the onset of the PETM (Schmitz and Pujalte, 2003, 2007). These sequences are also associated with increased kaolinite contents and high sedimentation rates, apparently contradicting this interpretation, but the authors instead suggest that they record episodic erosive rainfall events rather than a more humid climate (Section 4.1.2). Silcrete $\delta^{30}Si$ values also failed to record an increase in weathering in continental settings from northern France (Rad et al., 2009). In contrast, the Bogota Basin (Colombia) records an increase in iron and aluminium oxides and a decrease in carbonate nodules, suggesting enhanced precipitation or weathering during the Paleocene-Eocene transition (although they may not correspond to the PETM due to poorly constrained chronology; Morón et al., 2013). The $\delta^{15}N$ values of soil organic matter at Vasterival (Normandy, France) have been used to infer cycles of wet and dry conditions during the PETM (Storme et al., 2012), based on the assumption that ^{14}N is preferentially lost under dry conditions, but the complexity of this novel proxy remains poorly understood in deep-time settings (Garel et al., 2013).

Whilst their distribution is limited, paleosols indicate pronounced regional variation in the PETM hydrological response. Locations at which hydrological change has been inferred from paleosol characteristics are summarised within Fig. 1. Consistent and multiple lines of evidence indicate transient drying events occurred in the Bighorn Basin and Western Europe, but the former could be a localised response with evidence for a more varied hydrological response at other US sites. It is also likely that the complex and apparently contradictory results within a given depositional system arise from: 1) the fact that weathering changes at the PETM were governed by a range of factors other than precipitation alone, including temperature and vegetation; and 2) the different responses of weathering signals to prolonged versus episodic precipitation events. Paleosols also provide critical evidence for more complex changes in the hydrological cycle within the body of the PETM, with evidence for wet-dry cycles apparent at a number of locations, perhaps relating to orbital forcing.

3.2.1. Clay and iron oxide mineralogy in marine sediments

In addition to paleosol morphology and mineralogy, clay mineralogical changes have also been used to infer shifts in hydrology across the PETM. This is based upon the observed correlation between the abundance of different clay minerals and hydroclimatic regimes (Robert and Kennett, 1994; Gibson et al., 2000). In particular, a pulse of kaolinite, which commonly forms in tropical, moist climates with year-round precipitation (Egger et al., 2002; John et al., 2012), is coincident with the PETM in many marginal marine sections (Fig. 1), including along the eastern US coast (Gibson et al., 2000; John et al., 2012), offshore Antarctica (Robert and Kennett, 1994), various locations around the Tethyan Sea (Bolle and Adatte, 2001; Bolle et al., 2000), New Zealand (Kaiho et al., 1996), the eastern North Atlantic (Bornemann et al., 2014) and Svalbard (Dypvik et al., 2011). Whilst sea level could also play a role in controlling kaolinite deposition (e.g. Gibson et al., 2000), a lack of correlation between sea-level variation and kaolinite abundance argues that climatic variables are the dominant control on this signal (e.g. Bolle and Adatte, 2001; Robert and Chamley, 1991).

Variations in clay minerals indicative of other climatic regime

changes have resulted in increasingly nuanced interpretations of the clay-mineral record. Smectite has been used to examine changes in seasonality at the onset of PETM given its occurrence today in climates dominated by distinct wet and dry seasons. Its lower abundance relative to kaolinite along the New Jersey/Virginia coast at the PETM was used by Gibson et al. (2000) to suggest a shift from seasonal to year round precipitation, whilst continued dominance of smectite across the PETM has been interpreted as evidence for a seasonal climate throughout the PETM at Untersberg, Austria (Egger et al., 2005). Although a kaolinite pulse is observed at the onset of the PETM within the Southern Ocean, smectite dominates for the majority of the PETM (Robert and Kennett, 1994), perhaps indicating seasonally varying precipitation rates in Antarctica. Palygorskite is most commonly formed in arid climates either due to evaporative enrichment of Mg/Si in coastal seawaters or in calcrete soils (Bolle and Adatte, 2001). Robert and Chamley (1991) document the presence of palygorskite in the Angola basin off West Africa and suggest low latitude coastal environments were subject to intense evaporation during the PETM. Bolle and Adatte (2001) and Bolle et al. (2000) have also suggested a differentiation of Tethyan climates occurred between the Paleocene and Eocene, with evidence for aridity in coastal basins along the southern Tethyan margin, (e.g. Israel; Fig. 1) and more humid climates on the northern margin (e.g. Kazakhstan; Fig. 1), although whether this was a long-term response remains unclear.

The climatic origin of the observed shifts in clay mineral associations across the PETM has been widely challenged in recent years. Chemical weathering sufficient to result in extensive kaolinite deposits in marine sediments would typically take at least ~1 Ma to form (Thiry, 2000) and is incompatible with the suggested duration of the PETM (~120–220 kyr; Abdul Aziz et al., 2008; Murphy et al., 2010). John et al. (2012) show that at Bass River, New Jersey, increases in kaolinite occurred within 40 kyr of the PETM onset, two to three orders of magnitude faster than the assumed rate of kaolinite pedogenesis. Schmitz and Pujalte (2003) also argue that within PETM-aged deposits from the Tremp Basin, Spain, a small increase in kaolinite occurs at the Paleocene-Eocene boundary despite the identification of carbonate nodules and gypsum/calcite minerals indicative of a semi-arid climate. The exhumation of earlier Mesozoic aged sediments has been proposed as an alternative explanation (John et al., 2012; Schmitz and Pujalte, 2003; Bornemann et al., 2014), although this process would require global exhumation of previously buried kaolinite to result in the globally extensive signal shown in Fig. 1. In their study of a PETM section in North Dakota, Clechenko et al. (2007) note a lack of extensive kaolinite-rich sources in underlying strata, and propose a possible drying or preconditioning of the soil ahead of an increase in precipitation. Nonetheless, it appears likely that this kaolinite pulse was derived not from its increased formation under a more humid climate regime but from increased erosion, which could include the occurrence of more intense rainfall events. Given the widespread occurrence of the kaolinite pulse, this reinterpretation is vital when considering changes in precipitation, its sedimentological consequences, and data-model comparisons.

The presence of iron oxides (e.g. haematite, magnetite and maghemite) has also been used to infer changes in hydrology during the PETM due to climatic controls on the formation of these minerals (Hyland et al., 2015; Maxbauer et al., 2016a). In marginal marine sediments from New Jersey, USA, the presence of “giant” magnetite particles imply intense tropical weathering and the supply of reactive iron into a deltaic, shallow-marine setting (Schumann et al., 2008; Kopp et al., 2009), in turn driving changes in iron biogeochemical cycling in zones of relative oxygen depletion (Section 4.6). In other regions, such as the southern Kerguelen Plateau (ODP 738C), abundances of aeolian haematite grains increase at the start of the PETM, possibly reflecting drier, more seasonal, conditions on the nearby Antarctic continent (Larrasoaña et al., 2012). In contrast, a significant increase in haematite (relative to magnetite and maghemite) within the Belluno Basin lasting approximately 300 kyr likely indicates a warm and wet climate and enhanced weathering of iron-bearing silicates (Dallanave et al., 2009). The application of iron oxide proxies is currently limited in the terrestrial realm. However, variations in magnetic properties in subsurface paleosols at Polecat Bench, Bighorn Basin correlate with the trend towards aridification implied by independent geochemical proxies, although the impact of diagenesis, particularly on outcropping paleosols, currently prevents quantitative estimates of precipitation change (Maxbauer et al., 2016b).

3.3. Hydrological change inferred from δ^2H and $\delta^{18}O$ values of meteoric water, recorded by lipid biomarkers and teeth/bones, respectively

Evaporation and condensation processes fractionate stable isotopes of water during the global hydrological cycle, resulting in distinct spatial and temporal variations in the hydrogen and oxygen isotopic composition of meteoric water (Dansgaard, 1964; Gat, 1996; Bowen, 2010). Therefore, the $\delta^{18}O$ and δ^2H values of various sedimentary materials that have incorporated meteoric water, such as fossilised teeth and plant-derived organic matter, have been used to constrain both global and local changes in hydrology across the PETM.

3.3.1. Hydrogen isotopes of plant-derived lipid biomarkers

In the past decade, the hydrogen isotopic ratio of leaf wax-derived lipid biomarkers has emerged as a novel paleohydrological proxy given the potential for *n*-alkane compounds to persist in the geological record over many millions of years (Eglinton and Eglinton, 2008; Sachse et al., 2012). A range of climatic and plant physiological characteristics govern the δ^2H values of leaf waxes. These include the δ^2H composition of meteoric water (itself governed by a wide range of climatic controls e.g. Gat, 1996), the extent of evaporative enrichment prior to lipid biosynthesis (both external and internal to the plant e.g. (Polissar and Freeman, 2010; Feakins and Sessions, 2010), the degree of biological fractionation during lipid synthesis (Chikaraishi and Naraoka, 2003), and the timing of leaf wax production (Tipple and Pagani, 2013). By extension, changes in vegetation and the source of organic matter can significantly influence δ^2H values of leaf waxes in sediments. If these multiple, often antagonistic, parameters can be accounted for through corroboratory evidence (e.g. paleovegetation data and complementary proxies), constraints imposed by site latitude, or climate modelling, then variations in δ^2H can be used as a tracer of the hydrological cycle (Sachse et al., 2004; Schefuß et al., 2005; Tierney et al., 2008; Sachs et al., 2009).

Most hydrogen isotope records that span the PETM provide evidence for a hydrological perturbation during the event (Fig. 2). The first published record was from Lomonosov Ridge in the central Arctic Ocean, where long-chain *n*-alkanes exhibit a marked deuterium enrichment from δ^2H values $< -200‰$ prior to the PETM to ca. $-155‰$ at the CIE onset (Fig. 2), with a subsequent decline to pre-event values later during the PETM (Pagani et al., 2006). Assuming that the shift in δ^2H values mainly reflects a change in δ^2H of precipitation water and is not complicated by additional processes, the large enrichment in δ^2H implies a reduced isotopic distillation along the airmass trajectory, i.e. increased water vapour transport to the high latitudes and a possible associated decrease in rainout at lower-latitudes. An increase in precipitation in the high-latitudes is supported by the presence of low-salinity dinoflagellates in the Arctic (Pagani et al., 2006; Kender et al., 2012) and is also consistent with the inferred reduced latitudinal temperature gradient during the PETM (Speelman et al., 2010; Pagani et al., 2006).

A shift towards higher δ^2H values during the PETM also occurs in Tanzania (Handley et al., 2008; Fig. 2). These changes are difficult to explain via reduced rainout or a shift in vapour source given the tropical and coastal location of Tanzania during the PETM (Fig. 3). This shift does not appear to be associated with vegetation changes, based on pollen records and a lack of correlation of δ^2H values with *n*-alkane

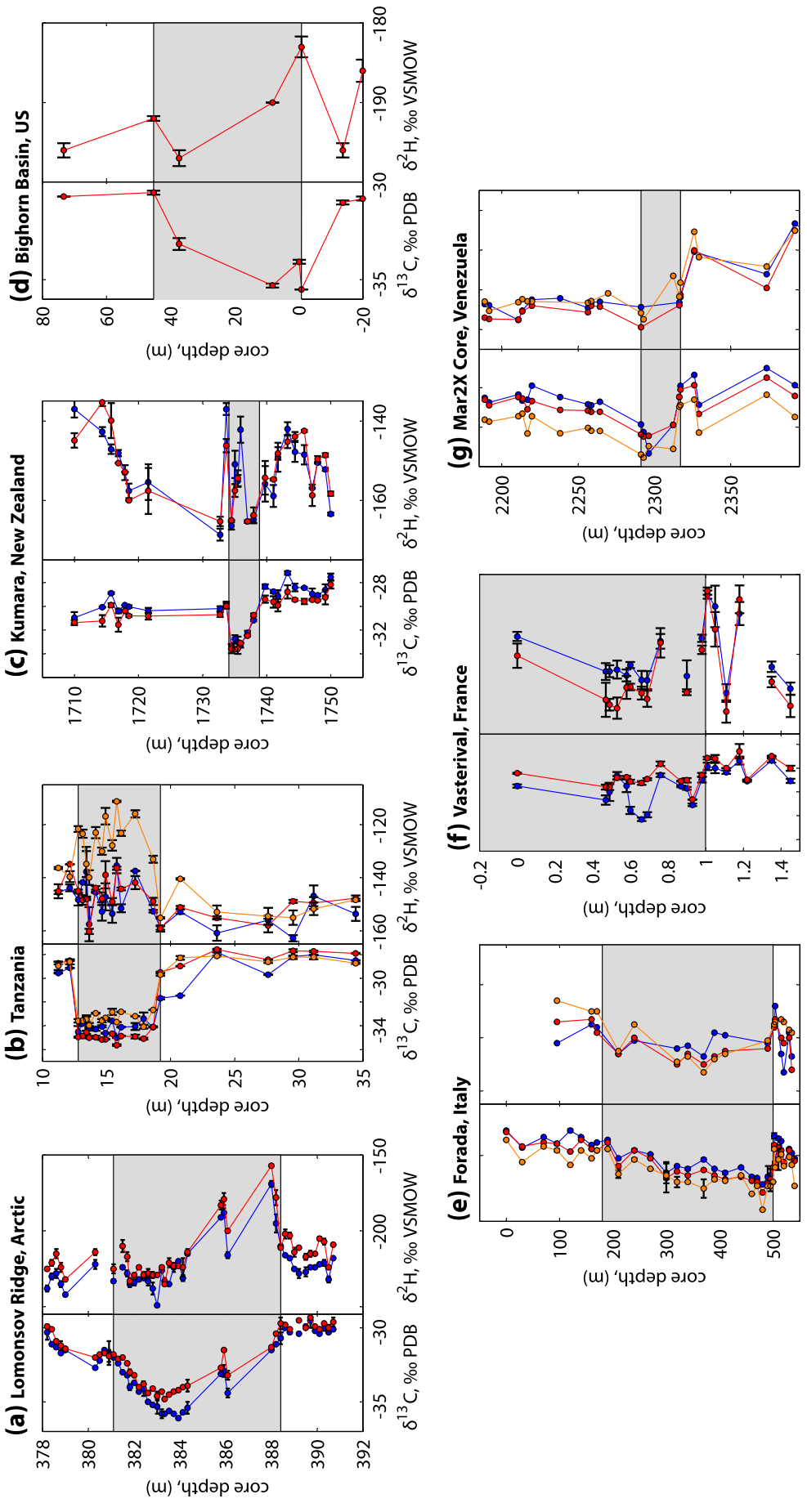

Fig. 2. Summary of published *n*-alkane δ^2H isotope records through the PETM for carbon chain lengths C_{27} (blue), C_{29} (red), C_{31} (orange), right hand panels, and associated carbon isotope variations shown in the left panels for (a) Lomonosov Ridge, Arctic (Pagani et al., 2006), (b) Tanzania (Handley et al., 2008, 2012), (c) Bighorn Basin, Wyoming (Smith et al., 2007), (d) Kumara, New Zealand (Handley et al., 2011) (e) Forada, Italy (Tipple et al., 2011), (f) Normandy, France (Garel et al., 2013), (g) Mar2X core, Venezuela (Jaramillo et al., 2010). Where shown, error bars are: for (a) range of values based on duplicate measurements and for (b)–(f) standard deviation for repeat measurements, as described in the original publications. The grey areas represent the CIE as inferred by the authors of each publication. (For interpretation of the references to colour in this figure legend, the reader is referred to the web version of this article.)

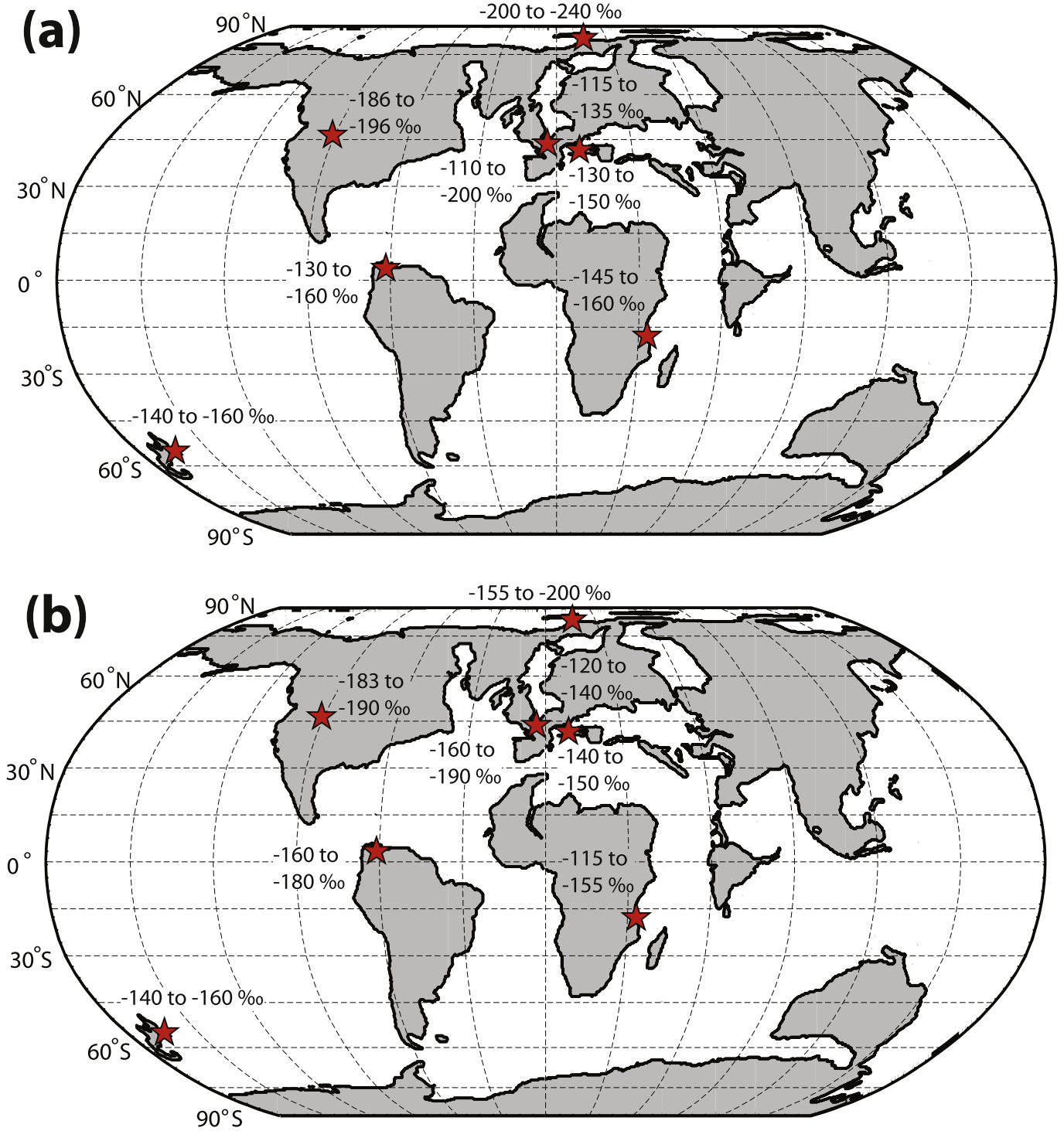

Fig. 3. Paleogeographic reconstruction for 56 Ma showing range of δ^2H values in long-chain *n*-alkanes for pre-PETM (a) and during the CIE at the onset of the PETM (b). Compilation based on records from Lomonosov Ridge, Arctic Ocean (Pagani et al., 2006), Bighorn Basin, USA (Smith et al., 2007), Vasterival, France (Garel et al., 2013), Forada, Italy (Tipple et al., 2011), Cicogna, Italy (Krishnan et al., 2015), Tanzania (Handley et al., 2012), Kumara Section, New Zealand (Handley et al., 2011) and Mar2X, Venezuela (Jaramillo et al., 2010).

distributions. Instead, an increase in soil evaporation or evapotranspiration was invoked to explain most of the deuterium enrichment during the PETM at this location, suggesting that a more arid climate dominated in east Africa. However the δ^2H values are highly variable during the CIE, by up to 18‰ between adjacent sediment horizons, and the secular shift in δ^2H is relatively small. A low-resolution record from the Bighorn Basin also indicates a shift to more enriched deuterium values at the onset of the CIE, but then followed by depleted values during the PETM body (Smith et al., 2007). Although based on a low-resolution record, this δ^2H pattern is compatible with the drying and then wetting scenario as inferred from paleosol and paleobotanic methods, with the shifts caused by changes in evaporative processes as invoked for Tanzania.

Complex variations in δ^2H across the PETM are recorded at Forada and Cicogna, Italy (Tipple et al., 2011; Krishnan et al., 2015) and in the Kumara section, New Zealand (Handley et al., 2011), with multiple possible interpretations. The increase in δ^2H values in the upper-PETM aged sediments at Kumara could be explained by both high-latitude

moisture export or evaporative-enrichment style mechanisms. However, this section is also characterised by a change in organic matter source across the PETM, necessitating caution in any climatic interpretation. In addition, these three records exhibit significant variations before the PETM and do not display a significant shift in δ^2H values across the CIE onset itself (Fig. 2). In Normandy, France, a shift to more δ^2H-depleted values of the order of 60‰ occurs across the onset of the CIE, which was interpreted by the authors to represent a possible increase in precipitation/humidity, followed by a drying event up-section (Garel et al., 2013). However, the magnitude of these variations is smaller than that seen during the Paleocene in the same record and the core is truncated within the CIE, preventing an assessment of the significance of PETM variations.

In contrast to the other low-latitude δ^2H record, the Venezuelan Mar2X section exhibits a deuterium depletion at the onset of the PETM. Whilst sampling within the body of the PETM is limited, and it is possible that changes in δ^2H values close to the CIE are not resolved, a shift by up to 35‰ is observed in the long chain *n*-alkanes (Jaramillo et al., 2010), and there is no return to pre-event values within the section (Fig. 2g). Given the tropical setting, an enhanced amount effect is suggested at the PETM with extensive airmass rainout resulting in a predominance of deuterium-depleted precipitation. However, whilst there is no change in the wet/dry preference of plant families across the PETM (Section 3.1), major changes in the vegetation composition do occur and the effect of a differing plant community on fractionation cannot be ruled out.

Taken together, the available δ^2H records that span the PETM are limited in both spatial coverage, as shown in Fig. 3 and temporal coverage, as shown in Fig. 2, due to a combination of low resolution in some records (e.g. Smith et al., 2007) and truncation in others (e.g. Handley et al., 2008, 2012). Furthermore, these interpretations require a degree of caution, particularly in assuming that the variability in leaf wax hydrogen isotopes reflects changes in isotopic composition of meteoric water. Vegetation, carbon dioxide concentrations and temperature varied markedly across the PETM (see above), all of which can have a large impact on water use efficiency (Farquhar et al., 1989; Wullschleger et al., 2002; Sachse et al., 2012) and, therefore, leaf wax hydrogen isotopes. Global warming will also impact precipitation δ^2H via changes in the temperature of source water and changes in air mass circulation. Some of these additional factors could account for the ~15‰ δ^2H offset between the two proximal Italian records, only ~25 km apart (Krishnan et al., 2015). They could also account for the unusual temporal trends: for example, the Arctic, Bighorn Basin and Kumara records all exhibit a transient positive excursion followed by a return to pre-CIE values, and it is unclear why the proxy response is largely limited to the earliest part of the PETM.

Nonetheless, the existing records do document some apparent temporal and spatial trends. Polar sites and continental interiors record an increase in δ^2H values, whereas marginal mid-latitude sites exhibit less clear trends. The two low-latitude, tropical sites exhibit contrasting trends at the onset of the PETM. Although low to high latitude δ^2H gradients decrease at the PETM, consistent with increased moisture transport to polar regions, this interpretation is dependent on the single, low-resolution Arctic record. We therefore suggest that additional records, including those with higher resolution and complementary proxy data are now required to fully evaluate spatial changes in the isotopic composition of meteoric water at the PETM; also required are longer-term records from prior to and following the PETM to fully contextualise the documented variability.

3.3.2. Oxygen isotopes within mammalian remains

In addition to biomarker based δ^2H values, $\delta^{18}O$ values of fossilised (mammalian) tooth enamel can be used to study variations in meteoric water isotopic composition and, by extension, Eocene hydrology. Biogenic apatite is resistant to isotopic exchange and diagenetic processes (Fricke, 2003; Clementz and Sewall, 2011), and as mammals homoregulate their body temperature, $\delta^{18}O$ variations over time reflect variations in the isotopic composition of the ingested water rather than temperature dependent fractionation. Early work identified a shift to more enriched $\delta^{18}O$ values at the PETM within Bighorn Basin *Coryphodon* teeth, which was suggested to indicate several degrees warming by assuming that the present day relation between oxygen isotope composition of precipitation and temperature existed during the early Eocene (Fricke et al., 1998). However, subsequent work indicated that these shifts likely also record changes in the hydrological cycle (Fricke, 2003).

In a recent study, tooth enamel of the putatively aridity-insensitive *Coryphodon*, a semi-aquatic hippo like mammal, has been compared with that of *Sifrhippus*, an early horse, to estimate regional aridity during the PETM within the US continental interior (Secord et al., 2012). *Coryphodon* likely grazed on submerged plant material, such that its $\delta^{18}O$ composition tracks riverine variations influenced by local temperature; *Sifrhippus* is thought to have grazed on terrestrial plant leaves, subject to additional evaporative enrichment. Whilst the absence of *Sifrhippus* teeth in the lower part of the section do not allow for pre-PETM estimates, the $\delta^{18}O$ anomaly between *Coryphodon* and *Sifrhippus* during the CIE suggests drier conditions at the beginning of the CIE, followed by wetter conditions ~68 kyr into the PETM. Crucially, this is consistent with previous inferences (including those based on leaf wax δ^2H values) from the Bighorn Basin.

3.4. Humidity change inferred from terrestrial CIEs

The magnitude of the PETM CIE is typically greater in terrestrial substrates compared to marine settings (e.g. see reviews in Schouten et al., 2007 and McInerney and Wing, 2011). For example, paleosol carbonates spanning the PETM from Wyoming, Spain and China are characterised by a CIE that is ~3‰ greater than that seen in planktonic foraminifera from the marine realm (Bowen et al., 2004). Leaf wax *n*-alkanes and pedogenic carbonates exhibit particularly large CIEs, with bulk terrestrial organic matter tending to yield smaller CIEs, albeit still larger than those observed in marine settings (McInerney and Wing, 2011). This offset can be partially attributed to the observation that terrestrial records are governed by plant biomass $\delta^{13}C$ values and therefore include a photosynthetic fractionation effect. Using an integrated model for soil organic carbon and CO_2, Bowen et al. (2004) proposed that a > 20% increase in soil moisture and relative humidity could explain the offset via larger carbon isotope fractionation by plants. However, this interpretation was not supported by subsequent proxy-based studies that indicated drier rather than wetter conditions within the Bighorn Basin (Wing et al., 2005; Smith et al., 2008; Kraus and Riggins, 2007; Section 3.2). An amplified CIE in the Cambay Shale formation, western India has also been suggested to reflect elevated precipitation at the PETM (Samanta et al., 2013). Increased rainfall is also supported by elevated lignin phenol concentrations at that location, which may serve as a marker for increased soil erosion under elevated tropical precipitation. Such an explanation was also explored by Handley et al. (2012) to explain the very large CIE in Tanzanian sediments, which are also characterised by an increased abundance of higher plant biomarkers, but it was ultimately dismissed due to contradictory evidence for increased aridity from leaf wax δ^2H values (similar to interpretations from the Bighorn Basin).

It now seems likely that alternative mechanisms account for the differences between marine and terrestrial CIEs at the PETM. Smith et al. (2007) argued for a floral change (gymnosperm to angiosperm) across the PETM that could have amplified the CIE in terrestrial records; however, it is hard to envision that this would have affected all records, especially those from tropical sites, and in fact there is no evidence for major floral change at either Tanzania or in the Cambay Shale. More recently, Schubert and Jahren (2013) proposed an alternative and more global explanation - that all or a large part of the difference between terrestrial and marine CIEs is due to greater discrimination against ^{13}C

during C_3 plant photosynthesis under elevated atmospheric CO_2. This interpretation remains the subject of much debate (i.e. Kohn, 2016), but it could be tested by investigating marine organic $\delta^{13}C$ records which would be affected by higher CO_2 (i.e. Bidigare et al., 1997) but not humidity (c.f. terrestrial settings). Regardless of the explanation, we suggest that the offset in CIE magnitude between terrestrial and marine substrates is uncertain evidence for increased humidity during the PETM.

4. Inferred consequences of hydrological changes at the PETM

As alluded to in Section 1, substantial changes in the hydrological cycle have a variety of impacts on sediments and both terrestrial and marine biogeochemistry. We explore these both as additional, albeit indirect, evidence for hydrological changes at the PETM, but also to better understand the consequences of a perturbed hydrological cycle on Earth system processes.

4.1. Sedimentological and geomorphological consequences

Some of the most compelling evidence for dramatic hydrological change at the PETM are geomorphological and sedimentological changes, documented in both terrestrial and marine archives. Many studies show direct evidence for greater export of terrigenous sediment to the marine realm coincident with the PETM CIE, as well as changes in the nature of the sediment. As discussed above (Section 3.2.1) some change could be due to greater chemical weathering, but it is increasingly accepted that much of the sedimentological signature reflects a change in erosion and, by extension, an increase in hydrological intensity (John et al., 2012), although quantitative interpretation remains challenging. Whilst terrestrial geomorphology and sediment transport to the marine realm reflect climatic controls, they are also strongly controlled by tectonics and filtered through interacting feedbacks such as vegetation, weathering, and transport (e.g. Romans et al., 2016; Macklin et al., 2012; Armitage et al., 2011). Furthermore, because fluvial systems are capable of responding to climatic and tectonic perturbations on short timescales (e.g. 1–10 ka, Goodbred et al., 2003; Simpson and Castelltort, 2012) but continue to re-equilibrate over a longer duration (e.g. 1–10 Ma, Allen, 2008; Armitage et al., 2011), the terrestrial erosion response to hydrological changes at the PETM is likely to be complex and prolonged (Foreman et al., 2012; Romans et al., 2016). Despite this, global trends are emerging, with sedimentological and geomorphological changes evidently indicating that precipitation became more episodic ("peaked" or "flashy") or occurred with greater seasonality, regardless of changes in total precipitation amount (Section 3.1).

4.1.1. Increased terrigenous sediment flux to marginal marine settings

Global changes in sediment export are caused by variations in climate and/or eustatic sea level. Sea level low-stands provide increased land area for erosion and bring river mouths closer to the shelf edge, thereby reducing continental shelf area (Egger et al., 2005; Sluijs et al., 2008a). Under this model, eustatic sea level rise during the PETM interval (Sluijs et al., 2008a) would be expected to result in reduced export of terrestrial sediments to marginal marine environments. However, many marginal marine sections document increased sedimentation rates at the onset of the PETM (John et al., 2008; Fig. 4), attributed to greater continental runoff and erosion (John et al., 2008; Giusberti et al., 2007)

Inferring the climatic signal underlying higher sedimentation rates is not straightforward (Romans et al., 2016; Armitage et al., 2011; Schumer and Jerolmack, 2009). In addition to the caveats mentioned above, determination of robust sedimentation rates across the PETM remains a particular challenge. Sedimentation rates decrease as the duration of temporal averaging increases (Sadler, 1981; Schumer and Jerolmack, 2009), such that comparing short (10 to 100 kyr CIEs) and long (e.g. hundreds to thousands of kyr magnetochrons or biozones) timescales will tend to result in higher sedimentation rates for the former. Incompleteness of the CIE due to erosional truncation (Khozyem et al., 2015; Stassen et al., 2012a) can also add substantial error. For example, at Tawanui, New Zealand, Kaiho et al. (1996) inferred a decrease in sedimentation rate, but Crouch et al. (2003) argued that this was due to poor age constraints and used an expanded section to infer elevated PETM rates. In other locations it is necessary to take into account potential variations in lysocline depth and associated changes in carbonate deposition (Egger et al., 2005). Such difficulties make direct comparisons of sedimentation rates between sites difficult (Sluijs et al., 2011; Stassen et al., 2012a; Kaiho et al., 1996; Crouch et al., 2003).

These caveats aside, the majority of records, for which both pre- and *syn*-PETM sedimentation rate estimates exist, document an increase coincident with the CIE (Fig. 4), as well as a change in mineralogy, suggesting enhanced delivery of terrigenous materials (Section 3.2). These data are largely based on the compilation of rates provided by John et al. (2008) who estimated background sedimentation rate using site-specific biostratigraphy and the estimated event duration of 220 kyr (Röhl et al., 2007). Only a few sites show a decrease in sedimentation rate. These include Tawanui, New Zealand - although see comment above; Abu Zenmia, Egypt (John et al., 2008) and Spitzbergen (Cui et al., 2011), where a reduction in sedimentation rate is possible, although climatic-induced changes could have been overprinted by local orographic change (Charles et al., 2012). Changes in either total annual precipitation or in the intra-annual distribution of precipitation could explain the increased terrigenous sediment flux (e.g., John et al., 2008). Whilst the former cannot be excluded, the timing of precipitation could be an even greater influence (Tucker and Slingerland, 1997). Runoff and erosion are maximised in strongly seasonal climates where vegetation cover is reduced and brief periods of intense rainfall result in higher energy discharge regimes (Bull, 1979; Plink-Björklund, 2015).

4.1.2. Terrestrial geomorphology and evidence for more episodic precipitation

As with sedimentation rates in marine sediments, interpretation of fluvial geomorphological changes is complex. Nonetheless, two of the most detailed studies, in the Spanish Pyrenees and Western United States, are both consistent with a shift to more episodic precipitation patterns. In northern Spain, semi-arid to arid conditions are indicated during the late Paleocene by red mudstones, carbonate- and gypsum-bearing paleosols, and discontinuous 10–200 m-scale fluvial channels (Schmitz and Pujalte, 2003, 2007). These paleosols are unconformably overlain by the PETM-aged Claret Conglomerate (CC). The CC comprises 1 to 4 m thick, clast-supported, imbricated conglomerates interbedded with paleosols (Schmitz and Pujalte, 2007). Rounded clasts as large as 65 cm require substantial current strength to originate from the putative source located ca. 10 km away. Although it is difficult to rule out a tectonically driven decrease in accommodation space, numerical modelling suggests that a precipitation increase can result in sheet conglomerate formation on a greater areal scale than a decrease in accommodation space (Armitage et al., 2011). The CC is also correlated with the deposition of a siliciclastic unit in offshore sections at Zumaia and Ermua (Schmitz et al., 2001; Manners et al., 2013), whilst coarse-grained siliciclastics have recently been identified within incised valleys in terrestrial sections (Pujalte et al., 2015). Despite the large spatial extent of the CC (500 to 2000 km^2), the carbonate-bearing red paleosols interbedded with it are consistent with semi-arid conditions both before and during the PETM. Schmitz and Pujalte (2007) reconcile these apparent contrasts through analogy with present-day megafan deposits, which form in subtropical regions where episodic precipitation drives large changes in discharge and channel migration (Leier et al., 2005). Thus, the CC appears not to reflect greater overall annual precipitation, but instead episodic high discharge events.

Further evidence for hydrological change has been documented in

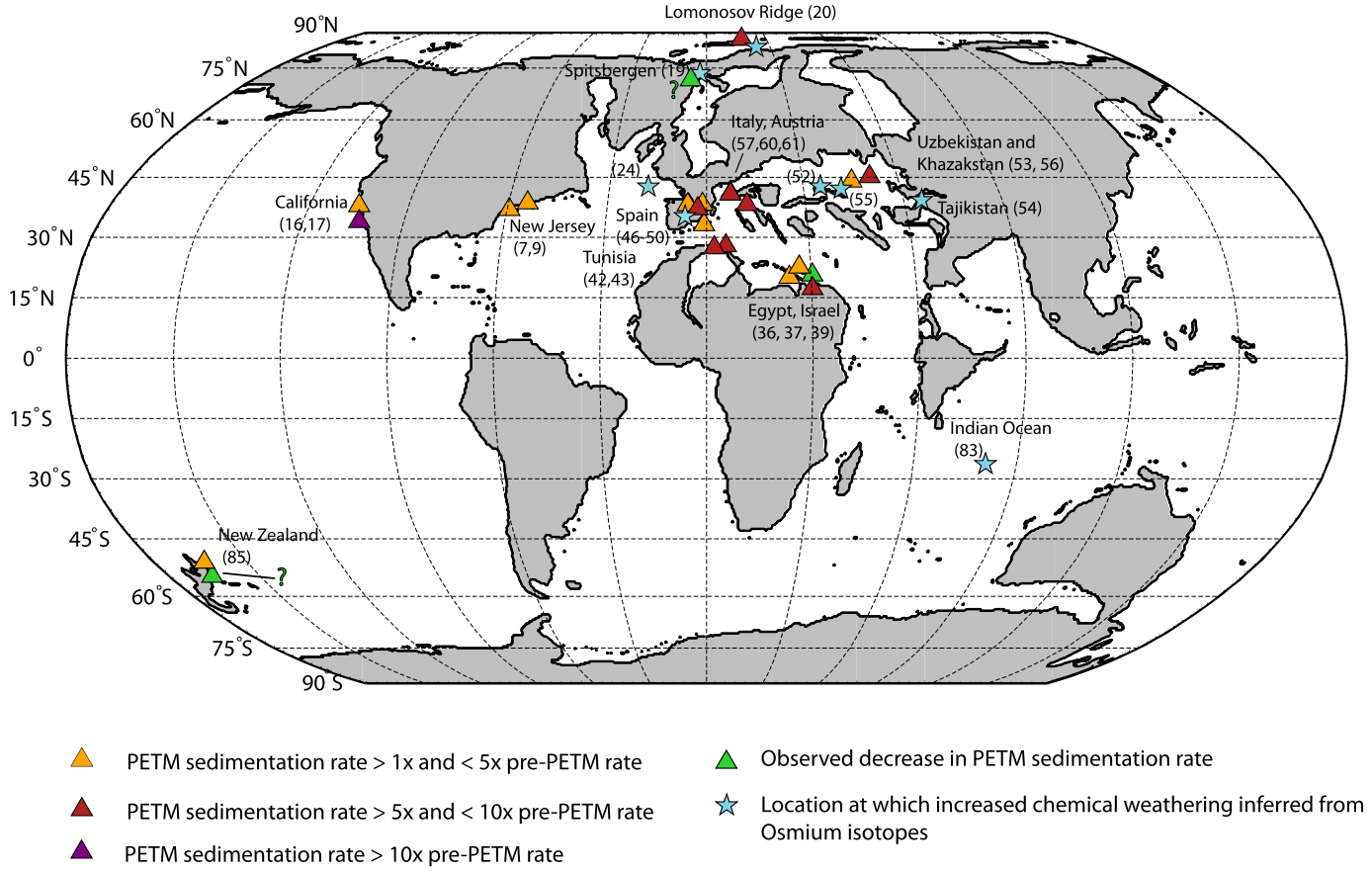

Fig. 4. Paleogeographic reconstruction for 56 Ma showing estimates of changes in sedimentation rate in marine-marginal sections at the PETM. Coloured triangles correspond to differences in ratio of CIE:pre-CIE sedimentation rate with values > 1 indicating sedimentation rate increases. Data are from John et al. (2008) and supplemented with estimates from Sluijs et al. (2008b; Lomonosov Ridge, Arctic), Giusberti et al. (2007; Forada, Italy), Stassen et al. (2012a; Tunisia) and Egger (2003, 2005, Paleotethys). Also shown are locations at which an increase in weathering has been inferred from Osmium isotopes (stars). Numbers provided after each location correspond to PETM sites and references provided in Supplementary Table 1.

the Piceance Creek Basin of Colorado, in the western US (Foreman et al., 2012). Paleocene-aged paleosols with restricted channels of dominantly cross-bedded sand (< 10 m thick, 200 m wide) indicate shallow, narrow rivers. The PETM CIE occurs roughly concurrently with the onset of crevasse-splay deposition characterised by much larger (up to 20 m thick, 500 m wide), dominantly planar laminated, upper flow regime sand bodies (Foreman et al., 2012). Although available age constraints are insufficient to fully exclude a tectonic driver for the change to crevasse-splay deposition, Foreman et al. (2012) note that the geographic context of the Piceance Creek Basin makes it unlikely that this change was driven by eustatic sea level. As in the CC, crevasse splay deposits could indicate more episodic intense precipitation, related to a monsoonal regime (Winguth et al., 2010). Unlike the CC, however, deposition of high flow regime alluvial sediments persists after the CIE, and Foreman et al. (2012) suggest that the delayed return to pre-PETM depositional conditions reflects protracted re-equilibration of erosional and depositional processes following the perturbation.

In the nearby Bighorn Basin an increase in the amalgamation of alluvial sandstones (the Boundary Sandstone of the Willwood Formation at Sand Coulee) occurs within the PETM CIE and has been recently reinterpreted by Foreman (2014) as climatically controlled. Detailed lithofacies examination of pre-, *syn*- and post-PETM sediments indicates individual sand bodies of the Boundary Sandstone are minimally different from non-PETM sand bodies indicating there was little net difference in fluvial discharge; thus, Foreman (2014) proposed two complementary potential explanations for deposition of the Boundary Sandstone. First, basin-wide aridification punctuated by periods of precipitation similar to pre- and post-PETM conditions could have resulted in sediment 'flushing' (Simpson and Castelltort, 2012) through the basin. Second, a decrease in dense forests and extensive root networks, coupled with seasonally variable soil moisture content, could have promoted landscape destabilization, river avulsion, and winnowing and export of finer-grained sediments (e.g. Gran and Paola, 2001). Kraus et al. (2015) examined these hypotheses at Polecat Bench, approximately 10 km to the southeast of Sand Coulee, and argued that drier conditions in the Bighorn Basin reduced vegetation density and increased sediment storage in the hinterland.

There is some evidence for a temporal lag between climate forcing and these responses. Deposition of the Claret Conglomerate is estimated to have taken place very close to the onset of the PETM carbon isotope excursion, with a lag of < 15 kyr (Domingo et al., 2009; Manners et al., 2013), and a total duration on the order of 10 kyr or less (Schmitz and Pujalte, 2007). Similarly, increased episodicity in the Bighorn (Foreman, 2014; Kraus et al., 2015) and Piceance Creek (Foreman et al., 2012) basins appears to come into effect around the onset of the PETM, although depositional hiatuses in these sections are difficult to constrain. A limited lag time between atmospheric forcing (CIE) and the terrestrial sedimentological response at the PETM is also supported by comparison of carbon isotope profiles from terrigenous *n*-alkanes and marine carbonates at the Forada section in Northern Italy and the nearby Cicogna Section, which suggest terrestrial residence times on the order of 5 kyr (Tipple et al., 2011) or effectively none (Krishnan et al., 2015), respectively. In combination, these studies clearly indicate that the PETM rapidly impacted terrestrial sedimentary systems, likely through shifting the timing and intensity of precipitation. As such there is a pressing need to further study episodicity and the occurrence of

extreme precipitation events.

4.2. Increased chemical weathering

As discussed above, paleosol geochemistry indicates changes in chemical weathering rates during the PETM, inferred to be evidence for local changes in precipitation (Section 3.2). Other records also document a link between local precipitation and weathering; for example, in central China, lacustrine deposits indicate elevated silica weathering coeval with lake freshening (Chen et al., 2016). Despite the complex regional patterns for chemical weathering change, osmium isotope records from multiple ocean basins suggest that global chemical weathering rates increased at the PETM (Fig. 4). $^{187}Os/^{188}Os$ ratios across the PETM have been generated for DSDP Site 213 (Indian Ocean), DSDP Site 549 (Atlantic Ocean), IODP Site M0004a (Arctic Ocean), Spitsbergen, the Zumaia land section (Spain), the Kheu River land section (Karbardino-Balkaria), the Dzhengutay land section (Dagestan), and the Guru-Fatima land section (Tajikistan). Most records show an antithetical relationship between $^{187}Os/^{188}Os$ and $\delta^{13}C$, with a shift towards more radiogenic $^{187}Os/^{188}Os$ during the PETM suggesting a pulse of increased continental weathering (Ravizza et al., 2001; Wieczorek et al., 2013; Dickson et al., 2015).

Therefore, we suggest that the range of responses recorded by paleosols (Section 3.2) reflects the profound geographical variability in precipitation change at the PETM, whereas signals integrated in marine sediments (including clay mineralogy, Section 3.2.1, and osmium isotopic signatures) provide collective evidence for a global increase in chemical weathering (Ravizza et al., 2001; Bowen and Zachos, 2010; Dickson et al., 2015). In this sense, the PETM appears to be similar to some of the Mesozoic OAEs that are also associated with an increase in atmospheric CO_2 and are characterised by a 2- to 3-fold increase in weathering rates as suggested by osmium, lithium, and calcium isotope records (Blättler et al., 2011; Pogge von Strandmann et al., 2013; Percival et al., 2016).

However, the magnitude of the increase in chemical weathering rates at the PETM, especially given the relatively poorly constrained hydrological changes, remains unclear; consequently, so does chemical weathering's potential role as a biogeochemical feedback on PETM warming. On geological time scales, weathering provides the ultimate negative feedback on CO_2-induced global warming (Berner and Berner, 2012) and enhanced silicate weathering has been both invoked and dismissed as a cause of CO_2 drawdown at the end of the PETM (Bowen and Zachos, 2010; Clechenko et al., 2007). Although the response of weathering rates is generally considered to be slow and operating on time-scales of millions of years, more rapid responses have been invoked for events lasting 10^3–10^4 years (Cohen et al., 2004). In fact, field studies on Iceland show a response of weathering rates to global warming over the last four decades (Gislason et al., 2009). However, modern observations clearly indicate that chemical weathering fluxes also largely depend on precipitation and the erosional regime as well as temperature (Lebedeva et al., 2010; Viers et al., 2014)

Within a given erosional regime, increased precipitation can promote rapid chemical weathering by flushing out dissolved weathering products to maintain thermodynamic undersaturation (White and Buss, 2014 and references therein). At present, warm and wet tropical regions with high relief are characterised by especially high weathering rates and constitute a large portion of global weathering (Rad et al., 2007; White and Blum, 1995). Even when mantled by thick, highly leached soils, very high precipitation rates are associated with rapid chemical weathering in the deep subsurface (Rad et al., 2007; West, 2012; Buss et al., 2013; Buss et al., 2017). As such, weathering rates during the PETM are expected to have increased not just due to temperature but due to an enhanced hydrological cycle; if that rainfall occurred as episodic events with associated increases in erosion (as inferred from sedimentological and geomorphological changes described in Sections 4.1) that could have further enhanced chemical weathering rates under some conditions. As such, it is critical that future work explores the chemical weathering response to the PETM with approaches that account for these factors.

4.3. Fate of terrestrial organic matter

It is likely that elevated temperatures during the PETM contributed to enhanced oxidation of organic matter. Bowen (2013) invoked this to explain the widely observed decreases in paleosol organic matter contents at the onset of the PETM (e.g. Wing et al., 2003). Subsequently, Cotton et al. (2015) used the offset in carbon isotopes between soil organic matter and pedogenic carbonates to also infer increased soil organic matter turnover rates during the PETM. Bowen (2013) also argued that organic matter oxidation could have contributed an additional source of ^{13}C-depleted carbon, a proposal that is similar or perhaps complementary to that of DeConto et al. (2012) who argued that the PETM CIE reflected oxidation of Antarctic permafrost. Observations from present-day systems, however, indicate that soil organic matter turnover times increase at both higher temperatures and higher precipitation (Raich and Schlesinger, 1992; Trumbore et al., 1996), the latter facilitating both leaching and direct oxidation of organic matter. Increased erosion and reworking of soils, as well as the deposition of coarser sediments in alluvial settings, will have also fostered organic matter degradation via greater oxygen exposure time. Consequently, inferred hydrological (and sedimentological) changes at the PETM likely also contributed to terrestrial organic matter oxidation as invoked by Bowen (2013).

Marginal marine sediments provide additional evidence for changes in the terrestrial carbon cycle. Organic carbon contents at the margin of the eastern Tethys Ocean increase up to 50-fold during the PETM (Dickson et al., 2014a) and similar changes are recorded in other ocean basins (Sluijs et al., 2008b). These changes are partly due to increased algal productivity and enhanced preservation due to marine anoxia (Section 4.6) and increased sediment accumulation rates (Section 4.1). However, the Tethyan section clearly records an increase in the abundance of terrestrial plant leaf waxes, such that the high organic carbon content could partially reflect a pulse of recalcitrant terrestrial organic matter and nutrients (Dickson et al., 2014a). A transfer of plant and soil matter as well as ancient reworked organic matter (thermally mature hopanes) to the ocean during the PETM has also been recorded in Tanzanian sediments (Handley et al., 2008; Section 5.1) and a transfer of plant matter recorded in India (Samanta et al., 2013). It seems likely, therefore, that the PETM was associated with the increased mobilisation and oxidation of terrestrial organic matter, and by extension, that multiple pools of terrestrial organic matter, including plants, soil and kerogen, could have contributed to the release of ^{13}C-depleted carbon. However, as with silicate weathering, the timing and magnitude of the carbon released remains contentious and is critical for understanding biogeochemical feedbacks; we suggest that future work that incorporates both temperature and hydrological controls will be critical to assessing the importance of these processes.

4.4. Methane cycling

Methane, an important trace greenhouse gas, is released to the atmosphere primarily from terrestrial wetlands (~60–90%; Denman et al., 2007; Kirschke et al., 2013). As such, changes in global hydrology have the potential to greatly influence wetland methane emissions, acting as a rapid and powerful positive feedback to warming. Ancient atmospheric methane concentrations are difficult to constrain and there are no direct proxies. However, model simulations suggest methane emissions are greater in greenhouse climates due to the expansion of wetlands and the impact of higher CO_2 and temperatures upon wetland methane production (Beerling et al., 2011). Although these inferences were made for the early Eocene, they would also be applicable to an increase in CO_2 at the PETM. Direct evidence of increased atmospheric

methane concentrations are not available for the PETM, however there is evidence of increased methane production in wetlands from the Cobham lignite (UK). Specifically, a dramatic decrease in the $\delta^{13}C$ values of hopanoids (biomarkers derived from bacteria; Pancost et al., 2007) and the unprecedented occurrence of bacteriohopanepolyols likely derived from methanotrophs (Talbot et al., 2015) suggests increased methane flux during the onset of the PETM (Pancost et al., 2007). This has been attributed to a change in the hydrological regime and increased waterlogging of the peatland. Inglis et al. (2015b) also investigated methane cycling in an early Eocene German lignite deposit at Schöningen. Although this did not span the PETM, carbon isotopic evidence for enhanced methane cycling was expected for this relatively warm wetland setting. Although increased methane processing was observed, it was not as dramatic as that observed in the Cobham Lignite. With the exception of these studies, there have been few subsequent investigations, and direct evidence for enhanced terrestrial methane cycling is not yet globally widespread. Given its potential importance as a positive feedback this is a vital topic for further investigation. Indeed, within the Eocene simulations of Beerling et al. (2011), methane feedbacks contributed an additional 2.7 °C of early Eocene warming.

4.5. Impacts on the marine realm – increased nutrients, algal productivity and anoxia

An increased hydrological cycle (alongside elevated temperatures and CO_2) would be expected to affect the marine realm, via increased marine primary productivity due to continental chemical weathering rates and nutrient runoff (Bralower, 2002). Annual or seasonal intensification of river runoff will also increase marginal marine nutrient inputs (Kopp et al., 2009), although this could have been partially countered by the global transgressive event at the start of the PETM (Speijer and Morsi, 2002; Sluijs et al., 2008a) and associated trapping of nutrients and sediments on continental margins. Therefore, it has been suggested that increased nutrient availability played an important role in increasing marginal marine productivity and carbon burial (Sluijs et al., 2014), manifested in changes in the assemblages of benthic foraminifers, calcareous nannofossils and dinoflagellate cysts (Sluijs et al., 2007; Sluijs and Brinkhuis, 2009; Gibbs et al., 2006).

This evidence is briefly summarised below, but it should be noted that the interpretation of environmental changes from the microfossil record is challenging and associated with significant uncertainties. For example, the majority of Paleogene calcareous nannoplankton taxa are extinct and the ecological preferences of their relatives may have changed over time. *Coccolithus* - common in Paleogene sequences - has been considered as both an oligotroph and mesotroph (Bown and Pearson, 2009). Moreover, trends in *Discoaster*, *Fasciculthus* and *Shpeholithus* abundances are uncorrelated at Walvis Ridge (ODP 1262/1263; Raffi et al., 2009), whereas previously all have been considered to be indicators of warm and oligotrophic environments. Perhaps most critically, fertility (nutrient) signals are difficult to separate from those of temperature (e.g. Bralower, 2002), and Bown and Pearson (2009) have questioned whether standard paleoecological affinities might have broken down with the rapid environmental perturbations of the PETM.

Calcareous nannoplankton exhibit significant changes at the PETM, including poleward migration, the emergence of excursion taxa and changes in productivity (Bown and Pearson, 2009; Raffi et al., 2009). Initial interpretations of nannoplankton assemblages disagreed on whether the PETM was marked by increased or decreased surface water productivity (Bralower, 2002; Self-Trail et al., 2012), hence the range of responses shown in Fig. 5. This discrepancy has more recently been rationalised by a productivity gradient model (Gibbs et al., 2006) that invokes a steepening of the shelf-offshelf concentration of nutrients, with increases in eutrophic species at the New Jersey shelf, whilst the open ocean (ODP 1209, equatorial Pacific) appears to become more oligotrophic. Nonetheless, other apparent inconsistencies persist. Bown and Pearson (2009) note that the Tanzanian coast is oligotrophic at the onset of the PETM and records a decline in the presumed mesotroph *Toweius*; this is difficult to rationalise with the likely increase in the delivery of nutrients associated with the changes in Tanzanian hydrology - although it is consistent with the dearth of algal biomarkers in the Tanzanian PETM sediments (Handley et al., 2012). Changes in calcareous nannoplankton across Egyptian outcrops indicate a decline in *Towieus* and increase in *Coccolithus* (Youssef, 2016), indicating warm yet oligotrophic conditions persisted across the PETM, with a later return to more nutrient-enriched conditions.

Dinoflagellate cysts have increasingly been used as an environmental proxy, especially in near shore settings. As with calcareous nannoplankton, their distributions are sensitive to small changes in nutrient state (Sluijs et al., 2005; Crouch et al., 2003). Sluijs et al. (2007) provide evidence for a bloom of eutrophic dinoflagellates in all known PETM sections. This is based on the occurrence of *Apectodinium*, a dinoflagellate that is generally regarded as both heterotrophic and thermophilic, such that its expansion at the PETM has been attributed to a combination of intense warmth and/or enhanced nutrient delivery to shallow marine settings (Crouch et al., 2001). Although further work is required to identify the key driving mechanism, the presence of *Apectodinium* in shallow marine settings often coincides with an increase in terrestrial palynomorphs (Crouch et al., 2003; Kender et al., 2012), providing further evidence for a causal link between runoff, nutrients and algal community structure. Beyond global insights, specific dinocyst records offer more nuanced interpretations of these relationships. For example, PETM variations in total dinocyst abundance and the number of *Apectodinium* cysts in New Jersey sediments have been invoked as evidence for fluctuations in precipitation and runoff on Milankovitch timescales (Sluijs and Brinkhuis, 2009).

The apparent increase in marine algal productivity, alongside evidence for warming and increased chemical weathering, has been used to invoke comparisons to Mesozoic OAEs. Crucially, the expansion of anoxia during OAEs is now linked to hydrological changes that impacted the marine realm via weathering-nutrient-productivity feedbacks (Jenkyns, 2010). However, the overall response of marine oxygen concentrations to collective PETM biogeochemical changes remains unclear (Speijer and Wagner, 2002; Sluijs et al., 2006; Sluijs et al., 2014; Chun et al., 2010; Dickson et al., 2012), although it was almost certainly less geographically widespread than the Mesozoic OAEs.

Several proxies indicate de-oxygenation in the deep Atlantic. At three Walvis Ridge Sites, representing different paleo-depths (ODP sites 1262, 1266, and 1263; South Atlantic), both manganese (Mn) and uranium (U) enrichment factors suggest that all sites experienced suboxic conditions during the PETM, with a possible vertical expansion of the oxygen minimum zone (OMZ) from shallow towards the deeper sites (Chun et al., 2010). Pälike et al. (2014) found similar results for Demerara Rise (ODP site 1258). The iodine calcium (I/Ca) ratios of the bulk coarse carbonate fraction at ODP Sites 1262 and 1266 (Zhou et al., 2014) support the previous findings of OMZ expansion, suggesting sea surface deoxygenation. Bralower et al. (1997) also observe lamination and absence of bioturbation in the Palaeocene-Eocene sediments of the West Atlantic (ODP sites 999 and 1001). None of these sites, however, are associated with the dramatic increase in organic matter accumulation rates observed during Mesozoic OAEs, and in fact, many remain organic-lean despite inferred increases in productivity.

The deep Pacific shows even more ambiguous evidence for a decrease in oxygenation. Pälike et al. (2014) and Zhou et al. (2014) find no evidence for deoxygenation in the Pacific at ODP sites 1209 and 1221 (Equatorial Pacific) from Mn and U enrichment factors and I/Ca ratios, respectively. However, other proxies point to at least some degree of deoxygenation in the Pacific. For example, a peak in pyrite abundance occurs just prior to the onset of the CIE at ODP sites 1209-1212 (West Pacific; Colosimo et al., 2005), whilst a significant reduction in the maximum diameter of benthic foraminifera test sizes at the peak of the PETM occurs at ODP site 1209 and 1210 (Kaiho et al.,

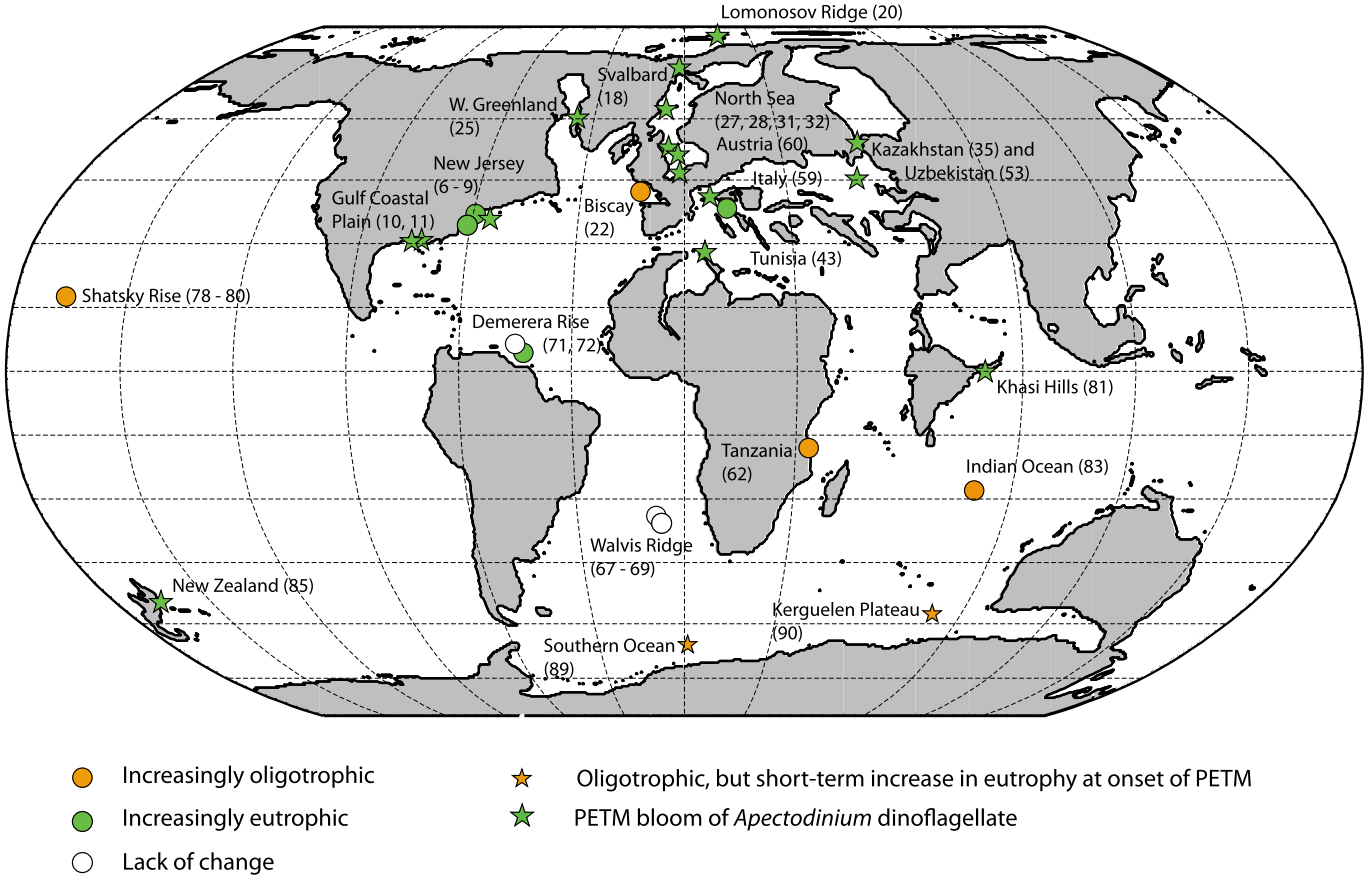

Fig. 5. Paleogeographic reconstruction for 56 Ma showing changes in nutrient distribution at the PETM (circles). Red star symbols indicate oligotrophic conditions at the PETM, but with a possible short-term increase in nutrients shortly before, or at the onset of the PETM, attributed to a change in ocean circulation by Jiang and Wise (2006). Also shown are locations where a bloom of Apectodinium has been documented (green stars). Numbers provided after each location correspond to PETM sites and references provided in Supplementary Table 1. (For interpretation of the references to colour in this figure legend, the reader is referred to the web version of this article.)

2006). Late Paleocene benthic foraminiferal extinctions have been reported in the Central Pacific (ODP site 865; Thomas and Shackleton, 1996) and West Pacific (ODP site 1209-1212 and 1220; Takeda and Kaiho, 2007), although these could have been due to a range of factors. ODP site 1220 also has weak laminations, which is paradoxical considering its sister site (1221) was shown to have experienced oxic conditions across the PETM (Pälike et al., 2014). I/Ca ratios in ODP site 865 indicate relative oxygen depletion (Zhou et al., 2014), which is in agreement with micropalaeontological evidence. As with the Atlantic sites, there is not strong evidence for an increase in organic matter contents.

Whilst deep-sea environments experienced only minimal deoxygenation during the PETM, there is growing evidence for deoxygenation in shelf and marginal marine settings (Sluijs et al., 2014). For example, in the eastern Gulf of Mexico, the presence of sulfur-bound isorenieratane in the PETM interval (Harrell Core) indicates development of intermittent photic zone euxinia during the PETM. Benthic foraminiferal turnover occurs across the New Jersey coastal plain (i.e. Wilson Lake, Ancora and Bass River; Stassen et al., 2012b) and there is an increase of magnetofossils within the same region (Kopp et al., 2009; Lippert and Zachos, 2007). Combined, these observations indicate suboxic conditions were present both within the sediment and in the bottom water in the eastern Gulf of Mexico. Similarly, the Eurasian shelves apparently experienced significant expansions of oxygen minimum zones, as suggested by a decrease in benthic foraminiferal diversity (Boltovskoy et al., 1992; Pak and Miller, 1992; Pardo et al., 1997; Gradstein et al., 1994); similarly, in the Bay of Biscay (DSDP Site 401) a short-term increase in the abundance of low-oxygen tolerant chiloguembelinids and low Mn and U enrichment ratios indicate expansion of the oxygen minimum zone (Pardo et al., 1997; Pälike et al., 2014). The Western Tethyan margins also experienced benthic turnover, notably in the Spanish sections of Zumaia and Caravaca, and in Possagno, Italy (Canudo et al., 1995; Braga et al., 1975). The presence of laminated sediments in Caravaca (Canudo et al., 1995) and the absence of bioturbation in Zumaia (Rodriguez-Tovar et al., 2011) coeval to the faunal turnover implicate deoxygenation as part of the cause of the benthic crisis. A benthic foraminiferal extinction has also been reported for Poland (Bak, 2005). TOC enrichments in Austria (Egger et al., 2003, 2005) suggest increased sea-surface productivity facilitating oxygen depletion in the bottom waters. The presence of isorenieratane in PETM sections from Denmark also indicate the development of photic zone euxinia on the epicontinental North Sea Basin (Schoon et al., 2013; Schoon et al., 2015). As with deep waters, evidence for deoxygenation in Pacific Ocean marginal settings is weaker than for the Atlantic Ocean. Nonetheless, the development of oxygen depletion in intermediate waters of the Southwest Pacific has been inferred from laminations and a decrease in ichnofossil abundance across the CIE in New Zealand (Nicolo et al., 2010), as well as a benthic foraminiferal turnover (Kaiho et al., 1996).

Evidence for extensive marine anoxia is most pronounced in the epicontinenal shelves of the Eastern Tethys and the Arctic Ocean. The former experienced anoxic bottom water conditions as evidenced by trace metal enrichments (Gavrilov et al., 1997; Gavrilov et al., 2003), the presence of pyrite (Gavrilov et al., 1997, 2003; Bolle et al., 2000), laminations (Gavrilov et al., 2003), and pronounced TOC enrichments (Frieling et al., 2014), documented from sites in the Caucasus and Central Asia. Isorenieratane is present in the West Siberian Sea indicating at least intermittent photic zone euxinia (Frieling et al., 2014),

and diaryl isoprenoids (potentially derived from isorenieratane) were found in Kurpai, Tadjikistan (Kodina et al., 1995). Lycopane, a C_{40} isoprenoid of unclear origin but associated with water column anoxia (Sinninghe Damsté et al., 2003) occurs in rocks from Aktumsuk, Uzbekistan (Bolle et al., 2000). Dickson et al. (2014a, 2014b) provided perhaps the most comprehensive evidence for strong and persistent anoxia along the northern margin of the Tethys during the PETM, based on a combination of TOC contents, trace metal enrichments, metal isotopes, characterisation of reactive iron species and biomarkers (lycopane) to show that anoxia occurred in both bottom waters and the water column during the PETM (CIE) but that the entire water column was well-oxygenated in pre and post-PETM intervals. The evidence for anoxia is also compelling for the southern Tethys, albeit less strong than for the northern margin sites. Benthic foraminiferal and nannofossil turnover occurred in sections in Egypt, Tunisia and Israel (Stassen et al., 2012a; Speijer and Wagner, 2002; Ernst et al., 2006; Khozyem et al., 2013). Supporting evidence for suboxic to euxinic environments coeval to the CIE comes from trace metal enrichments, laminated sediments and the presence of pyrite (Dupuis et al., 2003; Khozyem et al., 2013, 2015; Knox et al., 2003; Schulte et al., 2011; Soliman et al., 2011; Speijer and Schmitz, 1998).

The PETM section at Lomonosov Ridge (IODP Leg 302 Site 4) in the Central Arctic Ocean is characterised by a significant increase in the relative abundance of pyrite (Stein et al., 2006), a drastic decrease in C/S values and an increase in sulfur abundance (Sluijs et al., 2008b; Stein et al., 2006), elevated redox-sensitive trace metal concentrations (März et al., 2010; Sluijs et al., 2008a, 2008b; Dickson et al., 2012) and Mo-isotope compositions (Dickson et al., 2012), fine laminations and the occurrence of isorenieratane (Stein et al., 2006; Sluijs et al., 2006). In addition, the enrichment of Mn points to recycling of Mn(II) under restricted conditions in the Lomonosov Ridge PETM section (Sluijs et al., 2008b). Sediment lamination and pyrite abundances in the PETM interval in the Spitsbergen Central Basin, Longyearbyen section, represents a stratified water column during the PETM CIE (Harding et al., 2011). Cui et al. (2011) also infer reducing bottom water conditions at the margins of the Arctic Ocean indicated by well-developed parallel lamination in pyrite-rich shales (the Svalbard archipelago, BH9-05); this interpretation is reinforced by evidence of U and Re enrichment (Dypvik et al., 2011; Wieczorek et al., 2013), a benthic turnover, changes in benthic (agglutinated) foraminiferal relative morphogroup dominance and test size reduction (Nagy et al., 2013).

Collectively, these data suggest that during the PETM, deep-sea settings experienced a minor reduction in seafloor oxygen (Chun et al., 2010; Pälike et al., 2014) with a greater level of oxygen depletion occurring on some continental slopes (Nicolo et al., 2010) and shelves (Speijer and Wagner, 2002; Sluijs et al., 2008b; Sluijs et al., 2014). Water column anoxia and euxinia was restricted only to some marginal settings or partially restricted basins, i.e. the Arctic Ocean and Tethys. Locations at which deoxygenation has been inferred for the PETM are shown on Fig. 6, alongside those sites for which evidence exists for photic zone euxinia.

Moreover, many of these studies suggest that even where anoxia has been documented for the PETM Ocean, it was intermittent. It is noteworthy that even in the northern Tethys (Kheu River section, Dickson et al., 2014a), there appear to be cyclic variations in trace metal enrichments and lycopane concentrations. This cyclicity could be due to the sensitivity of shallow sites to oscillating depositional conditions, related to an enhanced hydrological cycle and fluctuations in nutrient input to marginal basins, which favours episodic oxygen depletion. By extension, the Arctic Ocean and Tethys could be considered nutrient traps, whereby increased nutrient inputs bring about increased productivity and anoxia only in restricted basins.

5. Synthesis

5.1. Integrating multiple proxies: a detailed example from Tanzania

As is apparent from the above, proxies for hydrological change - and the inferred consequences - are often contradictory. As such, we suggest it is critical to conduct multi-proxy, multi-parameter investigations at single sites in order to develop more nuanced interpretations. To illustrate this, we summarise and complement previous studies exploring changes in hydrology, sedimentology and carbon cycling from the Tanzanian PETM section. The Tanzania Drilling Project recovered the onset of the PETM interval and peak warmth at TDP site 14, first drilled in 2004 (9°16′S, 39°30′E, Nicholas et al., 2006). Micropaleontological and sedimentological evidence suggest the site represents a bathyal outer shelf or upper slope environment, with sediments comprising mainly clays and clayey siltstones, and with water depths estimated at 300 to 500 m (Nicholas et al., 2006). The clay-rich sediments have resulted in exceptional preservation of biomarkers, calcareous microfossils and nannofossils. Biostratigraphic and higher plant (*n*-alkane) carbon isotope records suggest that the onset and at least some of the core of the PETM interval is preserved, before being truncated by a probable hiatus prior to the CIE recovery.

The *n*-alkanes preserved at TDP-14a are composed of a homologous series with a predominance of odd- over- even carbon numbers at greater carbon numbers (Handley et al., 2008) typical of terrestrial higher plants (Eglinton and Hamilton, 1967). The PETM carbon isotope excursion is evident in *n*-alkane isotope records as a negative excursion of ~6‰, consistent with many other studies in which leaf waxes record a particularly high amplitude CIE. Initially, the CIE was thought to take place as an abrupt change at 19.5 m in the core, representing an abrupt onset of the PETM (Handley et al., 2008, 2012); however, more recent analyses at conducted at higher stratigraphic resolution across the PETM onset in TDP-14b (Aze et al., 2014) suggest a more complex picture of the PETM onset than previously recognised. The new records show rapid changes in *n*-alkane $\delta^{13}C$ values during the onset of the carbon isotope excursion, with fluctuations between −28 and −34‰ over several metres of core (Aze et al., 2014). By comparison to other CIEs, we argue that this fluctuation does not represent changes in the atmospheric carbon reservoir, but instead is evidence of significant reworking and remobilisation of older (pre-PETM) material during the onset of the PETM.

The *n*-alkane evidence of a complex onset at TDP14 is supported by dramatic and rapid fluctuations in both total organic carbon contents and $\delta^{13}C_{org}$ over the same interval in the core, both of which are evidence of highly variable delivery of organic matter to the site (Fig. 7; Aze et al., 2014). Further evidence of the episodic delivery of old, reworked organic matter comes from new records of bacterial biomarkers which likely represent erosion of even older organic matter, perhaps kerogen. Prior to the PETM interval, hopanes are dominated by thermally immature forms which are structurally similar to those produced by bacteria and consistent with the presence of other well preserved, thermally immature biomarkers in almost all Tanzanian Paleogene sediments (van Dongen et al., 2006); starting at the PETM onset these are replaced by increasing proportions of thermally mature, rearranged fossil biomarkers. Na/Al and Li/Al ratios of the bulk sediment also fluctuate together during the PETM onset interval, with higher Li/Al and lower Na/Al recording the delivery of older, more highly weathered clays to the core site, similar to previously reported kaolinite percentages (Handley et al., 2012). The BIT index of GDGTs also suggests an increase in the supply of soil-derived GDGTs to this marginal marine site.

Collectively, these new data suggest a sedimentologically complex onset to the PETM in Tanzania. Apparently, it was characterised by strongly erosive events leading to a mixture of contemporaneous plant-derived organic matter (*n*-alkanes), older soil-derived organic matter (branched GDGTs, but also some *n*-alkanes) and even kerogen-derived

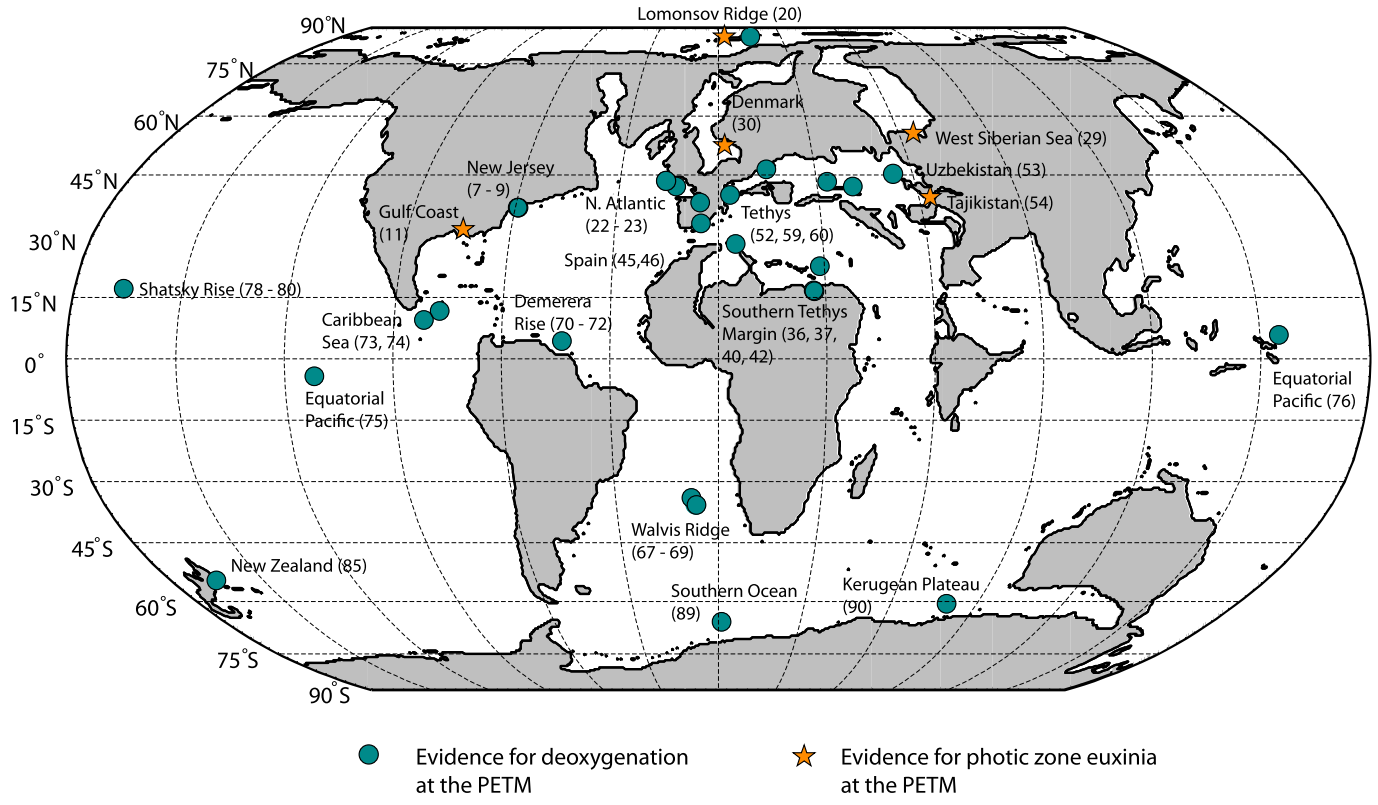

Fig. 6. Paleogeographic reconstruction for 56 Ma showing locations where evidence exists for deoxygenation in marine and marginal PETM sites. Also shown are locations where evidence for photic zone euxinia exists (stars). Numbers provided after each location correspond to PETM sites and references provided in Supplementary Table 1.

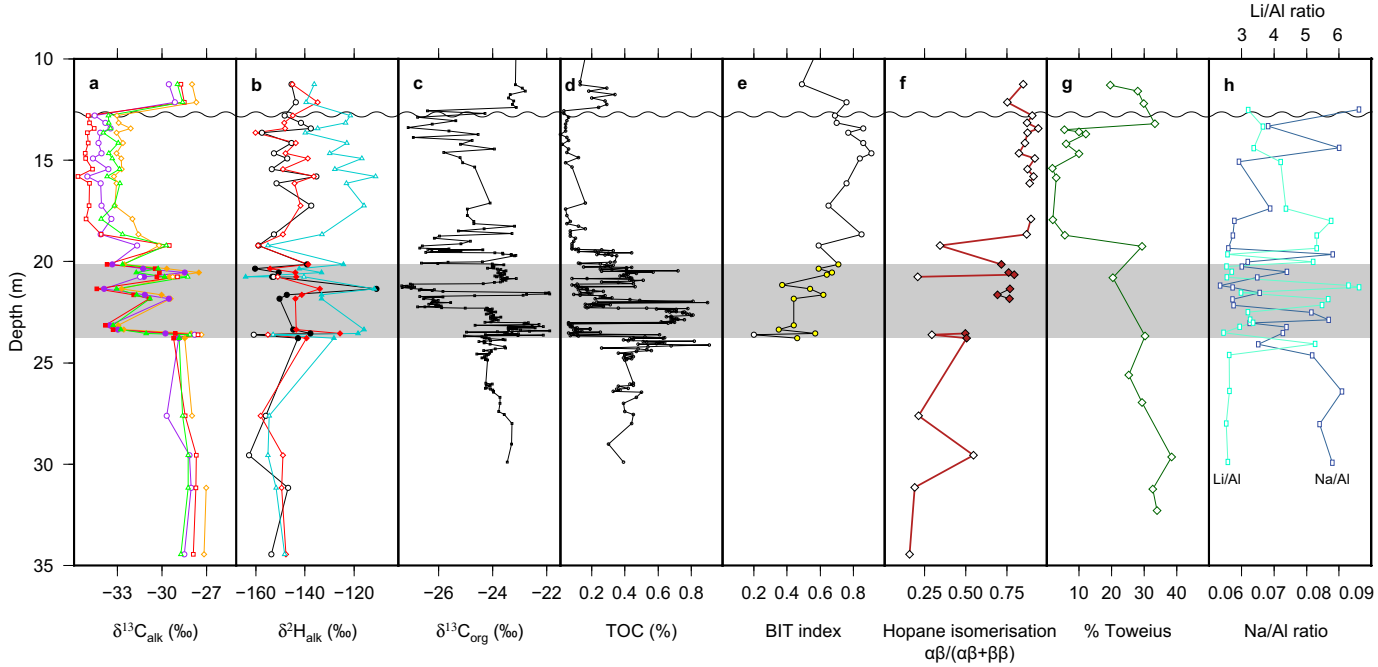

Fig. 7. Multiple proxy records from Tanzania Drilling Project Site 14 during the onset and core of the PETM; (a) Carbon isotope records from C_{25} (orange diamonds), C_{27} (purple circles), C_{29} (red squares) and C_{31} *n*-alkanes (green triangles), open symbols from Handley et al. (2008), filled symbols from Aze et al. (2014); (b) Hydrogen isotope records from C_{27} (black circles), C_{29} (red diamonds) and C_{31} alkanes (blue triangles), open symbols from Handley et al. (2008), filled symbols are new data; (c) Bulk organic carbon isotope record (Aze et al., 2014); (d) Total organic carbon (Aze et al., 2014); (e) BIT index, open symbols from Handley et al. (2008), with new data for the onset (filled symbols; this study); (f) hopane isomerisation index – ratio of mature (fossil) isomer to fossil and immature (biological) isomers; (g) percentage *Toweius* in nannoplankton community from Bown and Pearson (2009); (h) Na/Al and Li/Al ratios of bulk sediment. The wavy horizontal line represents a probable hiatus truncating the PETM interval, and the shading represents the "onset" as discussed in the text. (For interpretation of the references to colour in this figure legend, the reader is referred to the web version of this article.)

organic matter (thermally mature hopanes). These appear to have been delivered to the site via rather catastrophic and episodic sediment events, as reflected by the dramatic fluctuations in *n*-alkane $\delta^{13}C$ values. Potentially, this was related to an enhanced episodic hydrological regime. We have invoked a similar explanation for high variability in terrestrial biomarker concentrations and to resolve apparent discrepancies among proxies during the core of the CIE (Handley et al., 2008, 2012). The *n*-alkane hydrogen isotope record from TDP14 of Handley et al. (2012) exhibits a shift of up to 40‰ in the C_{31} alkane, starting at the same core depth as the initial carbon isotope excursion at the onset of the PETM. The new *n*-alkane carbon isotope record of Aze et al. (2014) puts this earliest shift deeper in the core, but our new alkane δ^2H record also starts at this lower, older horizon, such that the confluence of carbon and hydrogen isotopic change remains in our revised records. Therefore, we still argue that the increase in δ^2H values and increased variability during the PETM CIE represents a shift in east Africa to a more arid and but highly variable climate state with alternating wet-dry intervals.

Together, these records suggest a highly complex sedimentary environment at TDP-14 during the onset and core of the PETM CIE. The delivery of packages of recalcitrant terrestrial organic matter, evidence for highly weathered material, variability of the alkane isotopic compositions and increased BIT index (as well as increased kaolinite contents, quartz contents and inferred sedimentation rates, Handley et al., 2012) are broadly consistent with the suggestion that this location was characterised by more episodic rainfall, intensification of chemical weathering and erosion, and a mobilisation and perhaps oxidation of terrestrial organic matter. In fact, it potentially resolves some outstanding questions in PETM research. For example, the Tanzanian section is characterised by a small and very noisy $\delta^{13}C_{org}$ CIE, much smaller than that recorded by leaf wax biomarkers. We attribute that to the reworking of old organic matter into an overall organic-lean sedimentary setting; reworking of older soils would complicate both the bulk organic and leaf wax isotope records but reworking of kerogen would be particularly problematic for the former. We suggest that this reworking of kerogen is a likely explanation for small and noisy $\delta^{13}C_{org}$ records observed elsewhere (McInerney and Wing, 2011).

5.2. Integrating proxy data with the results of GCM simulations

Our proxy-data synthesis indicates that a varied range of proxies reflect a perturbed hydrological cycle at the PETM, incorporating changes in precipitation, continental runoff, evapotranspiration and humidity. Although many of the data are qualitative indicators of hydrological changes, they provide a way in which to evaluate the spatial patterns simulated within GCMs. Anomalies between low and high CO_2 simulations have been used previously as an analogue for pre-PETM and PETM climatology (Winguth et al., 2010; Lunt et al., 2010; Dunkley Jones et al., 2013). Fig. 8 shows the difference in P - E index between equilibrium simulations performed with the HadCM3L GCM at 2 × preindustrial concentrations of CO_2 (2 × CO_2, 560 ppmv) and 4 × CO_2 (1120 ppmv) and can be used to reconstruct first order changes in the hydrological cycle. The 4 × CO_2 simulation is the same as the early Eocene (Ypresian) simulation described by Inglis et al. (2015a) and Lunt et al. (2016). Both 2 × and 4 × simulations are also presented briefly in Inglis et al. (2017). The model is described in detail in Valdes et al. (2017), where it is called HadCM3L-M2.1E. The model simulations were run for > 1400 years; the spinup procedure and model configuration and initial conditions are described in full in Lunt et al. (2016).

Importantly, the model simulations indicate regions of both increased and decreased P – E associated with a doubling of pCO_2. Unlike the oceans, where moisture supply is unlimited, annually simulated P - E must exceed zero over terrestrial regions within both the 2 × CO_2 and 4 × CO_2 simulations (e.g. Byrne and O'Gorman, 2015). However, increased aridity is predicted in regions where the P - E balance becomes less positive in the high CO_2 simulation i.e. Δ(P-E) < 0. Whilst the simulations indicate a highly heterogeneous response in the hydrological cycle for a given latitude, some broad-scale trends are apparent. Above 50°N/S, P - E generally becomes more positive, driven by increases in precipitation within these regions (Supplementary Fig. S1). Within subtropical regions, there is a simulated shift towards greater aridity (i.e. the increase in evaporation is greater than that of precipitation, or precipitation declines), including over northern and southern Africa, around the Paleo-Tethys and within parts of South America. The deep tropics are associated with large increases in P - E, including over northern regions of South America, the western coast of Africa and the Indian subcontinent. Continental interior regions show highly variable changes, underlining the need for further proxy data and analyses, beyond those from the Bighorn Basin.

5.2.1. High northern latitudes

Relatively large increases in precipitation and precipitation - evaporation (and by extension runoff) are simulated across much of the high northern latitudes, including Greenland and the Arctic, particularly around the Turgai and Fram straits. This agrees well with various proxies which suggest increases in precipitation and runoff as indicated by hydrogen isotopes (Pagani et al., 2006) and the presence of low salinity dinoflagellate cysts (Sluijs et al., 2006), respectively. Isotopically-depleted $\delta^{18}O$ within tooth apatite of North Sea sharks (Zacke et al., 2009) and Norwegian-Greenland Sea fish (Andreasson et al., 1996) further suggested elevated terrestrial runoff, whilst plant fossils from Svalbard also indicate high mean annual precipitation (Harding et al., 2011).

Northern Europe, at a paleolatitude of ~45°N, is located at the boundary between a simulated increased and decreased P - E. Proxy evidence supports generally wetter climates in this region (Collinson et al., 2009; Pancost et al., 2007), increased runoff around the North Sea inferred from low-salinity dinoflagellate cysts (Kender et al., 2012) and a negative shift in *n*-alkane δ^2H values in France, interpreted to reflect a shift to moister conditions (Garel et al., 2013). Further proxy-model comparisons and analysis of the sensitivity of the simulated P-E boundary in other models is now required.

5.2.2. United States: Bighorn Basin and New Jersey

Over much of the United States an increase in P - E is simulated, although changes are strongly zonally-orientated with more arid climates in the western continental interior. This appears to relate to increased atmospheric subsidence within the model, which suppresses regional precipitation rates. This is partially consistent with evidence for transient aridification indicated by paleosols (Kraus and Riggins, 2007; Kraus et al., 2013), ichnofossils (Smith et al., 2008) and various geochemical studies (Woody et al., 2014; Adams et al., 2011). There is now a pressing need to improve understanding of the mechanisms which led to a return to higher precipitation during the PETM recovery (Wing et al., 2005; Kraus and Riggins, 2007), particularly as these processes cannot be represented within the equilibrium simulations. Despite a reduced P - E offshore, the eastern margin of the US has a much higher P - E within the 4xCO_2 model simulations which also qualitatively agrees with PETM increases in sedimentation (John et al., 2012), runoff (Sluijs and Brinkhuis, 2009) and consequent changes in the degree of oxygenation (Sluijs et al., 2014; Schumann et al., 2008) and shifts towards eutrophic algal-dominated communities (Gibbs et al., 2006; Stassen et al., 2012b). However, a variable P - E signal is simulated on the western US coast, whereas sedimentation rates from California indicate large increases in runoff (John et al., 2008). Potentially, this putative increase in erosion could reflect changes in the erodibility of the land surface or in sub-annual precipitation rates, which have not previously been considered within GCMs for the PETM. We show in Fig. S1 that the western US coast appears to experience a more seasonal distribution of precipitation at PETM, despite an overall decline in mean annual precipitation.

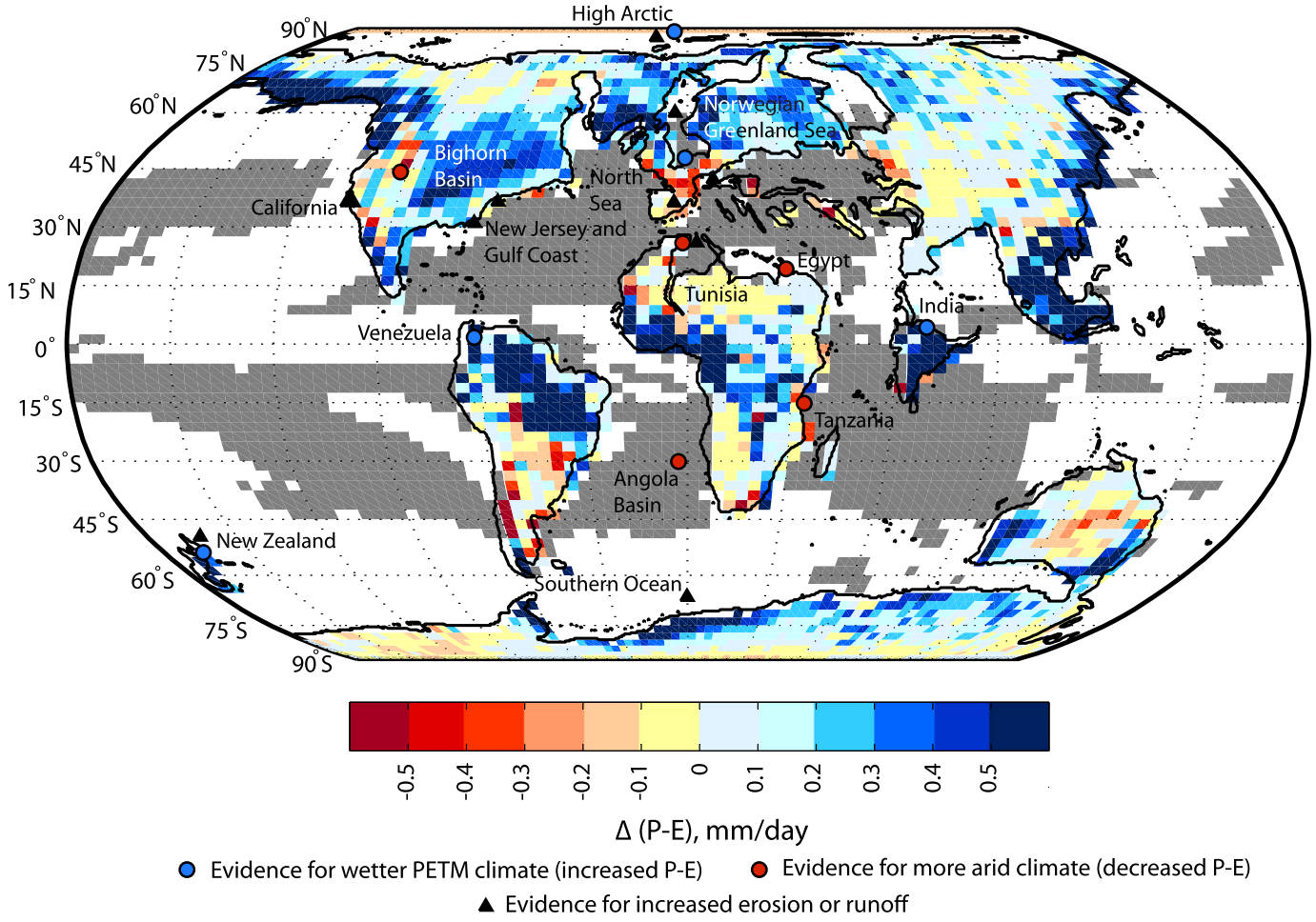

Fig. 8. Paleogeographic reconstruction for 56 Ma showing terrestrial changes in PETM precipitation - evaporation (P - E) distribution (mm/day) simulated within HadCM3L. The changes are calculated as an anomaly between 4 × CO_2 and 2 × CO_2 simulation. Regions where there is a simulation change to a more evaporative climate over the ocean (Δ(P-E) < −2.5) are masked in grey. Key proxy evidence for possible changes in P-E and runoff are also shown.

5.2.3. Paleo-Tethys, northern Africa and southern Europe

The north-eastern margin of the Paleo-Tethys is characterised by increased P - E which agrees qualitatively with proxies for increased runoff from Kazakhstan and Uzbekistan. In contrast, southern Europe shows a decline in P - E (and P) in model simulations, which is consistent with some proxy responses in that region (Bolle and Adatte, 2001; Schmitz and Pujalte, 2003) but does not agree with the increased runoff inferred for these locations from changes in sedimentation rate (e.g. Egger et al., 2003, 2005) or changes in nutrient state (Dickson et al., 2014a). Similarly, along the northern African margin, changes in sedimentation rate in the Tunisian and Egyptian sections imply elevated terrestrial runoff and erosion (Bolle et al., 2000; John et al., 2008), although a more negative P-E budget is simulated for the PETM within the continental interior. One possibility is that the hydroclimate regime became drier but more episodic in southern Europe and northern Africa as a response to global warming. The Claret Conglomerate in Spain has been interpreted as evidence for a flashy precipitation regime (Schmitz and Pujalte, 2007; Section 4.1) in an otherwise arid climate, and this is consistent with decreased P – E. Crucially, similar climatic controls could explain the increased sedimentation rates in marginal marine settings adjacent to land masses that apparently experienced greater annual aridity. Overall, the simulations do not show major changes in the seasonality of precipitation around the Paleo-Tethys (Supplementary Fig. S1), but our simulations do not allow an assessment of changes in extremes or episodicity, which should be examined more explicitly in future simulations.

5.2.4. The tropics

Tanzania is situated within a region of variable simulated changes, located at the boundary between wetter simulated tropics and a region of relatively small changes in P - E. As such, model simulations are consistent with but do not provide compelling support for the paradigm advanced in Section 5.1, i.e. a more arid climate punctuated with extreme and episodic precipitation events. Intriguingly, our simulations do show increases in the seasonality of precipitation in the region influenced by migration of the intertropical convergence zone (ITCZ), including regions where only minor changes in mean annual rainfall are simulated (Supplementary Fig. S1). As with the European and Northern African data-model comparison, we argue that this could indicate that the proxy response is driven by changes in subannual precipitation distribution – and possibly rainfall extremes - rather than annual averages. Aside from Tanzania, there is better data-model agreement elsewhere. The northern parts of South America are characterised by strong increases in P - E which agrees with floral assemblages and lower plant δ^2H values, interpreted to reflect an enhanced regional amount effect (Jaramillo et al., 2010). Similarly, higher simulated tropical precipitation in India is consistent with increased higher plant biomarker inputs to marginal marine sediments (Samanta et al., 2013). Greater aridity inferred for the Angola basin (Robert and Chamley, 1991) also agrees qualitatively with low-latitude subtropical drying implied by the model. Overall, the model indicates an increase in tropical P-E with a doubling of pCO_2 but with highly regional responses that are broadly consistent with the limited available proxy data.

5.2.5. High southern latitudes

The East Antarctic margin exhibits an increased P – E signal, which is consistent with some of the kaolinite evidence for increases in humidity or erosion (Robert and Kennett, 1994). The Antarctic continental interior exhibits a small absolute change to greater aridity, but given the low precipitation regime, this is likely a large relative change and perhaps consistent with interpretations from iron oxide deposits (Dallanave et al., 2009). New Zealand experienced relatively large increases in P and P-E which agrees with the suggestions of enhanced runoff and weathering indicated by elevated sedimentation rates (Crouch et al., 2003). Furthermore, enriched δ^2H within the upper-stages of the PETM could relate to increased moisture export (Handley et al., 2011), with which these simulations are qualitatively consistent, although isotope-enabled model simulations are now needed to mechanistically evaluate such hypotheses.

5.3. Conclusions

An enhanced or intensified hydrological cycle refers to the increased meridional transport of water vapour from low to high latitudes; it does not mean that precipitation simply increased across the globe (Pierrehumbert, 2002; Pagani et al., 2013; Huber, 2012). Assuming no fundamental changes in atmospheric dynamics, this results in a globally wet-wetter, dry-drier style response (Held and Soden, 2006), whereby evaporation increases within the net-evaporation zones of the subtropics, and precipitation increases within the net-precipitation zones of the high latitudes and deep tropics. Whilst changes over land are arguably more complex because of the limited moisture supply (Greve et al., 2014; Byrne and O'Gorman, 2015), our PETM climate model simulations support these broad-scale changes in hydrological response with latitude, although the responses are highly regionalised.

At present, PETM proxies provide some support for this paradigm, with consistent evidence from multiple proxies for high latitude increases in precipitation. However, there is currently relatively little evidence for associated subtropical drying due to the limited number of low-latitude sections. Evidence for increases in palygorskite around the northern Africa-Tethyan margin (Bolle and Adatte, 2001) and offshore of western Africa (Robert and Chamley, 1991), along with the interpretation of increased aridity in Tanzania (Handley et al., 2012) and perhaps the western United States (Wing et al., 2005; Kraus and Riggins, 2007) provide the first indications of this, but a denser assemblage of PETM records is needed to substantiate these changes. However, interpretation of the data compilation presented here must be done with caution, particularly given that the proxies incorporate signals of different processes associated with a perturbed hydrological cycle. Furthermore, as we have shown, a number of proxies record transient changes in hydrology throughout the PETM; the data are not, therefore, a global 'snapshot', but also integrate variability, possibly arising from feedbacks due to enhanced global warmth or orbital cyclicity. Several recent studies have invoked environmental instability in the aftermath of the CIE to explain apparent variability in the hydrological cycle. This includes rapid alternations in microfossil distributions, including dinocyst assemblages at New Jersey (Sluijs and Brinkhuis, 2009) and benthic forams at Forada, Italy (Giusberti et al., 2016); the sedimentary cycles recorded within the Bighorn Basin (Section 3.2; Kraus and Riggins, 2007; Kraus et al., 2015); and the cycles of humid and arid conditions inferred from organic matter nitrogren isotopes in Normandy, France (Storme et al., 2012). Below, we make some suggestions of directions for future research to fully understand the complexity of the hydrological response at the PETM, drawing on our data compilation and proxy-model comparison.

First, hydrological proxies with good stratigraphic age control will be necessary to probe regional synchroneity, system leads and lags, and the duration of hydrological change during the PETM. This requires archives that have the potential to yield high resolution records, such as vertically-stacked paleosols (or similar terrigenous deposits) or marginal (high sedimentation rate) marine sedimentary archives of hydrological change (e.g. leaf wax hydrogen isotopes), continental runoff, or chemical weathering. Such records could provide insight into leads and lags in the terrestrial environmental response, although caution is required due to the lags in sedimentary responses; for example, a rapid biotic or hydrological change could appear to lag warming if there is delay in transferring that signal to marine sediments. Moreover, the difficulty in unambiguously interpreting proxies as indicative of hydrological change (Section 3.2), means that considerable caution is necessary when comparing different proxies from different archives.

Second, more records from mid- and low latitudes, but especially arid regions, are necessary. With the exception of the Paleo-Tethys - including the northern margin of Africa and southern Europe - and the Bighorn Basin, nearly all existing PETM sections fall within regions where GCM simulations predict PETM Δ(P-E) $>$ 0. Furthermore, previous work has indicated that the terrestrial aridification of the Paleotethys could be a model-dependent result (Carmichael et al., 2016). One avenue for future research is to target marine sections which fall within zones of Δ (P-E) $<$ 0, such as the Indian Ocean and Walvis Ridge, for evidence of PETM salinification, analogous to modern-day changes detected in response to global warming (Stott et al., 2008; Curry et al., 2003). However, there is also a dearth of PETM data from continental interior sites and these exhibit a regionally-variable model response (Fig. 8) which requires data model comparison.

Third, multi-proxy approaches appear to be essential for more nuanced insights into hydrological changes, as illustrated by the case study for Tanzania where a combination of proxies was required to reveal the complex onset of PETM, a likely episodic precipitation regime, and the interplay of more arid conditions but more extreme rainfall events. Similar insights have been revealed by multi-proxy investigations in the Bighorn Basin and Spain. Such investigations also allow the consequences of hydrological change to be interrogated, including chemical weathering responses and mobilisation of different organic carbon pools. Multi-proxy approaches have also revealed evidence for heightened mid-latitude seasonality (Schmitz and Pujalte, 2003, 2007; Garel et al., 2013 and Storme et al., 2012; Giusberti et al., 2016). Multi-proxy approaches are also necessary because the PETM (and similar events) resulted in pervasive and wide-ranging environmental impacts and feedbacks that have complex synergistic and antagonistic impacts on some proxies. For example, it has been argued that under elevated CO_2 conditions the closing of stomata could have resulted in less rapid soil water uptake (although perhaps partially offset by a CO_2-fertilisation effect) and/or higher temperatures could have favoured drought-tolerant plants with a lower water demand (Wing and Currano, 2013). Both of these changes could impact paleosol characteristics or botanic indicators for drier climates in the absence of precipitation change. Adopting a multiproxy approach is thus essential to disentangle synergestic effects - particularly in the terrestrial regions, where land-surface processes introduce complex feedbacks. Crucially, given that all of these proxies have the potential to record wider (non-hydrological) environmental processes, are increasingly understood to integrate different time signals (e.g. see Tipple and Pagani, 2013; Foreman, 2014), and could suffer from Eocene non-analogue problems (e.g. Carmichael et al., 2016; Eberle and Greenwood, 2012), we suggest it is important to avoid reliance on any single proxy, where possible.

The use of GCMs to simulate changes in the Eocene hydrological cycle remains relatively limited, despite an increasing number of studies which have explored various manifestations of the hydrological cycle (Pagani et al., 2006; Winguth et al., 2010; Speelman et al., 2010; Sagoo et al., 2013; Kiehl and Shields, 2013; Loptson et al., 2014; Carmichael et al., 2016). There are a number of potential approaches by which further insights may be gained. First, future studies should explore the sensitivity of the simulated hydrological cycle to model boundary conditions and parameterisation schemes. Carmichael et al.

Table 1
Summary of the opportunities and threats in making proxy-model comparisons using isotope-enabled GCMs for the PETM hydrological cycle.

Opportunities	Threats
1. Isotopic proxies provide an opportunity to evaluate GCM simulations quantitatively, including whether the *magnitude* of hydrological change is correctly simulated, rather than the direction of change. 2. Isotope-enabled simulations provide a direct and mechanistic way to test proxy-inferred hypotheses e.g. whether a GCM-simulated water isotope excursion accompanies a change in source water temperature, precipitation or evapotranspiration rate. 3. Even in locations where no hydrological change has been explicitly invoked, any material which incorporates stable water isotopes (e.g. bone, shell or tooth enamel) can be directly compared to isotope-enabled simulations.	1. Each proxy requires a separate correction to estimate meteoric isotopic composition. Paleogene fractionation factors are poorly constrained and rely on simplistic vegetation reconstructions or nearest living relative calibrations. 2. Existing proxy data show significant pre-PETM and within-CIE variation in water isotope signals. This temporal complexity in the hydrological cycle response cannot be captured in equilibrium GCM simulations. 3. For meaningful proxy-model comparisons, the model must adequately represent the governing real-world processes (e.g. Rayleigh distillation, tropical amount effects) and include appropriate boundary conditions (e.g. seawater $\delta^{18}O$ and $\delta^{2}H$).

(2016) highlighted possible differences in the spatial pattern of PETM-simulated precipitation changes between HadCM3L and CCSM3, including declines in Paleotethyan precipitation within HadCM3L and increased high-latitude precipitation within CCSM3 at elevated atmospheric CO_2. However, the ability to explain these observations was limited given differences in various model boundary conditions and parameterisation scheme (Lunt et al., 2012). Coordinated Paleogene model simulations are now planned as part of the Paleoclimate Modelling Intercomparison Project (Lunt et al., 2016) which will lead to an improved ability to explain inter-model differences and potentially to evaluate the robustness of simulated changes.

Secondly, there is a need to study sub-annual (i.e. seasonal and episodic) precipitation and hydrological characteristics within GCMs. Although first-order mean annual changes in P and P-E show good correspondence with some of the proxy data (Fig. 8), it is clear that sedimentological and biotic proxies are often sensitive to the seasonal distribution of precipitation, water table or redox conditions (e.g. Sections 3.2 and 4.1) or the incidence of intense episodic precipitation events (e.g. Section 4.1.2) - or a filtered combination of these signals. Whilst sub-annual characteristics of the hydrological cycle are less well represented within GCMs (Sun et al., 2006; Dai, 2006), new generations of climate models better represent seasonal and daily variability and could lead to improved proxy-model comparisons in some regions.

Third, although the majority of the records discussed within this paper are qualitative changes in the hydrological cycle, isotopic proxies can be quantitatively compared with isotope-enabled model simulations (e.g. Sturm et al., 2009; Xi, 2014). Such comparisons could lead to an improved understanding of whether GCMs adequately simulate both the spatial pattern and magnitude of hydrological change (e.g. Speelman et al., 2010; Table 1).

Overall, we propose that new approaches for data-model integration are required, that incorporate the multiple dimensions of hydrological change (amount, seasonality, episodicity, intensity) and the complexity of hydrologically-impacted proxies. Such data-model integration requires caution, particularly given long-standing problems in the simulation of high-latitude temperatures and equable continental interior temperatures. If models do not adequately represent these characteristics of background Eocene climatology, then their ability to simulate changes at the PETM could be impaired (e.g. Speelman et al., 2010; Huber and Caballero, 2011; Carmichael et al., 2016). However, comparing hydrological proxies to model-simulated parameters has an important role to play; whilst CO_2 results in temperature increases across the Earth's surface, the response of the hydrological cycle is bi-directional, with regions of both increased wetting and drying. Qualitative comparisons of proxies to these spatial patterns can serve as a critical test, alongside temperatures, for the evaluation of GCM simulations. With a dense enough record of hydrological indicators, the responsible climate mechanisms can identified and the skill of individual GCMs benchmarked.

Supplementary data to this article can be found online at http://dx.doi.org/10.1016/j.gloplacha.2017.07.014.

Acknowledgements

The research leading to these results has received funding from the European Research Council under the European Union's Seventh Framework Programme (FP/2007–2013)/ERC Grant Agreement number 340923 (T-GRES, awarded to RDP). We thank the NERC LSMSF (Bristol) for analytical support. RDP acknowledges the Royal Society Wolfson Research Merit Award. DJL and AF acknowledge NERC grant CPE (NE/K012479/1) and thank Getech Plc for providing the Ypresian paleogeography. Finally, we thank the two anonymous reviewers for their comments and thoughtful suggestions which greatly improved this manuscript.

References

Abdul Aziz, H., Hilgen, F.J., van Luijk, G.M., Sluijs, A., Kraus, M.J., Pares, J.M., Gingerich, P.D., 2008. Astronomical climate control on paleosol stacking patterns in the upper Paleocene-lower Eocene Willwood Formation, Bighorn Basin, Wyoming. Geology 36, 531–534. http://dx.doi.org/10.1130/G24734A.1.

Acreman, M.C., Blake, J.R., Booker, D.J., Harding, R.J., Reynard, N., Mountford, J.O., Stratford, C.J., 2009. A simple framework for evaluating regional wetland ecohydrological response to climate change with case studies from Great Britain. Ecohydrology 2, 1–17. http://dx.doi.org/10.1002/eco.37.

Adams, J.S., Kraus, M.J., Wing, S.L., 2011. Evaluating the use of weathering indices for determining mean annual precipitation in the ancient stratigraphic record. Palaeogeogr. Palaeoclimatol. Palaeoecol. 309, 358–366. http://dx.doi.org/10.1016/j.palaeo.2011.07.004.

Allen, P.A., 2008. Time scales of tectonic landscapes and their sediment routing systems. Geol. Soc. Lond. Spec. Publ. 296, 7–28. http://dx.doi.org/10.1144/SP296.2.

Allen, M.R.R., Ingram, W.J.J., 2002. Constraints on future changes in climate and the hydrologic cycle. Nature 419, 224–232. http://dx.doi.org/10.1038/nature01092.

Anagnostou, E., John, E.H., Edgar, K.M., Foster, G.L., Ridgwell, A., Inglis, G.N., Pancost, R.D., Lunt, D.J., Pearson, P.N., 2016. Changing atmospheric CO_2 concentration was the primary driver of early Cenozoic climate. Nature 533, 380–384.

Andreasson, F.P., Schmitz, B., Spiegler, D., 1996. Stable isotopic composition ($\delta^{18}O$ CO_{32}-, $\delta^{13}C$) of early Eocene fish-apatite from Hole 913B: an indicator of the early Norwegian-Greenland Sea paleosalinity. In: Thiede, J., Myhre, A.M., Firth, J., Johnson, G.L., Ruddiman, W.F. (Eds.), Proceedings of the Ocean Drilling Program, Scientific Results. North Atlantic - Arctic Gateways I. Ocean Drilling Program, College Station, TX Vol. 151. pp. 583–591.

Armitage, J.J., Duller, R.a., Whittaker, A.C., Allen, P.a., 2011. Transformation of tectonic and climatic signals from source to sedimentary archive. Nat. Geosci. 4, 231–235. http://dx.doi.org/10.1038/ngeo1087.

Aze, T., Pearson, P.N., Dickson, A.J., Badger, M.P.S., Bown, P.R., Pancost, R.D., Gibbs, S.J., Huber, B.T., Leng, M.J., Coe, A.L., Cohen, A.S., Foster, G.L., 2014. Extreme warming of tropical waters during the Paleocene-Eocene thermal maximum. Geology 42, 739–742. http://dx.doi.org/10.1130/G35637.1.

Bains, S., Norris, R.D., Corfield, R.M., Faul, K.L., 2000. Termination of global warmth at the Palaeocene/Eocene boundary through productivity feedback. Nature 407, 171–174. http://dx.doi.org/10.1038/35025035.

Bak, K., 2005. Deep-water agglutinated foraminiferal changes across the Cretaceous/Tertiary and Paleocene/Eocene transitions in the deep flysch environment: eastern outer Carpathians (Boiesczady Mts, Poland). In: Proceedings of the 6th International Workshop on Agglutinated Foraminifera, Grzybowski Foundation Special Publication. Volume 8. pp. 1–56.

Beerling, D.J., Fox, A., Stevenson, D.S., Valdes, P.J., 2011. Enhanced chemistry-climate feedbacks in past greenhouse worlds. Proc. Natl. Acad. Sci. U. S. A. 108, 9770–9775. http://dx.doi.org/10.1073/pnas.1102409108.

Berner, E.K., Berner, R.A., 2012. GLobal Environment. Water, Air, and Geochemical Cycles, Second Ed. Princeton University Press, New Jersey.

Bidigare, R.R., Fluegge, A., Freeman, K.H., Hanson, K.L., Hayes, J.M., Hollander, D., Jasper, J.P., King, L.L., Laws, E.A., Milder, J., Millero, F.J., Pancost, R., Popp, B.N., Steinberg, P.A., Wakeham, S.G., 1997. Consistent fractionation of ^{13}C in nature and in

the laboratory: growth-rate effects in some haptophyte algae. Glob. Biogeochem. Cycles 11, 279–292.
Bijl, P.K., Schouten, S., Sluijs, A., Reichart, G.-J., Zachos, J.C., Brinkhuis, H., 2009. Early Palaeogene temperature evolution of the southwest Pacific Ocean. Nature 461, 776–779. http://dx.doi.org/10.1038/nature08399.
Blättler, C.L., Jenkyns, H.C., Reynard, L.M., Henderson, G.M., 2011. Significant increases in global weathering during Oceanic Anoxic Events 1a and 2 indicated by calcium isotopes. Earth Planet. Sci. Lett. 309, 77–88. http://dx.doi.org/10.1016/j.epsl.2011.06.029.
Bolle, M.P., Adatte, T., 2001. Palaeocene early Eocene climatic evolution in the Tethyan realm: clay mineral evidence. Clay Miner. 36, 249–261. http://dx.doi.org/10.1180/000985501750177979.
Bolle, M.P., Pardo, A., Adatte, T., Tantawy, A.A., Hinrichs, K.U., Von Salis, K., Burns, S., 2000. Climatic evolution on the southern and northern margins of the Tethys from the Paleocene to the early Eocene. GFF 122, 31–32.
Boltovskoy, E., Watanabe, S., Totah, V.I., Vera Ocampo, J., 1992. Cenozoic benthic bathyal foraminifers of DSDP Site 548 (North Atlantic). Micropaleontology 38, 183–207.
Bornemann, A., Norris, R.D., Lyman, J.A., D'Haenens, S., Groeneveld, J., Röhl, U., Farley, K.A., Speijer, R.P., 2014. Persistent environmental change after the Paleocene-Eocene Thermal Maximum in the eastern North Atlantic. Earth Planet. Sci. Lett. 394, 70–81. http://dx.doi.org/10.1016/j.epsl.2014.03.017.
Bowen, G.J., 2010. Isoscapes: spatial pattern in isotopic biogeochemistry. Annu. Rev. Earth Planet. Sci. 38, 161–187. http://dx.doi.org/10.1146/annurev-earth-040809-152429.
Bowen, G.J., 2013. Up in smoke: a role for organic carbon feedbacks in Paleogene hyperthermals. Glob. Planet. Chang. 109, 18–29. http://dx.doi.org/10.1016/j.gloplacha.2013.07.001.
Bowen, G.J., Bowen, B.B., 2008. Mechanisms of PETM global change constrained by a new record from central Utah. Geology 36, 379–382. http://dx.doi.org/10.1130/G24597A.1.
Bowen, G.J., Zachos, J.C., 2010. Rapid carbon sequestration at the termination of the Palaeocene–Eocene Thermal Maximum. Nat. Geosci. 3, 866–869. http://dx.doi.org/10.1038/ngeo1014.
Bowen, G.J., Beerling, D.J., Koch, P.L., Zachos, J.C., Quattlebaum, T., 2004. A humid climate state during the Palaeocene/Eocene thermal maximum. Nature 432, 495–499. http://dx.doi.org/10.1038/Nature03115.
Bown, P., Pearson, P., 2009. Calcareous plankton evolution and the Paleocene/Eocene thermal maximum event: new evidence from Tanzania. Mar. Micropaleontol. 71, 60–70. http://dx.doi.org/10.1016/j.marmicro.2009.01.005.
Braga, G., De, B.R., Grunig, A., Proto Decima, F., 1975. Foraminiferi bentonici del Paleocene ed Eocene della Sezione di Possagno. Schweiz Palaontol Abh 97, 85–111.
Bralower, T.J., 2002. Evidence of surface water oligotrophy during the Paleocene-Eocene thermal maximum: Nannofossil assemblage data from Ocean Drilling Program Site 690, Maud Rise, Weddell Sea. Paleoceanography 17, 12–13. http://dx.doi.org/10.1029/2001PA000662.
Bralower, T.J., Thomas, D.J., Zachos, J.C., Hirschmann, M.M., Röhl, U., Sigurdsson, H., Thomas, E., Whitney, D.L., 1997. High-resolution records of the late Paleocene thermal maximum and circum-Caribbean volcanism: is there a causal link? Geology 25, 963–966. http://dx.doi.org/10.1130/0091-7613(1997)025<0963:HRROTL>2.3.CO.
Bull, W.B., 1979. Threshold of critical power in streams. Bull. Geol. Soc. Am. 90, 453–464. http://dx.doi.org/10.1130/0016-7606(1979)90<453:TOCPIS>2.0.CO;2.
Buss, H.L., Brantley, S.L., Scatena, F.N., Bazilievskaya, E.A., Blum, A., Schulz, M., Jiménez, R., White, A.F., Rother, G., Cole, D., 2013. Probing the deep critical zone beneath the luquillo experimental forest, Puerto Rico. Earth Surf. Process. Landf. 38, 1170–1186. http://dx.doi.org/10.1002/esp.3409.
Buss, H.L., Chapela Lara, M., Moore, O.W., Kurtz, A.C., Schulz, M.S., White, A.F., 2017. Lithological influences on contemporary and long-term regolith weathering at the Luquillo Critical Zone Observatory. Geochim. Cosmochim. Acta 196, 224–251. http://dx.doi.org/10.1016/j.gca.2016.09.038.
Byrne, M.P., O'Gorman, P.A., 2015. The response of precipitation minus evapotranspiration to climate warming: why the "wet-get-wetter, dry-get-drier" scaling does not hold over land. J. Clim. 28, 8078–8092. http://dx.doi.org/10.1175/JCLI-D-15-0369.1.
Canudo, J., Keller, G., Molina, E., Ortiz, N., 1995. Planktic foraminiferal turnover and $\delta^{13}C$ isotopes across the Paleocene-Eocene transition at Caravaca and Zumaya, Spain. Palaeogeogr. Palaeoclimatol. Palaeoecol. 114, 75–100. http://dx.doi.org/10.1016/0031-0182(95)00073-U.
Carmichael, M.J., Lunt, D.J., Huber, M., Heinemann, M., Kiehl, J., LeGrande, A., Loptson, C.A., Roberts, C.D., Sagoo, N., Shields, C., Valdes, P.J., Winguth, A., Winguth, C., Pancost, R.D., 2016. A model–model and data–model comparison for the early Eocene hydrological cycle. Clim. Past 12, 455–481. http://dx.doi.org/10.5194/cp-12-455-2016.
Charles, A.J., Condon, D.J., Harding, I.C., Pälike, H., Marshall, J.E.A., Cui, Y., Kump, L., Croudace, I.W., 2012. Constraints on the numerical age of the Paleocene-Eocene boundary. Geochem. Geophys. Geosyst. 12. http://dx.doi.org/10.1029/2010GC003426.
Chen, Z., Ding, Z., Yang, S., Zhang, C., Wang, X., 2016. Increased precipitation and weathering across the Paleocene-Eocene Thermal Maximum in central China. Geochem. Geophys. Geosyst. 17, 2286–2297. http://dx.doi.org/10.1002/2016GC006333.
Chikaraishi, Y., Naraoka, H., 2003. Compound-specific dD-d13C analyses of n-alkanes extracted from terrestrial and aquatic plants. Phytochemistry 63, 361–371. http://dx.doi.org/10.1016/S0031-9422(02)00749-5.
Chou, C., Neelin, J.D., 2004. Mechanisms of global warming impacts on regional tropical precipitation. J. Clim. 17, 2688–2701. http://dx.doi.org/10.1175/1520-0442(2004)017<2688:MOGWIO>2.0.CO;2.
Chun, C.O.J., Delaney, M.L., Zachos, J.C., 2010. Paleoredox changes across the Paleocene-Eocene thermal maximum, Walvis Ridge (ODP Sites 1262, 1263, and 1266): evidence from Mn and U enrichment factors. Paleoceanography 25. http://dx.doi.org/10.1029/2009PA001861.
Clechenko, E.R., Kelly, D.C., Harrington, G.J., Stiles, C.A., 2007. Terrestrial records of a regional weathering profile at the Paleocene-Eocene boundary in the Williston Basin of North Dakota. Bull. Geol. Soc. Am. 119, 428–442. http://dx.doi.org/10.1130/B26010.1.
Clementz, M.T., Sewall, J.O., 2011. Latitudinal gradients in greenhouse seawater δ(18) O: evidence from Eocene sirenian tooth enamel. Science 80 (332), 455–458. http://dx.doi.org/10.1126/science.1201182.
Cohen, A.S., Coe, A.L., Harding, S.M., Schwark, L., 2004. Osmium isotope evidence for the regulation of atmospheric {CO} (sub 2) by continental weathering. Geology 32, 157–160. http://dx.doi.org/10.1130/G20158.1.
Collinson, M.E., Steart, D.C., Harrington, G.J., Hooker, J.J., Scott, A.C., Allen, L.O., Glasspool, I.J., Gibbons, S.J., 2009. Palynological evidence of vegetation dynamics in response to palaeoenvironmental change across the onset of the Paleocene-Eocene Thermal Maximum at Cobham, Southern England. Grana 48, 38–66. http://dx.doi.org/10.1080/00173130802707980.
Colosimo, A.B., Bralower, T.J., Zachos, J.C., 2005. Evidence for lysocline shoaling at the Paleocene/Eocene Thermal Maximum on Shatsky Rise, northwest Pacific. In: Bralower, T.J., Silva, I.P., Malone, M.J. (Eds.), Proceedings of the Ocean Drilling Program, Scientific Results. Ocean Drilling Program Vol. 198. College Station, TX, pp. 1–36.
Conant, R.T., Ryan, M.G., Ågren, G.I., Birge, H.E., Davidson, E.A., Eliasson, P.E., Evans, S.E., Frey, S.D., Giardina, C.P., Hopkins, F.M., Hyvönen, R., Kirschbaum, M.U.F., Lavallee, J.M., Leifeld, J., Parton, W.J., Megan Steinweg, J., Wallenstein, M.D., Martin Wetterstedt, J.Å., Bradford, M.A., 2011. Temperature and soil organic matter decomposition rates - synthesis of current knowledge and a way forward. Glob. Chang. Biol. http://dx.doi.org/10.1111/j.1365-2486.2011.02496.x.
Contreras, L., Pross, J., Bijl, P.K., Koutsodendris, A., Raine, J.I., van de Schootbrugge, B., Brinkhuis, H., 2013. Early to Middle Eocene vegetation dynamics at the Wilkes Land Margin (Antarctica). Rev. Palaeobot. Palynol. 197, 119–142. http://dx.doi.org/10.1016/j.revpalbo.2013.05.009.
Cotton, J.M., Sheldon, N.D., Hren, M.T., Gallagher, T.M., 2015. Positive feedback drives carbon release from soils to atmosphere during Paleocene/Eocene warming. Am. J. Sci. 315, 337–361. http://dx.doi.org/10.2475/04.2015.03.
Cramer, B.S., 2003. Orbital climate forcing of d13C excursions in the late Paleocene–early Eocene (chrons C24n–C25n). Paleoceanography 18, 1–25. http://dx.doi.org/10.1029/2003PA000909.
Creech, J.B., Baker, J.A., Hollis, C.J., Morgans, H.E.G., Smith, E.G.C., 2010. Eocene sea temperatures for the mid-latitude southwest Pacific from Mg/Ca ratios in planktonic and benthic foraminifera. Earth Planet. Sci. Lett. 299, 483–495. http://dx.doi.org/10.1016/j.epsl.2010.09.039.
Crouch, E.M., Heilmann-Clausen, C., Brinkhuis, H., Morgans, H.E.G., Rogers, K.M., Egger, H., Schmitz, B., 2001. Global dinoflagellate event associated with the late Paleocene Thermal Maximum. Geology 29, 315–318. http://dx.doi.org/10.1130/0091-7613(2001)029<0315:GDEAWT>2.0.CO;2.
Crouch, E.M., Dickens, G.R., Brinkhuis, H., Aubry, M.P., Hollis, C.J., Rogers, K.M., Visscher, H., 2003. The Apectodinium acme and terrestrial discharge during the Paleocene-Eocene thermal maximum: new palynological, geochemical and calcareous nannoplankton observations at Tawanui, New Zealand. Palaeogeogr. Palaeoclimatol. Palaeoecol. 194, 387–403. http://dx.doi.org/10.1016/S0031-0182(03)00334-1.
Cui, Y., Kump, L.R., Ridgwell, A.J., Charles, A.J., Junium, C.K., Diefendorf, A.F., Freeman, K.H., Urban, N.M., Harding, I.C., 2011. Slow release of fossil carbon during the Palaeocene–Eocene Thermal Maximum. Nat. Geosci. 4, 481–485. http://dx.doi.org/10.1038/ngeo1179.
Curry, R., Dickson, B., Yashayaev, I., 2003. A change in the freshwater balance of the Atlantic Ocean over the past four decades. Nature 426, 826–829.
Dai, A., 2006. Precipitation characteristics in eighteen coupled climate models. J. Clim. 19, 4605–4630. http://dx.doi.org/10.1175/Jcli3884.1.
Dallanave, E., Agnini, C., Muttoni, G., Rio, D., 2009. Magneto-biostratigraphy of the Cicogna section (Italy): implications for the late Paleocene-early Eocene time scale. Earth Planet. Sci. Lett. 285, 39–51.
Dansgaard, W., 1964. Stable isotopes in precipitation. Tellus 16, 436–468. http://dx.doi.org/10.3402/tellusa.v16i4.8993.
DeConto, R.M., Galeotti, S., Pagani, M., Tracy, D., Schaefer, K., Zhang, T., Pollard, D., Beerling, D.J., 2012. Corrigendum: past extreme warming events linked to massive carbon release from thawing permafrost. Nature 490 292–292. http://dx.doi.org/10.1038/nature11424.
Denis, E.H., Pedentchouk, N., Schouten, S., Pagani, M., Freeman, K.H., 2017. Fire and ecosystem change in the Arctic across the Paleocene-Eocene Thermal Maximum. Earth Planet. Sci. Lett. 467, 149–156.
Denman, K.L., Brasseur, G., Chidthaisong, A., Ciais, P., Cox, P.M., Dickinson, R.E., Hauglustaine, D., Heinze, C., Holland, E., Jacob, D., Lohmann, U., Ramachandran, S., Leite da Silva Dias, P., Wofsy, S.C., Zhang, X., Steffen, W., 2007. Couplings between changes in the climate system and biogeochemistry. In: Climate Change 2007: The Physical Science Basis. 21. pp. 499–587.
Dickens, G.R., O'Neil, J.R., Rea, D.K., Owen, R.M., 1995. Dissociation of oceanic methane hydrate as a cause of the carbon isotope excursion at the end of the Paleocene. Paleoceanography 10, 965–971. http://dx.doi.org/10.1029/95PA02087.
Dickson, A.J., Cohen, A.S., Coe, A.L., 2012. Seawater oxygenation during the Paleocene-Eocene Thermal Maximum. Geology 40, 639–642. http://dx.doi.org/10.1130/

G32977.1.
Dickson, A.J., Cohen, A.S., Coe, A.L., 2014a. Continental margin molybdenum isotope signatures from the Early Eocene. Earth Planet. Sci. Lett. 404, 389–395.
Dickson, A.J., Rees-Owen, R.L., Marz, C., Coe, A.L., Cohen, A.S., Pancost, R.D., Taylor, K., Shcherbinina, E., 2014b. The spread of marine anoxia on the northern Tethys margin during the Paleocene-Eocene thermal maximum. Paleoceanography 29, 471–488. http://dx.doi.org/10.1002/2014PA002629.
Dickson, A.J., Cohen, A.S., Coe, A.L., Davies, M., Shcherbinina, E.A., Gavrilov, Y.O., 2015. Evidence for weathering and volcanism during the PETM from Arctic Ocean and Peri-Tethys osmium isotope records. Palaeogeogr. Palaeoclimatol. Palaeoecol. 438, 300–307. http://dx.doi.org/10.1016/j.palaeo.2015.08.019.
Domingo, L., López-Martínez, N., Leng, M.J., Grimes, S.T., 2009. The Paleocene-Eocene Thermal Maximum record in the organic matter of the Claret and Tendruy continental sections (South-central Pyrenees, Lleida, Spain). Earth Planet. Sci. Lett. 281, 226–237. http://dx.doi.org/10.1016/j.epsl.2009.02.025.
van Dongen, B.E., Talbot, H.M., Schouten, S., Pearson, P.N., Pancost, R.D., 2006. Well preserved Palaeogene and Cretaceous biomarkers from the Kilwa area, Tanzania. Org. Geochem. 37, 539–557. http://dx.doi.org/10.1016/j.orggeochem.2006.01.003.
Doria, G., Royer, D.L., Wolfe, A.P., Fox, A., Westgate, J.A., Beerling, D.J., 2011. Declining atmospheric CO_2 during the late Middle Eocene climate transition. Am. J. Sci. 311, 63–75. http://dx.doi.org/10.2475/01.2011.03.
Dunkley Jones, T., Ridgwell, A., Lunt, D.J., Maslin, M.A., Schmidt, D.N., Valdes, P.J., 2010. A Palaeogene perspective on climate sensitivity and methane hydrate instability. Philos. Trans. R. Soc. A - Math. Phys. Eng. Sci. 368, 2395–2415. http://dx.doi.org/10.1098/rsta.2010.0053.
Dunkley Jones, T., Lunt, D.J., Schmidt, D.N., Ridgwell, A., Sluijs, A., Valdes, P.J., Maslin, M., 2013. Climate model and proxy data constraints on ocean warming across the Paleocene-Eocene Thermal Maximum. Earth-Sci. Rev. 125, 123–145. http://dx.doi.org/10.1016/j.earscirev.2013.07.004.
Dupuis, C., Aubry, M.P., Steurbat, E., Berggren, W.A., Ouda, K., Magioncalda, R., Cramer, B.S., Kent, D.V., Speijer, R.P., Heilmann-Clausen, C., 2003. The Dababiya Quarry section: lithostratigraphy, clay mineralogy, geochemistry and paleontology. Micropaleontology 49, 41–59. http://dx.doi.org/10.2113/49.Suppl_1.41.
Dypvik, H., Riber, L., Burca, F., Ruther, D., Jargvoll, D., Nagy, J.J., Jochmann, M., Rüther, D., 2011. The Paleocene-Eocene Thermal Maximum (PETM) in Svalbard - clay mineral and geochemical signals. Palaeogeogr. Palaeoclimatol. Palaeoecol. 302, 156–169. http://dx.doi.org/10.1016/j.palaeo.2010.12.025.
Eberle, J.J., Greenwood, D.R., 2012. Life at the top of the greenhouse Eocene world - a review of the Eocene flora and vertebrate fauna from Canada's high Arctic. Geol. Soc. Am. Bull. 124, 3–23.
Egger, H., Homayoun, M., Schnabel, W., 2002. Tectonic and climatic control of Paleogene sedimentation in the Rhenodanubian Flysch basin (eastern Alps, Austria). Sediment. Geol. 152, 247–262. http://dx.doi.org/10.1016/S0037-0738(02)00072-6.
Egger, H., Fenner, J., Heilmann-Clausen, C., Rögl, F., Sachsenhofer, R.F., Schmitz, B., 2003. Paleoproductivity of the northwestern Tethyan margin (Anthering section, Austria) across the Paleocene-Eocene transition. Geol. Soc. Am. Spec. Pap. 369, 133–146.
Egger, H., Homayoun, M., Huber, H., Rögl, F., Schmitz, B., 2005. Early Eocene climatic, volcanic, and biotic events in the northwestern Tethyan Untersberg section, Austria. Palaeogeogr. Palaeoclimatol. Palaeoecol. 217, 243–264. http://dx.doi.org/10.1016/j.palaeo.2004.12.006.
Eglinton, T.I., Eglinton, G., 2008. Molecular proxies for paleoclimatology. Earth Planet. Sci. Lett. 275, 1–16. http://dx.doi.org/10.1016/j.epsl.2008.07.012.
Eglinton, G., Hamilton, R.J., 1967. Leaf epicuticular waxes. Science 80 (156), 1322–1335. http://dx.doi.org/10.1126/science.156.3780.1322.
Ernst, S.R., Guasti, E., Dupuis, C., Speijer, R.P., 2006. Environmental perturbation in the southern Tethys across the Paleocene/Eocene boundary (Dababiya, Egypt): foraminiferal and clay mineral records. Mar. Micropaleontol. 60, 89–111. http://dx.doi.org/10.1016/j.marmicro.2006.03.002.
Fabricius, K.E., 2005. Effects of terrestrial runoff on the ecology of corals and coral reefs: review and synthesis. Mar. Pollut. Bull. 50, 125–146. http://dx.doi.org/10.1016/j.marpolbul.2004.11.028.
Farquhar, G.D., Hubick, K.T., Condon, A.G., Richards, R.A., 1989. Carbon isotope fractionation and plant water-use efficiency. In: Stable Isotopes in Ecological Research, pp. 21–40. http://dx.doi.org/10.1007/978-1-4612-3498-2_2.
Feakins, S.J., Sessions, A.L., 2010. Controls on the D/H ratios of plant leaf waxes in an arid ecosystem. Geochim. Cosmochim. Acta 74, 2128–2141. http://dx.doi.org/10.1016/j.gca.2010.01.016.
Fletcher, B.J., Brentnall, S.J., Anderson, C.W., Berner, R.A., Beerling, D.J., 2008. Atmospheric carbon dioxide linked with Mesozoic and early Cenozoic climate change. Nat. Geosci. 1, 43–48. http://dx.doi.org/10.1038/ngeo.2007.29.
Foreman, B.Z., 2014. Climate-driven generation of a fluvial sheet sand body at the Paleocene-Eocene boundary in north-west Wyoming (USA). Basin Res. 26, 225–241. http://dx.doi.org/10.1111/bre.12027.
Foreman, B.Z., Heller, P.L., Clementz, M.T., 2012. Fluvial response to abrupt global warming at the Palaeocene/Eocene boundary. Nature 490, 92–95. http://dx.doi.org/10.1038/nature11513.
Fricke, H.C., 2003. Investigation of early Eocene water-vapor transport and paleoelevation using oxygen isotope data from geographically widespread mammal remains. Geol. Soc. Am. Bull. 115, 1088–1096. http://dx.doi.org/10.1130/B25249.1.
Fricke, H.C., Clyde, W.C., O'Neil, J.R., Gingerich, P.D., 1998. Evidence for rapid climate change in North America during the latest Paleocene thermal maximum: oxygen isotope compositions of biogenic phosphate from the Bighorn Basin (Wyoming). Earth Planet. Sci. Lett. 160, 193–208. http://dx.doi.org/10.1016/S0012-821X(98)00088-0.
Frieling, J., Iakovleva, A.I., Reichart, G.J., Aleksandrova, G.N., Gnibidenko, Z.N., Schouten, S., Sluijs, A., 2014. Paleocene-Eocene warming and biotic response in the epicontinental West Siberian Sea. Geology 42, 767–770. http://dx.doi.org/10.1130/G35724.1.
Garel, S., Schnyder, J., Jacob, J., Dupuis, C., Boussafir, M., Le Milbeau, C., Storme, J.Y., Iakovleva, A.I., Yans, J., Baudin, F., Flehoc, C., Quesnel, F., Fléhoc, C., Quesnel, F., Flehoc, C., Quesnel, F., Fléhoc, C., Quesnel, F., 2013. Paleohydrological and paleoenvironmental changes recorded in terrestrial sediments of the Paleocene-Eocene boundary (Normandy, France). Palaeogeogr. Palaeoclimatol. Palaeoecol. 376, 184–199. http://dx.doi.org/10.1016/j.palaeo.2013.02.035.
Gat, J.R., 1996. Oxygen and hydrogen isotopes in the hydrologic cycle. Annu. Rev. Earth Planet. Sci. 24, 225–262. http://dx.doi.org/10.1146/annurev.earth.24.1.225.
Gavrilov, Y.O., Kodina, L.A., Lubchenko, I.Y., Muzylöv, N.G., 1997. The Late Paleocene anoxic event in epicontinental seas of Peri-Tethys and formation of the sapropelite unit: sedimentology and geochemistry. Lithol. Miner. Resour. 32, 427–450.
Gavrilov, Y.O., Shcherbinina, E.A., Oberhänsli, H., 2003. Paleocene-Eocene boundary events in the northeastern Peri-Tethys. Geol. Soc. Am. Spec. Pap. 369, 147–168. http://dx.doi.org/10.1130/0-8137-2369-8.147.
Gibbs, S.J., Bralower, T.J., Bown, P.R., Zachos, J.C., Bybell, L.M., 2006. Shelf and open-ocean calcareous phytoplankton assemblages across the Paleocene-Eocene thermal maximum: implications for global productivity gradients. Geology 34, 233–236. http://dx.doi.org/10.1130/G22381.1.
Gibson, T.G., Bybell, L.M., Mason, D.B., 2000. Stratigraphic and climatic implications of clay mineral changes around the Paleocene/Eocene boundary of the northeastern US margin. Sediment. Geol. 134, 65–92. http://dx.doi.org/10.1016/S0037-0738(00)00014-2.
Gislason, S.R., Oelkers, E.H., Eiriksdottir, E.S., Kardjilov, M.I., Gisladottir, G., Sigfusson, B., Snorrason, A., Elefsen, S., Hardardottir, J., Torssander, P., Oskarsson, N., 2009. Direct evidence of the feedback between climate and weathering. Earth Planet. Sci. Lett. 277, 213–222. http://dx.doi.org/10.1016/j.epsl.2008.10.018.
Giusberti, L., Rio, D., Agnini, C., Backman, J., Fornaciari, E., Tateo, F., Oddone, M., 2007. Mode and tempo of the Paleocene-Eocene thermal maximum in an expanded section from the Venetian pre-Alps. Bull. Geol. Soc. Am. 119, 391–412. http://dx.doi.org/10.1130/B25994.1.
Giusberti, L., Boscolo Galazzo, F., Thomas, E., 2016. Variability in climate and productivity during the Paleocene-Eocene Thermal Maximum in the western Tethys (Forada section). Clim. Past 12, 213–240.
Goodbred, S.L., Kuehl, S.A., Steckler, M.S., Sarker, M.H., 2003. Controls on facies distribution and stratigraphic preservation in the Ganges-Brahmaputra delta sequence. Sediment. Geol. 155, 301–316. http://dx.doi.org/10.1016/S0037-0738(02)00184-7.
Gradstein, F.M., Kaminski, M.A., Berggren, W.A., Kristiansen, I.L., D'lorio, M.A., 1994. Cenozoic biostratigraphy of the North Sea and Labrador Shelf. Micropaleontology 40 (i-ii + 1–152).
Gran, K., Paola, C., 2001. Riparian vegetation controls on braided stream dynamics. Water Resour. Res. 37, 3275–3283. http://dx.doi.org/10.1029/2000WR000203.
Greenwood, D.R., Moss, P.T., Rowett, A.I., Vadala, A.J., Keefe, R.L., 2003. Plant communities and climate change in southeastern Australia during the early Paleogene. In: Causes and Consequences of Globally Warm Climates in the Early Paleogene, pp. 365–380. http://dx.doi.org/10.1130/0-8137-2369-8.365.
Greve, P., Orlowsky, B., Mueller, B., Sheffield, J., Reichstein, M., Seneviratne, S.I., 2014. Global assessment of trends in wetting and drying over land. Nat. Geosci. 7, 716–721. http://dx.doi.org/10.1038/ngeo2247.
Handley, L., Pearson, P.N., McMillan, I.K., Pancost, R.D., 2008. Large terrestrial and marine carbon and hydrogen isotope excursions in a new Paleocene/Eocene boundary section from Tanzania. Earth Planet. Sci. Lett. 275, 17–25. http://dx.doi.org/10.1016/j.epsl.2008.07.030.
Handley, L., Crouch, E.M., Pancost, R.D., 2011. A New Zealand record of sea level rise and environmental change during the Paleocene-Eocene Thermal Maximum. Palaeogeogr. Palaeoclimatol. Palaeoecol. 305, 185–200. http://dx.doi.org/10.1016/j.palaeo.2011.03.001.
Handley, L., O'Halloran, A., Pearson, P.N., Hawkins, E., Nicholas, C.J., Schouten, S., McMillan, I.K., Pancost, R.D., 2012. Changes in the hydrological cycle in tropical East Africa during the Paleocene-Eocene Thermal Maximum. Palaeogeogr. Palaeoclimatol. Palaeoecol. 329, 10–21. http://dx.doi.org/10.1016/j.palaeo.2012.02.002.
Harding, I.C., Charles, A.J., Marshall, J.E.A., Pälike, H., Roberts, A.P., Wilson, P.A., Jarvis, E., Thorne, R., Morris, E., Moremon, R., Pearce, R.B., Akbari, S., 2011. Sea-level and salinity fluctuations during the Paleocene-Eocene thermal maximum in Arctic Spitsbergen. Earth Planet. Sci. Lett. 303, 97–107. http://dx.doi.org/10.1016/j.epsl.2010.12.043.
Harrington, G., Kemp, S., Koch, P., 2004. Palaeocene-Eocene paratropical floral change in North America: responses to climate change and plant immigration. J. Geol. Soc. Lond. 161, 173–184. http://dx.doi.org/10.1144/0016-764903-100.
Harrington, G.J., Clechenko, E.R., Kelly, D.C., 2005. Palynology and organic-carbon isotope ratios across a terrestrial Palaeocene/Eocene boundary section in the Williston Basin, North Dakota, USA. Palaeogeogr. Palaeoclimatol. Palaeoecol. 226, 214–232. http://dx.doi.org/10.1016/j.palaeo.2005.05.013.
Haywood, A.M., Ridgwell, A., Lunt, D.J., Hill, D.J., Pound, M.J., Dowsett, H.J., Dolan, A.M., Francis, J.E., Williams, M., 2011. Are there pre-Quaternary geological analogues for a future greenhouse warming? Philos. Trans. R. Soc. A Math. Phys. Eng. Sci. 369, 933–956. http://dx.doi.org/10.1098/rsta.2010.0317.
Held, I.M., Soden, B.J., 2006. Robust responses of the hydrological cycle to global warming. J. Clim. 19, 5686–5699. http://dx.doi.org/10.1175/JCLI3990.1.
Hollis, C.J., Taylor, K.W.R., Handley, L., Pancost, R.D., Huber, M., Creech, J.B., Hines, B.R., Crouch, E.M., Morgans, H.E.G., Crampton, J.S., Gibbs, S., Pearson, P.N., Zachos, J.C., 2012. Early Paleogene temperature history of the Southwest Pacific Ocean: reconciling proxies and models. Earth Planet. Sci. Lett. 349–350, 53–66. http://dx.doi.org/10.1016/j.epsl.2012.06.024.

Huber, M., Caballero, R., 2011. The early Eocene equable climate problem revisited. Clim. Past 7, 603–633.
Huber, M., 2012. Progress in greenhouse climate modeling. Reconstr. Earth Deep. Clim. State Art 18, 213–262.
Hyland, E.G., Sheldon, N.D., Van der Voo, R., Badgley, C., Abrajevitch, A., 2015. A new paleoprecipitation proxy based on soil magnetic properties: implications for expanding paleoclimate reconstructions. Bull. Geol. Soc. Am. 127, 975–981. http://dx.doi.org/10.1130/B31207.1.
Inglis, G.N., Collinson, M.E., Riegel, W., Wilde, V., Robson, B.E., Lenz, O.K., Pancost, R.D., 2015a. Ecological and biogeochemical change in an early Paleogene peat-forming environment: linking biomarkers and palynology. Palaeogeogr. Palaeoclimatol. Palaeoecol. 438, 245–255. http://dx.doi.org/10.1016/j.palaeo.2015.08.001.
Inglis, G.N., Farnsworth, A., Lunt, D., Foster, G.L., Hollis, C.J., Pagani, M., Jardine, P.E., Pearson, P.N., Markwick, P., Galsworthy, A.M.J., Raynham, L., Taylor, K.W.R., Pancost, R.D., 2015b. Descent toward the Icehouse: Eocene sea surface cooling inferred from GDGT distributions. Paleoceanography 30, 1000–1020. http://dx.doi.org/10.1002/2014PA002723.
Inglis, G.N., Collinson, M.E., Riegel, W., Wilde, V., Farnsworth, A., Lunt, D.J., Valdes, P., Robson, B.E., Scott, A.C., Lenz, O.K., Naafs, B.D.A., Pancost, R.D., 2017. Mid-latitude continental temperatures through the early Eocene in western Europe. Earth Planet. Sci. Lett. 460, 86–96.
IPCC, 2013. Climate Change 2013: The Physical Science Basis. Contribution of Working Group I to the Fifth Assessment Report of the Intergovernmental Panel on Climate Change. Cambridge University Press, Cambridge, UK and New York, NY, USA.
Jagniecki, E.A., Lowenstein, T.K.T.K., Jenkins, D.M., Demicco, R.V., 2015. Eocene atmospheric CO_2 from the nahcolite proxy. Geology 43, 1075–1078. http://dx.doi.org/10.1130/G36886.1.
Jaramillo, C., Ochoa, D., Contreras, L., Pagani, M., Carvajal-Ortiz, H., Pratt, L.M., Krishnan, S., Cardona, A., Romero, M., Quiroz, L., Rodriguez, G., Rueda, M.J., de la Parra, F., Morón, S., Green, W., Bayona, G., Montes, C., Quintero, O., Ramirez, R., Mora, G., Schouten, S., Bermudez, H., Navarrete, R., Parra, F., Alvarán, M., Osorno, J., Crowley, J.L., Valencia, V., Vervoort, J., 2010. Effects of rapid global warming at the Paleocene-Eocene boundary on neotropical vegetation. Science 330, 957–961. http://dx.doi.org/10.1126/science.1193833.
Jenkyns, H.C., 2010. Geochemistry of oceanic anoxic events. Geochem. Geophys. Geosyst. 11. http://dx.doi.org/10.1029/2009GC002788.
Jiang, S., Wise Jr., S.W., 2006. Surface-water chemistry and fertility variations in the tropical Atlantic across the Paleocene/Eocene Thermal Maximum as evidenced by calcareous nannoplankton from ODP Leg 207, Hole 1259B. Rev. Micropaleontol. 49, 227–244. http://dx.doi.org/10.1016/j.revmic.2006.10.002.
Jiang, Y., Zhuang, Q., Schaphoff, S., Sitch, S., Sokolov, A., Kicklighter, D., Melillo, J., 2012. Uncertainty analysis of vegetation distribution in the northern high latitudes during the 21st century with a dynamic vegetation model. Ecol. Evol. 2, 593–614. http://dx.doi.org/10.1002/ece3.85.
Jiménez Cisneros, B.E., Oki, T., Arnell, N.W., Benito, G., Cogley, J.G., Döll, P., Jiang, T., Mwakalila, S.S., 2014. Freshwater resources. In: Field, C.B., Barros, V.R., Dokken, D.J., Mach, K.J., Mastrandrea, M.D., Bilir, T.E., Chatterjee, M., Ebi, K.L., Estrada, Y.O., Genova, R.C., Girma, B., Kissel, E.S., Levy, A.N., MacCracken, S., Mastrandrea, P.R., White, L.L. (Eds.), Climate Change 2014: Impacts, Adaptation, and Vulnerability. Part A: Global and Sectoral Aspects. Contribution of Working Group II to the Fifth Assessment Report of the Intergovernmental Panel of Climate Change. Cambridge University Press, Cambridge, United Kingdom and New York, NY, USA, pp. 229–269.
Jobbagy, E.G., Jackson, R., 2000. The vertical distribution of soil organic carbon and its relation to climate and vegetation. Ecol. Appl. 10 (2), 423–436. http://dx.doi.org/10.2307/2641104.
John, C.M., Bohaty, S.M., Zachos, J.C., Sluijs, A., Gibbs, S., Brinkhuis, H., Bralower, T.J., 2008. North American continental margin records of the Paleocene-Eocene thermal maximum: implications for global carbon and hydrological cycling. Paleoceanography 23. http://dx.doi.org/10.1029/2007PA001465.
John, C.M., Banerjee, N.R., Longstaffe, F.J., Sica, C., Law, K.R., Zachos, J.C., 2012. Clay assemblage and oxygen isotopic constraints on the weathering response to the Paleocene-Eocene thermal maximum, east coast of North America. Geology 40, 591–594. http://dx.doi.org/10.1130/G32785.1.
Kaiho, K., Arinobu, T., Ishiwatari, R., Morgans, H.E.G., Okada, H., Takeda, N., Tazaki, K., Zhou, G., Kajiwara, Y., Matsumoto, R., Hirai, A., Niitsuma, N., Wada, H., 1996. Latest Paleocene benthic foraminiferal extinction and environmental changes at Tawanui, New Zealand. Paleoceanography 11, 447–465. http://dx.doi.org/10.1029/96PA01021.
Kaiho, K., Takeda, K., Petrizzo, M.R., Zachos, J.C., 2006. Anomalous shifts in tropical Pacific planktonic and benthic foraminiferal test size during the Paleocene-Eocene thermal maximum. Palaeogeogr. Palaeoclimatol. Palaeoecol. 237, 456–464. http://dx.doi.org/10.1016/j.palaeo.2005.12.017.
Kelly, D.C., Zachos, J.C., Bralower, T.J., Schellenberg, S.A., 2005. Enhanced terrestrial weathering/runoff and surface ocean carbonate production during the recovery stages of the Paleocene-Eocene thermal maximum. Paleoceanography 20. http://dx.doi.org/10.1029/2005PA001163.
Kender, S., Stephenson, M.H., Riding, J.B., Leng, M.J., Knox, R.W.O.B., Peck, V.L., Kendrick, C.P., Ellis, M.A., Vane, C.H., Jamieson, R., 2012. Marine and terrestrial environmental changes in NW Europe preceding carbon release at the Paleocene-Eocene transition. Earth Planet. Sci. Lett. 353–354, 108–120. http://dx.doi.org/10.1016/j.epsl.2012.08.011.
Khozyem, H., Adatte, T., Spangenberg, J.E., Tantawy, A.A., Keller, G., 2013. Palaeoenvironmental and climatic changes during the Palaeocene–Eocene Thermal Maximum (PETM) at the Wadi Nukhul Section, Sinai, Egypt. J. Geol. Soc. Lond. 170, 341–352. http://dx.doi.org/10.1144/jgs2012-046.
Khozyem, H., Adatte, T., Spangenberg, J.E., Keller, G., Tantawy, A.A., Ulianov, A., 2015. New geochemical constraints on the Paleocene-Eocene thermal maximum: Dababiya GSSP, Egypt. Palaeogeogr. Palaeoclimatol. Palaeoecol. 429, 117–135. http://dx.doi.org/10.1016/j.palaeo.2015.04.003.
Kiehl, J.T., Shields, C.A., 2013. Sensitivity of the Palaeocene-Eocene Thermal Maximum climate to cloud properties. Philos. Trans. R. Soc. A-Mathematical Phys. Eng. Sci. 371. http://dx.doi.org/10.1098/Rsta.2013.0093.
Kirschke, S., Bousquet, P., Ciais, P., Saunois, M., Canadell, J.G., Dlugokencky, E.J., Bergamaschi, P., Bergmann, D., Blake, D.R., Bruhwiler, L., Cameron-Smith, P., Castaldi, S., Chevallier, F., Feng, L., Fraser, A., Heimann, M., Hodson, E.L., Houweling, S., Josse, B., Fraser, P.J., Krummel, P.B., Lamarque, J.-F., Langenfelds, R.L., Le Quéré, C., Naik, V., O'Doherty, S., Palmer, P.I., Pison, I., Plummer, D., Poulter, B., Prinn, R.G., Rigby, M., Ringeval, B., Santini, M., Schmidt, M., Shindell, D.T., Simpson, I.J., Spahni, R., Steele, L.P., Strode, S.A., Sudo, K., Szopa, S., van der Werf, G.R., Voulgarakis, A., van Weele, M., Weiss, R.F., Williams, J.E., Zeng, G., 2013. Three decades of global methane sources and sinks. Nat. Geosci. 6, 813–823. http://dx.doi.org/10.1038/ngeo1955.
Knox, R.W.O., Aubry, M.P., Berggren, W.A., Dupuis, C., Ouda, K., Magioncalda, R., Soliman, M., 2003. The Qreiya section at Gebel Abu Had: lithostratigraphy, clay mineralogy, geochemistry and biostratigraphy. Micropaleontology 49, 93–104. http://dx.doi.org/10.2113/49.Suppl_1.93.
Knutti, R., Sedláček, J., 2013. Robustness and uncertainties in the new CMIP5 climate model projections. Nat. Clim. Chang. 3, 369–373. http://dx.doi.org/10.1038/Nclimate1716.
Kodina, L.A., Huang, Y., Gavrilov, Y.O., Jones, M., Eglinton, G., 1995. Environment of upper Paleocene black shale deposition in Southern Russia and adjacent regions as revealed by isotope and biomarker study. In: Grimalt, J.O., Dorrosoro, C. (Eds.), Organic Geochemistry: Developments and Applications to Energy, Climate, Environment and Human History: Selected Papers from the 17th International Meeting on Organic Geochemistry, Special Papers. Volume 369. Geological Society of America, pp. 192–194.
Kohn, M.J., 2016. Carbon isotope discrimination in C3 land plants is independent of natural variations in pCO_2. Geochem. Perspect. Lett. 2, 35–43. http://dx.doi.org/10.7185/geochemlet.1604.
Kopp, R.E.R.E., Schumann, D., Raub, T.D.T.D., Powars, D.S.D.S., Godfrey, L.V.L.V., Swanson-Hysell, N.L.N.L., Maloof, A.C.A.C., Vali, H., 2009. An Appalachian Amazon? Magnetofossil evidence for the development of a tropical river-like system in the mid-Atlantic United States during the Paleocene-Eocene thermal maximum. Paleoceanography 24, 1–17. http://dx.doi.org/10.1029/2009PA001783.
Kraus, M.J., McInerney, F.A., Wing, S.L., Secord, R., Baczynski, A.A., Bloch, J.I., 2013. Paleohydrologic response to continental warming during the Paleocene-Eocene Thermal Maximum, Bighorn Basin, Wyoming. Palaeogeogr. Palaeoclimatol. Palaeoecol. 370, 196–208. http://dx.doi.org/10.1016/j.palaeo.2012.12.008.
Kraus, M.J., Woody, D.T., Smith, J.J., Dukic, V., 2015. Alluvial response to the Paleocene-Eocene Thermal Maximum climatic event, Polecat Bench, Wyoming (U.S.A.). Palaeogeogr. Palaeoclimatol. Palaeoecol. 435, 177–192. http://dx.doi.org/10.1016/j.palaeo.2015.06.021.
Kraus, M., Riggins, S., 2007. Transient drying during the Paleocene–Eocene Thermal Maximum (PETM): analysis of paleosols in the bighorn basin, Wyoming. Palaeogeogr. Palaeoclimatol. Palaeoecol. 245, 444–461.
Krishnan, S., Pagani, M., Agnini, C., 2015. Leaf waxes as recorders of paleoclimatic changes during the Paleocene-Eocene Thermal Maximum: regional expressions from the Belluno Basin. Org. Geochem. 80, 8–17. http://dx.doi.org/10.1016/j.orggeochem.2014.12.005.
Larrasoaña, J.C., Roberts, A.P., Chang, L., Schellenberg, S.A., Fitz Gerald, J.D., Norris, R.D., Zachos, J.C., 2012. Magnetotactic bacterial response to Antarctic dust supply during the Palaeocene-Eocene thermal maximum. Earth Planet. Sci. Lett. 333–334, 122–133. http://dx.doi.org/10.1016/j.epsl.2012.04.003.
Lebedeva, M.I., Fletcher, R.C., Brantley, S.L., 2010. A mathematical model for steady-state regolith production at constant erosion rate. Earth Surf. Process. Landf. 35, 508–524. http://dx.doi.org/10.1002/esp.1954.
Leier, A.L., DeCelles, P.G., Pelletier, J.D., 2005. Mountains, monsoons, and megafans. Geology 33, 289–292. http://dx.doi.org/10.1130/G21228.1.
Lippert, P.C., Zachos, J.C., 2007. A biogenic origin for anomalous fine-grained magnetic material at the Paleocone-Eocene boundary at Wilson Lake, New Jersey. Paleoceanography 22. http://dx.doi.org/10.1029/2007PA001471.
Littler, K., Röhl, U., Westerhold, T., Zachos, J.C., 2014. A high-resolution benthic stable-isotope record for the South Atlantic: implications for orbital-scale changes in Late Paleocene-Early Eocene climate and carbon cycling. Earth Planet. Sci. Lett. 401, 18–30. http://dx.doi.org/10.1016/j.epsl.2014.05.054.
Loptson, C.A., Lunt, D.J., Francis, J.E., 2014. Investigating vegetation-climate feedbacks during the early Eocene. Clim. Past 10, 419–436. http://dx.doi.org/10.5194/cp-10-419-2014.
Lourens, L., Sluijs, A., Kroon, D., Zachos, J.C., Thomas, E., Röhl, U., Bowles, J., Raffi, I., 2005. Astronomical pacing of late Palaeocene to early Eocene global warming events. Nature 435, 1083–1087. http://dx.doi.org/10.1038/nature03814.
Lunt, D.J., Valdes, P.J., Jones, T.D., Ridgwell, A., Haywood, A.M., Schmidt, D.N., Marsh, R., Maslin, M., 2010. CO_2-driven ocean circulation changes as an amplifier of Paleocene-Eocene thermal maximum hydrate destabilization. Geology 38, 875–878. http://dx.doi.org/10.1130/G31184.1.
Lunt, D.J., Dunkley Jones, T., Heinemann, M., Huber, M., LeGrande, A., Winguth, A., Loptson, C., Marotzke, J., Roberts, C.D., Tindall, J., Valdes, P., Winguth, C., Jones, T.D., Heinemann, M., Huber, M., LeGrande, A., Winguth, A., Loptson, C., Marotzke, J., Roberts, C.D., Tindall, J., Valdes, P., Winguth, C., 2012. A model-data comparison for a multi-model ensemble of early Eocene atmosphere-ocean simulations: EoMIP. Clim. Past 8, 1717–1736. http://dx.doi.org/10.5194/cp-8-1717-2012.

Lunt, D.J., Elderfield, H., Pancost, R., Ridgwell, A., Foster, G.L., Haywood, A., Kiehl, J., Sagoo, N., Shields, C., Stone, E.J., Valdes, P., 2013. Warm climates of the past—a lesson for the future? Philos. Trans. A. Math. Phys. Eng. Sci. 371, 20130146. http://dx.doi.org/10.1098/rsta.2013.0146.

Lunt, D.J., Huber, M., Baatsen, M.L.J., Caballero, R., DeConto, R., Donnadieu, Y., Evans, D., Feng, R., Foster, G., Gasson, E., von der Heydt, A.S., Hollis, C.J., Kirtland Turner, S., Korty, R.L., Kozdon, R., Krishnan, S., Ladant, J.-B., Langebroek, P., Lear, C.H., LeGrande, A.N., Littler, K., Markwick, P., Otto-Bliesner, B., Pearson, P., Poulsen, C., Salzmann, U., Shields, C., Snell, K., Starz, M., Super, J., Tabour, C., Tierney, J., Tourte, G.J.L., Upchurch, G.R., Wade, B., Wing, S.L., Winguth, A.M.E., Wright, N., Zachos, J.C., Zeebe, R., 2016. DeepMIP: experimental design for model simulations of the EECO, PETM, and pre-PETM. Geosci. Model Dev. Discuss. 2016, 1–16. http://dx.doi.org/10.5194/gmd-2016-127.

Macklin, M.G., Lewin, J., Woodward, J.C., 2012. The fluvial record of climate change. Philos. Trans. R. Soc. A Math. Phys. Eng. Sci. 370, 2143–2172. http://dx.doi.org/10.1098/rsta.2011.0608.

Manners, H.R., Grimes, S.T., Sutton, P.A., Domingo, L., Leng, M.J., Twitchett, R.J., Hart, M.B., Dunkley Jones, T., Pancost, R.D., Duller, R., Lopez-Martinez, N., 2013. Magnitude and profile of organic carbon isotope records from the Paleocene-Eocene Thermal Maximum: evidence from northern Spain. Earth Planet. Sci. Lett. 376, 220–230. http://dx.doi.org/10.1016/j.epsl.2013.06.016.

März, C., Schnetger, B., Brumsack, H.-J., 2010. Paleoenvironmental implications of Cenozoic sediments from the Central Arctic Ocean (IODP expedition 302) using inorganic geochemistry. Paleoceanography 25, PA3206. http://dx.doi.org/10.1029/2009PA001860.

Maxbauer, D.P., Feinberg, J.M., Fox, D.L., 2016a. Magnetic mineral assemblages in soils and paleosols as the basis for paleoprecipitation proxies: a review of magnetic methods and challenges. Earth-Sci. Rev. 155, 28–48. http://dx.doi.org/10.1016/j.earscirev.2016.01.014.

Maxbauer, D.P., Feinberg, J.M., Fox, D.L., Clyde, W.C., 2016b. Magnetic minerals as recorders of weathering, diagenesis, and paleoclimate: a core-outcrop comparison of Paleocene-Eocene paleosols in the Bighorn Basin, WY, USA. Earth Planet. Sci. Lett. 452, 15–26. http://dx.doi.org/10.1016/j.epsl.2016.07.029.

McInerney, F.a., Wing, S.L., 2011. The Paleocene-Eocene thermal maximum: a perturbation of carbon cycle, climate, and biosphere with implications for the future. Annu. Rev. Earth Planet. Sci. 39, 489–516. http://dx.doi.org/10.1146/annurev-earth-040610-133431.

Meire, L., Soetaert, K.E.R., Meysman, F.J.R., 2013. Impact of global change on coastal oxygen dynamics and risk of hypoxia. Biogeosciences 10, 2633–2653. http://dx.doi.org/10.5194/bg-10-2633-2013.

Milzow, C., Burg, V., Kinzelbach, W., 2010. Estimating future ecoregion distributions within the Okavango Delta Wetlands based on hydrological simulations and future climate and development scenarios. J. Hydrol. 381, 89–100. http://dx.doi.org/10.1016/j.jhydrol.2009.11.028.

Morón, S., Fox, D.L., Feinberg, J.M., Jaramillo, C., Bayona, G., Montes, C., Bloch, J.I., 2013. Climate change during the Early Paleogene in the Bogotá Basin (Colombia) inferred from paleosol carbon isotope stratigraphy, major oxides, and environmental magnetism. Palaeogeogr. Palaeoclimatol. Palaeoecol. 388, 115–127. http://dx.doi.org/10.1016/j.palaeo.2013.08.010.

Mosbrugger, V., Utescher, T., 1997. The coexistence approach - a method for quantitative reconstructions of Tertiary terrestrial palaeoclimate data using plant fossils. Palaeogeogr. Palaeoclimatol. Palaeoecol. 134, 61–86. http://dx.doi.org/10.1016/S0031-0182(96)00154-X.

Murphy, B.H., Farley, K.A., Zachos, J.C., 2010. An extraterrestrial ^{3}He-based timescale for the Paleocene-Eocene thermal maximum (PETM) from Walvis Ridge, IODP Site 1266. Geochim. Cosmochim. Acta 74, 5098–5108. http://dx.doi.org/10.1016/j.gca.2010.03.039.

Nagy, J., Jargvoll, D., Dypvik, H., Jochmann, M., Riber, L., 2013. Environmental changes during the paleocene-eocene thermal maximum in spitsbergen as reflected by benthic foraminifera. Polar Res. 32. http://dx.doi.org/10.3402/polar.v32i0.19737.

Nearing, M.A., Pruski, F.F., O'Neal, M.R., 2004. Expected climate change impacts on soil erosion rates: a review. J. Soil Water Conserv. 59, 43–50.

Nicholas, C.J., Pearson, P.N., Bown, P.R., Jones, T.D., Huber, B.T., Karega, A., Lees, J.A., McMillan, I.K., O'Halloran, A., Singano, J.M., Wade, B.S., 2006. Stratigraphy and sedimentology of the Upper Cretaceous to Paleogene Kilwa Group, southern coastal Tanzania. J. Afr. Earth Sci. 45, 431–466. http://dx.doi.org/10.1016/j.jafrearsci.2006.04.003.

Nicolo, M.J., Dickens, G.R., Hollis, C.J., 2010. South Pacific intermediate water oxygen depletion at the onset of the Paleocene-Eocene Thermal Maximum as depicted in New Zealand margin sections. Paleoceanography 25, Pa4210. http://dx.doi.org/10.1029/2009pa001904.

Pagani, M., Pedentchouk, N., Huber, M., Sluijs, A., Schouten, S., Brinkhuis, H., Damsté, J.S.S., Dickens, G.R., 2006. Arctic hydrology during global warming at the Palaeocene/Eocene thermal maximum. Nature 442, 671–675. http://dx.doi.org/10.1038/nature05043.

Pagani, M., Huber, M., Sageman, B., 2013. Greenhouse climates. In: Treatise on Geochemistry, Second Edition. pp. 281–304. http://dx.doi.org/10.1016/B978-0-08-095975-7.01314-0.

Pak, D.K., Miller, K.G., 1992. Paleocene to Eocene benthic foraminiferal isotopes and assemblages: implications for deepwater circulation. Paleoceanography 7, 405–422. http://dx.doi.org/10.1029/92PA01234.

Pälike, C., Delaney, M.L., Zachos, J.C., 2014. Deep-sea redox across the Paleocene-Eocene thermal maximum. Geochem. Geophys. Geosyst. 15, 1038–1053. http://dx.doi.org/10.1002/2013GC005074.

Pancost, R.D., Steart, D.S., Handley, L., Collinson, M.E., Hooker, J.J., Scott, A.C., Grassineau, N.V., Glasspool, I.J., 2007. Increased terrestrial methane cycling at the Palaeocene-Eocene thermal maximum. Nature 449, 332–335. http://dx.doi.org/10.1038/nature06012.

Pardo, A., Keller, G., Molina, E., Canudo, J.I., 1997. Planktic foraminiferal turnover across the Paleocene-Eocene transition at DSDP Site 401, Bay of Biscay, North Atlantic. Mar. Micropaleontol. 29, 129–158. http://dx.doi.org/10.1016/S0377-8398(96)00035-7.

Pearson, P.N., Ditchfield, P.W., Singano, J., Harcourt-Brown, K.G., Nicholas, C.J., Olsson, R.K., Shackleton, N.J., Hall, M., 2001. Warm tropical sea surface temperatures in the Late Cretaceous and Eocene epochs. Nature 413, 481–487. http://dx.doi.org/10.1038/35106617.

Pearson, P.N., van Dongen, B.E., Nicholas, C.J., Pancost, R.D., Schouten, S., Singano, J.M., Wade, B.S., 2007. Stable warm tropical climate through the Eocene Epoch. Geology 35, 211–214. http://dx.doi.org/10.1130/G23175A.1.

Peppe, D.J., Royer, D.L., Cariglino, B., Oliver, S.Y., Newman, S., Leight, E., Enikolopov, G., Fernandez-Burgos, M., Herrera, F., Adams, J.M., Correa, E., Currano, E.D., Erickson, J.M., Hinojosa, L.F., Hoganson, J.W., Iglesias, A., Jaramillo, C.A., Johnson, K.R., Jordan, G.J., Kraft, N.J.B., Lovelock, E.C., Lusk, C.H., Niinemets, Ü., Peñuelas, J., Rapson, G., Wing, S.L., Wright, I.J., 2011. Sensitivity of leaf size and shape to climate: global patterns and paleoclimatic applications. New Phytol. 190, 724–739. http://dx.doi.org/10.1111/j.1469-8137.2010.03615.x.

Percival, L.M.E., Cohen, A.S., Davies, M.K., Dickson, A.J., Hesselbo, S.P., Jenkyns, H.C., Leng, M.J., Mather, T.A., Storm, M.S., Xu, W., 2016. Osmium isotope evidence for two pulses of increased continental weathering linked to Early Jurassic volcanism and climate change. Geology 44, 759–762. http://dx.doi.org/10.1130/G37997.1.

Pierrehumbert, R.T., 2002. The hydrologic cycle in deep-time climate problems. Nature 419, 191–198.

Plink-Björklund, P., 2015. Morphodynamics of rivers strongly affected by monsoon precipitation: review of depositional style and forcing factors. Sediment. Geol. 323, 110–147. http://dx.doi.org/10.1016/j.sedgeo.2015.04.004.

Pogge von Strandmann, P.A.E., Jenkyns, H.C., Woodfine, R.G., 2013. Lithium isotope evidence for enhanced weathering during Oceanic Anoxic Event 2. Nat. Geosci. 6, 668–672. http://dx.doi.org/10.1038/ngeo1875.

Pole, M., 2010. Ecology of Paleocene-Eocene vegetation at Kakahu, South Canterbury, New Zealand. Palaeontol. Electron. 13, 14A–29.

Polissar, P.J., Freeman, K.H., 2010. Effects of aridity and vegetation on plant-wax dD in modern lake sediments. Geochim. Cosmochim. Acta 74, 5785–5797. http://dx.doi.org/10.1016/j.gca.2010.06.018.

Pujalte, V., Baceta, J.I., Schmitz, B., 2015. A massive input of coarse-grained siliciclastics in the Pyrenean Basin during the PETM: the missing ingredient in a coeval abrupt change in hydrological regime. Clim. Past 11, 1653–1672.

Rabalais, N.N., Turner, R.E., Díaz, R.J., Justić, D., 2009. Global change and eutrophication of coastal waters. ICES J. Mar. Sci. 66, 1528–1537. http://dx.doi.org/10.1093/icesjms/fsp047.

Rad, S.D., Allègre, C.J., Louvat, P., 2007. Hidden erosion on volcanic islands. Earth Planet. Sci. Lett. 262, 109–124. http://dx.doi.org/10.1016/j.epsl.2007.07.019.

Rad, S., Basile-Doelsch, I., Quesnel, F., Dupuis, C., 2009. Silicium isotopes as a proxy of weathering processes during the PETM. In: Goldschmidt Conference 2009: Challenges to Our Volatile Planet, June 2009, Davos, Switzerland, pp. A1066.

Raffi, I., Backman, J., Zachos, J.C., Sluijs, A., 2009. The response of calcareous nannofossil assemblages to the Paleocene Eocene Thermal Maximum at the Walvis Ridge in the South Atlantic. Mar. Micropaleontol. 70, 201–212. http://dx.doi.org/10.1016/j.marmicro.2008.12.005.

Raich, J.W., Schlesinger, W.H., 1992. The global carbon-dioxide flux in soil respiration and its relationship to vegetation and climate. Tellus Ser. B Chem. Phys. Meteorol. 44, 81–99. http://dx.doi.org/10.1034/j.1600-0889.1992.t01-1-00001.x.

Ravizza, G., Norris, R.N., Blusztajn, J., Aubry, M.-P., 2001. An osmium isotope excursion associated with the Late Paleocene thermal maximum: evidence of intensified chemical weathering. Paleoceanography 16, 155–163. http://dx.doi.org/10.1029/2000PA000541.

Retallack, G.J., 2005. Pedogenic carbonate proxies for amount and seasonality of precipitation in paleosols. Geology 33, 333–336.

Retallack, G.J., Bowen, G.J., Bowen, B.B., 2009. Mechanisms of PETM global change constrained by a new record from central Utah: COMMENT and REPLY: COMMENT. Geology 37, e184–e185. http://dx.doi.org/10.1130/G25070C.1.

Robert, C., Chamley, H., 1991. Development of early Eocene warm climates, as inferred from clay mineral variations in oceanic sediments. Glob. Planet. Chang. 3, 315–331. http://dx.doi.org/10.1016/0921-8181(91)90114-C.

Robert, C., Kennett, J.P., 1994. Antarctic subtropical humid episode at the Paleocene-Eocene boundary - clay-mineral evidence. Geology 22, 211–214. http://dx.doi.org/10.1130/0091-7613(1994)022<0211:Asheat>2.3.Co;2.

Rodriguez-Tovar, F.J., Uchman, A., Alegret, L., Molina, E., 2011. Impact of the Paleocene-Eocene Thermal Maximum on the macrobenthic community: ichnological record from the Zumaia section, northern Spain. Mar. Geol. 282, 178–187. http://dx.doi.org/10.1016/j.margeo.2011.02.009.

Röhl, U., Westerhold, T., Bralower, T.J., Zachos, J.C., 2007. On the duration of the Paleocene-Eocene thermal maximum (PETM). Geochem. Geophys. Geosyst. 8. http://dx.doi.org/10.1029/2007GC001784.

Romans, B.W., Castelltort, S., Covault, J.A., Fildani, A., Walsh, J.P., 2016. Environmental signal propagation in sedimentary systems across timescales. Earth-Sci. Rev. 153, 7–29. http://dx.doi.org/10.1016/j.earscirev.2015.07.012.

Royer, D.L., Wing, S.L., Beerling, D.J., Jolley, D.W., Koch, P.L., Hickey, L.J., Berner, R.A., 2001. Paleobotanical evidence for near present-day levels of atmospheric CO_2 during part of the tertiary. Science 292, 2310–2313. http://dx.doi.org/10.1126/science.292.5525.2310.

Royer, D.L., Wilf, P., Janesko, D.A., Kowalski, E.A., Dilcher, D.L., 2005. Correlations of climate and plant ecology to leaf size and shape: potential proxies for the fossil record. Am. J. Bot. 92, 1141–1151. http://dx.doi.org/10.3732/ajb.92.7.1141.

Sachs, J.P., Sachse, D., Smittenberg, R.H., Zhang, Z., Battisti, D.S., Golubic, S., 2009. Southward movement of the Pacific intertropical convergence zone AD 1400–1850. Nat. Geosci. 2, 519–525. http://dx.doi.org/10.1038/ngeo554.

Sachse, D., Radke, J., Gaupp, R., Schwark, L., Luniger, G., Gleixner, G., 2004. Reconstruction of palaeohydrological conditions in a lagoon during the 2nd Zechstein cycle through simultaneous use of dD values of individual n-alkanes and d18O and d13C values of carbonates. Int. J. Earth Sci. 93, 554–564. http://dx.doi.org/10.1007/s00531-004-0408-5.

Sachse, D., Billault, I., Bowen, G.J., Chikaraishi, Y., Dawson, T.E., Feakins, S.J., Freeman, K.H., Magill, C.R., McInerney, F.A., van der Meer, M.T.J., Polissar, P., Robins, R.J., Sachs, J.P., Schmidt, H.L., Sessions, A.L., White, J.W.C., West, J.B., Kahmen, A., 2012. Molecular paleohydrology: interpreting the hydrogen-isotopic composition of lipid biomarkers from photosynthesizing organisms. Annu. Rev. Earth Planet. Sci. 40, 221–249. http://dx.doi.org/10.1146/annurev-earth-042711-105535.

Sadler, P.M., 1981. Sediment accumulation rates and the completeness of stratigraphic sections. J. Geol. 89, 569–584. http://dx.doi.org/10.1086/628623.

Sagoo, N., Valdes, P.J., Flecker, R., Gregoire, L.J., 2013. The Early Eocene equable climate problem: can perturbations of climate model parameters identify possible solutions? Philos. Trans. A. Math. Phys. Eng. Sci. 371, 20130123. http://dx.doi.org/10.1098/Rsta.2013.0123.

Samanta, A., Bera, M.K., Ghosh, R., Bera, S., Filley, T., Pande, K., Rathore, S.S., Rai, J., Sarkar, A., 2013. Do the large carbon isotopic excursions in terrestrial organic matter across Paleocene-Eocene boundary in India indicate intensification of tropical precipitation? Palaeogeogr. Palaeoclimatol. Palaeoecol. 387, 91–103. http://dx.doi.org/10.1016/j.palaeo.2013.07.008.

Schaller, N., Mahlstein, I., Cermak, J., Knutti, R., 2011. Analyzing precipitation projections: a comparison of different approaches to climate model evaluation. J. Geophys. Res. Atmos. 116. http://dx.doi.org/10.1029/2010JD014963.

Schefuß, E., Schouten, S., Schneider, R.R., 2005. Climatic controls on central African hydrology during the past 20,000 years. Nature 437, 1003–1006. http://dx.doi.org/10.1038/nature03945.

Schmitz, B., Pujalte, V., 2003. Sea-level, humidity, and land-erosion records across the initial Eocene thermal maximum from a continental-marine transect in northern Spain. Geology 31, 689–692. http://dx.doi.org/10.1130/G19527.1.

Schmitz, B., Pujalte, V., 2007. Abrupt increase in seasonal extreme precipitation at the Paleocene-Eocene boundary. Geology 35, 215–218. http://dx.doi.org/10.1130/G23261A.1.

Schmitz, B., Pujalte, V., Nunez-Betelu, K., Núñez-Betelu, K., 2001. Climate and sea-level perturbations during the initial eocene thermal maximum: evidence from siliciclastic units in the Basque Basin (Ermua, Zumaia and Trabakua Pass), northern Spain. Palaeogeogr. Palaeoclimatol. Palaeoecol. 165, 299–320. http://dx.doi.org/10.1016/S0031-0182(00)00167-X.

Schoon, P.L., Heilmann-Clausen, C., Pagh Schultz, B., Sluijs, A., Sinninghe Damsté, J.S., Schouten, S., 2013. Recognition of Early Eocene global carbon isotope excursions using lipids of marine Thaumarchaeota. Earth Planet. Sci. Lett. 373, 160–168. http://dx.doi.org/10.1016/j.epsl.2013.04.037.

Schoon, P.L., Heilmann-Clausen, C., Pagh Schultz, B., Sinninghe Damste, J.S., Schouten, S., 2015. Warming and environmental changes in the eastern North Sea Basin during the Palaeocene-Eocene Thermal Maximum as revealed by biomarker lipids. Org. Geochem. 78, 79–88.

Schouten, S., Woltering, M., Rijpstra, W.I.C., Sluijs, A., Brinkhuis, H., Sinninghe Damsté, J.S., 2007. The Paleocene-Eocene carbon isotope excursion in higher plant organic matter: differential fractionation of angiosperms and conifers in the Arctic. Earth Planet. Sci. Lett. 258, 581–592. http://dx.doi.org/10.1016/j.epsl.2007.04.024.

Schubert, B.A., Jahren, A.H., 2013. Reconciliation of marine and terrestrial carbon isotope excursions based on changing atmospheric CO_2 levels. Nat. Commun. 4, 1653. http://dx.doi.org/10.1038/ncomms2659.

Schulte, P., Scheibner, C., Speijer, R.P., 2011. Fluvial discharge and sea-level changes controlling black shale deposition during the Paleocene-Eocene Thermal Maximum in the Dababiya Quarry section, Egypt. Chem. Geol. 285, 167–183. http://dx.doi.org/10.1016/j.chemgeo.2011.04.004.

Schumann, D., Raub, T.D., Kopp, R.E., Guerquin-Kern, J.-L., Wu, T.-D., Rouiller, I., Smirnov, A. V, Sears, S.K., Lücken, U., Tikoo, S.M., Hesse, R., Kirschvink, J.L., Vali, H., 2008. Gigantism in unique biogenic magnetite at the Paleocene–Eocene Thermal Maximum. Proc. Natl. Acad. Sci. 105, 17648–17653.

Schumer, R., Jerolmack, D.J., 2009. Real and apparent changes in sediment deposition rates through time. J. Geophys. Res. Solid Earth 114. http://dx.doi.org/10.1029/2009JF001266.

Secord, R., Bloch, J.I., Chester, S.G.B., Boyer, D.M., Wood, A.R., Wing, S.L., Kraus, M.J., McInerney, F.A., Krigbaum, J., 2012. Evolution of the earliest horses driven by climate change in the Paleocene-Eocene Thermal Maximum. Science 335, 959–962. http://dx.doi.org/10.1126/science.1213859.

Self-Trail, J.M., Powars, D.S., Watkins, D.K., Wandless, G.A., 2012. Calcareous nannofossil assemblage changes across the Paleocene-Eocene Thermal Maximum: evidence from a shelf setting. Mar. Micropaleontol. 92–93, 61–80. http://dx.doi.org/10.1016/j.marmicro.2012.05.003.

Simpson, G., Castelltort, S., 2012. Model shows that rivers transmit high-frequency climate cycles to the sedimentary record. Geology 40, 1131–1134. http://dx.doi.org/10.1130/G33451.1.

Sinninghe Damsté, J.S., Kuypers, M.M.M., Schouten, S., Schulte, S., Rullkötter, J., 2003. The lycopane/C31 n-alkane ratio as a proxy to assess palaeoxicity during sediment deposition. Earth Planet. Sci. Lett. 209, 215–226. http://dx.doi.org/10.1016/S0012-821X(03)00066-9.

Sluijs, A., Brinkhuis, H., 2009. A dynamic climate and ecosystem state during the Paleocene-Eocene Thermal Maximum: inferences from dinoflagellate cyst assemblages on the New Jersey Shelf. Biogeosciences 6, 1755–1781.

Sluijs, A., Pross, J., Brinkhuis, H., 2005. From greenhouse to icehouse; organic-walled dinoflagellate cysts as paleoenvironmental indicators in the Paleogene. Earth-Sci. Rev. 68, 281–315. http://dx.doi.org/10.1016/j.earscirev.2004.06.001.

Sluijs, A., Schouten, S., Pagani, M., Woltering, M., Brinkhuis, H., Damste, J.S.S., Dickens, G.R., Huber, M., Reichart, G.J., Stein, R., Matthiessen, J., Lourens, L.J., Pedentchouk, N., Backman, J., Moran, K., Scientists, E., 2006. Subtropical arctic ocean temperatures during the Palaeocene/Eocene thermal maximum. Nature 441, 610–613. http://dx.doi.org/10.1038/Nature04668.

Sluijs, A., Bowen, G.J., Brinkhuis, H., Lourens, L.J., Thomas, E., 2007. The Palaeocene-Eocene Thermal Maximum super greenhouse: biotic and geochemical signatures, age models and mechanisms of global change. In: Geological Society Special Publication, pp. 323–349 (doi:1747-602X/07/$15.00).

Sluijs, A., Brinkhuis, H., Crouch, E.M., John, C.M., Handley, L., Munsterman, D., Bohaty, S.M., Zachos, J.C., Reichart, G.J., Schouten, S., Pancost, R.D., Damste, J.S.S., Welters, N.L.D., Lotter, A.F., Dickens, G.R., 2008a. Eustatic variations during the Paleocene-Eocene greenhouse world. Paleoceanography 23, Pa4216. http://dx.doi.org/10.1029/2008pa001615.

Sluijs, A., Röhl, U., Schouten, S., Brumsack, H.J., Sangiorgi, F., Sinninghe Damsté, J.S., Brinkhuis, H., 2008b. Article late Paleocene - Early Eocene paleoenvironments with special emphasis on the Paleocene-Eocene thermal maximum (Lomonosov Ridge, Integrated Ocean Drilling Program Expedition 302). Paleoceanography 23. http://dx.doi.org/10.1029/2007PA001495.

Sluijs, A., Bijl, P.K., Schouten, S., Röhl, U., Reichart, G.J., Brinkhuis, H., Röhl, U., 2011. Southern ocean warming, sea level and hydrological change during the Paleocene-Eocene thermal maximum. Clim. Past 7, 47–61. http://dx.doi.org/10.5194/Cp-7-47-2011.

Sluijs, A., Van Roij, L., Harrington, G.J., Schouten, S., Sessa, J.A., Levay, L.J., Reichart, G.J., Slomp, C.P., 2014. Warming, euxinia and sea level rise during the Paleocene-Eocene thermal maximum on the gulf coastal plain: implications for ocean oxygenation and nutrient cycling. Clim. Past 10, 1421–1439. http://dx.doi.org/10.5194/cp-10-1421-2014.

Smith, F., Wing, S., Freeman, K., 2007. Magnitude of the carbon isotope excursion at the Paleocene–Eocene thermal maximum: the role of plant community change. Earth Planet. Sci. Lett. 262, 50–65. http://dx.doi.org/10.1016/j.epsl.2007.07.021.

Smith, J.J., Hasiotis, S.T., Woody, D.T., Kraus, M.J., 2008. Paleoclimatic implications of crayfish-mediated prismatic structures in paleosols of the Paleogene Willwood Formation, Bighorn Basin, Wyoming, U.S.A. J. Sediment. Res. 78, 323–334. http://dx.doi.org/10.2110/jsr.2008.040.

Soliman, M.F., Aubry, M.P., Schmitz, B., Sherrell, R.M., 2011. Enhanced coastal paleoproductivity and nutrient supply in Upper Egypt during the Paleocene/Eocene Thermal Maximum (PETM): mineralogical and geochemical evidence. Palaeogeogr. Palaeoclimatol. Palaeoecol. 310, 365–377. http://dx.doi.org/10.1016/j.palaeo.2011.07.027.

Speelman, E.N., Sewall, J.O., Noone, D., Huber, M., von der Heydt, A., Damste, J.S., Reichart, G.J., 2010. Modeling the influence of a reduced equator-to-pole sea surface temperature gradient on the distribution of water isotopes in the Early/Middle Eocene. Earth Planet. Sci. Lett. 298, 57–65. http://dx.doi.org/10.1016/j.epsl.2010.07.026.

Speijer, R.P., Morsi, M.M., 2002. Ostracode turnover and sea-level changes associated with the Paleocene-Eocene thermal maximum. Geology 30, 23–26.

Speijer, R.P., Schmitz, B., 1998. A benthic foraminiferal record of Paleocene sea level and trophic/redox conditions at Gebel Aweina, Egypt. Palaeogeogr. Palaeoclimatol. Palaeoecol. 137, 79–101. http://dx.doi.org/10.1016/S0031-0182(97)00107-7.

Speijer, R.P., Wagner, T., 2002. Sea-level changes and black shales associated with the late Paleocene thermal maximum: organic-geochemical and micropaleontologic evidence from the southern Tethyan margin (Egypt-Israel). Geol. Soc. Am. Spec. Pap. 356, 533–549.

Stassen, P., Dupuis, C., Steurbaut, E., Yans, J., Speijer, R.P., 2012a. Perturbation of a Tethyan coastal environment during the Paleocene-Eocene thermal maximum in Tunisia (Sidi Nasseur and Wadi Mezaz). Palaeogeogr. Palaeoclimatol. Palaeoecol. 317–318, 66–92. http://dx.doi.org/10.1016/j.palaeo.2011.12.011.

Stassen, P., Thomas, E., Speijer, R.P., 2012b. Integrated stratigraphy of the Paleocene-Eocene thermal maximum in the New Jersey Coastal Plain: Toward understanding the effects of global warming in a shelf environment. Paleoceanography 27. http://dx.doi.org/10.1029/2012PA002323.

Steart, D.C., Collinson, M.E., Scott, A.C., Glasspool, I.J., Hooker, J.J., 2007. The Cobham Lignite Bed: the palaeobotany of two petrographically contrasting lignites from either side of the Paleocene - Eocene carbon isotope excursion. Acta Palaeobot. 47, 109–125.

Stein, R., Boucsein, B., Meyer, H., 2006. Anoxia and high primary production in the Paleogene central Arctic Ocean: first detailed records from Lomonosov ridge. Geophys. Res. Lett. 33. http://dx.doi.org/10.1029/2006GL026776.

Steurbaut, E., Magioncalda, R., Dupuis, C., van Simaeys, S., Roche, E., Roche, M., 2003. Palynology, paleoenvironments, and organic carbon isotope evolution in lagoonal Paleocene-Eocene boundary settings in North Belgium. Spec. Pap. Geol. Soc. Am. 369, 291–317. http://dx.doi.org/10.1130/0-8137-2369-8.

Storme, J.Y., Dupuis, C., Schnyder, J., Quesnel, F., Garel, S., Iakovleva, A.I., Iacumin, P., Di Matteo, A., Sebilo, M., Yans, J., 2012. Cycles of humid-dry climate conditions around the P/E boundary: new stable isotope data from terrestrial organic matter in Vasterival section (NW France). Terra Nova 24, 114–122. http://dx.doi.org/10.1111/j.1365-3121.2011.01044.x.

Stott, P.A., Sutton, R.T., Smith, D.M., 2008. Detection and attribution of Atlantic salinity changes. Geophys. Res. Lett. 35. http://dx.doi.org/10.1029/2008GL035874.

Sturm, C., Zhang, Q., Noone, D., 2009. An introduction to stable water isotopes in climate models: benefits of forward proxy modelling for paleoclimatology. Clim. Past Discuss. 5, 1697–1729. http://dx.doi.org/10.5194/cpd-5-1697-2009.

Suarez, M.B., Gonzalez, L.A., Ludvigson, G.A., Vega, F.J., Alvarado-Ortega, J., 2009. Isotopic composition of low-latitude paleoprecipitation during the Early Cretaceous. Geol. Soc. Am. Bull. 121, 1584–1595. http://dx.doi.org/10.1130/B26453.1.

Sun, Y., Solomon, S., Dai, A., Portmann, R.W., 2006. How often does it rain? J. Clim. 19, 916–934. http://dx.doi.org/10.1175/JCLI3672.1.

Takeda, K., Kaiho, K., 2007. Faunal turnovers in central Pacific benthic foraminifera during the Paleocene-Eocene thermal maximum. Palaeogeogr. Palaeoclimatol. Palaeoecol. 251, 175–197. http://dx.doi.org/10.1016/j.palaeo.2007.02.026.

Talbot, H.M., Bischoff, J., Inglis, G.N., Collinson, M.E., Pancost, R.D., 2015. Polyfunctionalised bio- and geohopanoids in the Eocene Cobham lignite. Org. Geochem. http://dx.doi.org/10.1016/j.orggeochem.2016.03.006.

Thiry, M., 2000. Palaeoclimatic interpretation of clay minerals in marine deposits: an outlook from the continental origin. Earth Sci. Rev. 49, 201–221. http://dx.doi.org/10.1016/S0012-8252(99)00054-9.

Thomas, E., Shackleton, N.J., 1996. The Paleocene-Eocene benthic foraminiferal extinction and stable isotope anomalies. Geol. Soc. Lond. Spec. Publ. 101, 401–441. http://dx.doi.org/10.1144/GSL.SP.1996.101.01.20.

Tierney, J.E., Tingley, M.P., 2014. A Bayesian, spatially-varying calibration model for the TEX_{86} proxy. Geochim. Cosmochim. Acta 127, 83–106. http://dx.doi.org/10.1016/j.gca.2013.11.026.

Tierney, J.E., Russell, J.M., Huang, Y., Damste, J.S.S., Hopmans, E.C., Cohen, A.S., 2008. Northern hemisphere controls on tropical southeast African climate during the past 60,000 years. Science 322, 252–255. http://dx.doi.org/10.1126/science.1160485.

Tipple, B.J., Pagani, M., 2013. Environmental control on eastern broadleaf forest species' leaf wax distributions and D/H ratios. Geochim. Cosmochim. Acta 111, 64–77. http://dx.doi.org/10.1016/j.gca.2012.10.042.

Tipple, B.J., Pagani, M., Krishnan, S., Dirghangi, S.S., Galeotti, S., Agnini, C., Giusberti, L., Rio, D., 2011. Coupled high-resolution marine and terrestrial records of carbon and hydrologic cycles variations during the Paleocene-Eocene Thermal Maximum (PETM). Earth Planet. Sci. Lett. 311, 82–92. http://dx.doi.org/10.1016/j.epsl.2011.08.045.

Trenberth, K.E., 2011. Changes in precipitation with climate change. Clim. Res. 47, 123–138. http://dx.doi.org/10.3354/cr00953.

Trenberth, K.E., Dai, A., Rasmussen, R.M., Parsons, D.B., 2003. The changing character of precipitation. Bull. Am. Meteorol. Soc. 84, 1205–1217. http://dx.doi.org/10.1175/BAMS-84-9-1205.

Tripati, A., Elderfield, H., 2005. Deep-sea temperature and circulation changes at the Paleocene-Eocene Thermal Maximum. Science 308, 1894–1898. http://dx.doi.org/10.1126/science.1109202.

Trumbore, S.E., Chadwick, O., Amundson, R., 1996. Rapid exchange between soil carbon and atmospheric carbon dioxide driven by temperature change. Science 272, 393–396. http://dx.doi.org/10.1126/science.272.5260.393.

Tucker, G.E., Slingerland, R., 1997. Drainage basin responses to climate change. Water Resour. Res. 33, 2031–2047. http://dx.doi.org/10.1029/97WR00409.

Valdes, P.J., Armstrong, E., Badger, M.P.S., Bradshaw, C.D., Bragg, F., Davies-Barnard, T., Day, J.J., Farnsworth, A., Hopcroft, P.O., Kennedy, A.T., Lord, N.S., Lunt, D.J., Marzocchi, A., Parry, L.M., Roberts, W.H.G., Stone, E.J., Tourte, G.J.L., Williams, J.H.T., 2017. The BRIDGE HadCM3 family of climate models: HadCM3@Bristol v1.0. Geosci. Model Dev. Discuss. http://dx.doi.org/10.5194/gmd-2017-16.

VanDeVelde, J.H., Bowen, G.J., Passey, B.H., Bowen, B.B., 2013. Climatic and diagenetic signals in the stable isotope geochemistry of dolomitic paleosols spanning the Paleocene-Eocene boundary. Geochim. Cosmochim. Acta 109, 254–267. http://dx.doi.org/10.1016/j.gca.2013.02.005.

Viers, J., Oliva, P., Dandurand, J.-L., Dupré, B., Gaillardet, J., 2014. 7.6 - Chemical weathering rates, CO_2 consumption, and control parameters deduced from the chemical composition of rivers. In: Holland, H.D., Turekian, K.K. (Eds.), Treatise on Geochemistry, Second Edition. Elsevier, Oxford, pp. 175–194. http://dx.doi.org/10.1016/B978-0-08-095975-7.00506-4.

Walling, D.E., 2009. The impact of global change on erosion and sediment transport by rivers: current progress and future challenges. The impact of global change publications series. In: United Nations World Water Assess. Program. 81. pp. 1–26.

West, J.A., 2012. Thickness of the chemical weathering zone and implications for erosional and climatic drivers of weathering and for carbon-cycle feedbacks. Geology 40, 811–814. http://dx.doi.org/10.1130/G33041.1.

Westerhold, T., Röhl, U., McCarren, H.K., Zachos, J.C., 2009. Latest on the absolute age of the Paleocene-Eocene Thermal Maximum (PETM): new insights from exact stratigraphic position of key ash layers + 19 and − 17. Earth Planet. Sci. Lett. 287, 412–419.

White, A.F., Blum, A.E., 1995. Effects of climate on chemical-weathering in watersheds. Geochim. Cosmochim. Acta 59, 1729–1747. http://dx.doi.org/10.1016/0016-7037(95)00078-e.

White, A.F., Buss, H.L., 2014. 7.4 - Natural weathering rates of silicate minerals. In: Holland, H.D., Turekian, K.K. (Eds.), Treatise on Geochemistry, Second Edition. Elsevier, Oxford, pp. 115–155. http://dx.doi.org/10.1016/B978-0-08-095975-7.00504-0.

White, P.D., Schiebout, J., 2008. Paleogene paleosols and changes in pedogenesis during the initial Eocene thermal maximum: Big Bend National Park, Texas, USA. Bull. Geol. Soc. Am. 120, 1347–1361. http://dx.doi.org/10.1130/B25987.1.

White, T., Gonzalez, L., Ludvigson, G., Poulsen, C., 2001. Middle Cretaceous greenhouse hydrologic cycle of North America. Geology 29, 363–366. http://dx.doi.org/10.1130/0091-7613(2001)029<0363:Mcghco>2.0.Co;2.

Wieczorek, R., Fantle, M.S., Kump, L.R., Ravizza, G., 2013. Geochemical evidence for volcanic activity prior to and enhanced terrestrial weathering during the Paleocene Eocene Thermal Maximum. Geochim. Cosmochim. Acta 119, 391–410. http://dx.doi.org/10.1016/j.gca.2013.06.005.

Wilf, P., Wing, S.L., Greenwood, D.R., Greenwood, C.L., 1998. Using fossil leaves as paleoprecipitation indicators: an Eocene example. Geology 26, 203–206. http://dx.doi.org/10.1130/0091-7613(1998)026<0203:UFLAPI>2.3.CO.

Wing, S.L., Currano, E.D., 2013. Plant response to a global greenhouse event 56 million years ago. Am. J. Bot. 100, 1234–1254. http://dx.doi.org/10.3732/ajb.1200554.

Wing, S.L., Harrington, G.J., Bowen, G.J., Koch, P.L., 2003. Floral change during the initial Eocene Thermal Maximum in the Powder River Basin, Wyoming. GSA Spec. Pap. 369, 425–440. http://dx.doi.org/10.1130/0-8137-2369-8.425.

Wing, S.L., Harrington, G.J., Smith, F.A., Bloch, J.I., Boyer, D.M., Freeman, K.H., 2005. Transient floral change and rapid global warming at the Paleocene-Eocene boundary. Science 310, 993–996. http://dx.doi.org/10.1126/science.1116913.

Winguth, A., Shellito, C., Shields, C., Winguth, C., 2010. Climate response at the Paleocene-Eocene Thermal Maximum to greenhouse gas forcing-a model study with CCSM3. J. Clim. 23, 2562–2584. http://dx.doi.org/10.1175/2009JCLI3113.1.

Wolfe, J.A., 1993. A method of obtaining climatic parameters from leaf assemblages. U.S. Geol. Surv. Bull. 2040, 1–71.

Wolfe, J.A., 1995. Paleoclimatic estimates from tertiary leaf assemblages. Annu. Rev. Earth Planet. Sci. 23, 119–142. http://dx.doi.org/10.1017/CBO9781107415324.004.

Woody, D.T., Smith, J.J., Kraus, M.J., Hasiotis, S.T., 2014. Manganese-bearing rhizocretions in the Willwood Formation, Wyoming, USA: implications for paleoclimate during the Paleocene-Eocene Thermal Maximum. Palaios 29, 266–276.

Wullschleger, S.D., Tschaplinski, T.J., Norby, R.J., 2002. Plant water relations at elevated CO_2 - implications for water-limited environments. Plant Cell Environ. 25, 319–331. http://dx.doi.org/10.1046/j.1365-3040.2002.00796.x.

Xi, X., 2014. A review of water isotopes in atmospheric general circulation models: recent advances and future prospects. Int. J. Atmos. Sci. 2014 (16 pp.). http://dx.doi.org/10.1155/2014/250920.

Yang, F., Kumar, A., Schlesinger, M.E., Wang, W., 2003. Intensity of hydrological cycles in warmer climates. J. Clim. 16, 2419–2423. http://dx.doi.org/10.1175/2779.1.

Yapp, C.J., 2004. $Fe(CO_3)OH$ in goethite from a mid-latitude North American Oxisol: Estimate of atmospheric CO_2 concentration in the Early Eocene "climatic optimum.". Geochim. Cosmochim. Acta 68, 935–947. http://dx.doi.org/10.1016/j.gca.2003.09.002.

Youssef, M., 2016. Calcareous nannofossils and paleoenvironments of the Paleocene-Eocene thermal maximum (PETM) interval in central Egypt. J. Afr. Earth Sci. 114, 203–219.

Yu, M., Wang, G., Chen, H., 2016. Quantifying the impacts of land surface schemes and dynamic vegetation on the model dependency of projected changes in surface energy and water budgets. J. Adv. Model. Earth Syst. 8, 370–386. http://dx.doi.org/10.1002/2015MS000492.

Zachos, J., Pagani, M., Sloan, L., Thomas, E., Billups, K., 2001. Trends, rhythms, and aberrations in global climate 65 Ma to present. Science 292, 686–693. http://dx.doi.org/10.1126/science.1059412.

Zachos, J.C., Schouten, S., Bohaty, S., Quattlebaum, T., Sluijs, A., Brinkhuis, H., Gibbs, S.J., Bralower, T.J., 2006. Extreme warming of mid-latitude coastal ocean during the Paleocene-Eocene Thermal Maximum: inferences from TEX86 and isotope data. Geology 34, 737–740. http://dx.doi.org/10.1130/G22522.1.

Zacke, A., Voigt, S., Joachimski, M.M., Gale, A.S., Ward, D.J., Tutken, T., 2009. Surface-water freshening and high-latitude river discharge in the Eocene North Sea. J. Geol. Soc. Lond. 166, 969–980. http://dx.doi.org/10.1144/0016-76492008-068.

Zeebe, R.E., Zachos, J.C., Dickens, G.R., 2009. Carbon dioxide forcing alone insufficient to explain Paleocene-Eocene Thermal Maximum warming. Nat. Geosci. 2.

Zhang, Y., Hernandez, M., Anson, E., Nearing, M.A., Wei, H., Stone, J.J., Heilman, P., 2012. Modeling climate change effects on runoff and soil erosion in southeastern Arizona rangelands and implications for mitigation with conservation practices. J. Soil Water Conserv. 67, 390–405. http://dx.doi.org/10.2489/jswc.67.5.390.

Zhou, X., Thomas, E., Rickaby, R.E.M., Winguth, A.M.E., Lu, Z., 2014. I/Ca evidence for upper ocean deoxygenation during the PETM. Paleoceanography 29, 964–975. http://dx.doi.org/10.1002/2014PA002702.